D E S I G N A N D O P E R A T I O N

O F A W I D E G A P

S T R E A M E R C H A M B E R

A thesis submitted for the Degree of
Doctor of Philosopy in the
University of London,

by

Seeta Ram MISHRA M.Sc. (Pat.) M.Sc. (Lond.)

Physics Department
Bedford College
(University of London)

March, 1969

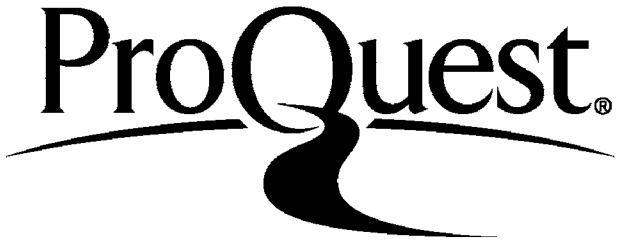

A B S T R A C T

A wide gap streamer chamber has been designed and constructed. Its performance in various modes has been investigated. It is shown that an angular accuracy of 1.5 m rad can be achieved for a 20 centimetre track.

The chamber has been applied to the study of multiple scattering of 100 Mev muons in one inch of lead. A large departure from theory has been observed, and the analysis has indicated a second narrow component of the distribution of the particles plotted against the projected angles of scattering.

The chamber has been modified to study low energy particles.

C O N T E N T S

CHAPTER II (contd.) Page

CHAPTER III

CHAPTER IV

CHAPTER IV (contd.) Page

CHAPTER V

C H A P T E R VI

C H A P T E R I

INTRODUCTION

The spark chamber is the most recent addition to the family of instruments known as visual detectors of charged particles. It is a device in which the trajectories of charged particles in a noble gas are made visible by electrical sparks taking place almost along them. The main advantages of this visual technique are its very small time resolution (of the order of 1 microsecond), a rapid cycling rate which can go up to about 100 per sec., and above all, it can be triggered which makes it possible to record only the desired events, unlike bubble chambers. These advantages, together with the isotropy of the streamer chamber can enable one to perform such experiments which might be impracticable with other visual techniques.

1.1. Early Development.

The standard equipment for particle detection in 1930's was the cloud chamber triggered by Geiger counters. But it has two serious drawbacks. First, the device is slow to set in operation, and ionisation trails persist for a large fraction of a second, with the result that the number of incoming particles must be limited, otherwise chamber pictures may contain more tracks than one can read. Secondly, only a few widely spaced plates may be placed in the chamber to see the interaction, otherwise the chamber will not work. If much material is required it must be a thick plate, with the result that the interaction takes place deep inside, where the tracks cannot be

/seen.

seen.

The bubble chamber developed by Glaser in early 1950's has an important virtue that it can be filled with various liquids such as liquid hydrogen, liquid propane etc. But the bubble chamber shares with emulsion method one serious disadvantage; it cannot be triggered. So one has to examine thousands of exposures for events of interest. It is exclusively used with large accelerators. Here a timing sequence expands the chamber before the bursts of particles arrive. After that at least a second is required for recovery. This puts a limit on its cycling rate.

In late 1940's a few physicists were trying to use electrical sparks to make tracks visible. Keuffel (1949) built several parallel plate spark counters, and suggested the use of arrays of them to obtain tracks. Conversi and Gozzine (1955) made a hodoscope chamber, consisting of many neon-filled glass tubes stacked between a pair of parallel plates. They used a triggering device to apply a high voltage pulse on the plate when a charged particle had passed through the chamber. Only the neon tubes through which particle had passed glowed. The only defect of this chamber is that it gives a two dimensional view of particles three-dimensional path.

In 1957, Cranshaw and de Beer made the next significant advance towards a practical spark chamber. They conbined the parallel plate geometry of the spark counter with the pulse triggering technique of the hodoscope chamber, and made the

/first

efficient spark chamber with six one cm gaps. They also used a clearing field to remove ions older than a few microseconds. They used air which made the detection of two or more simultaneous tracks impossible. Also the quality of tracks was very poor.

In 1959, Fukui and Miyamoto found that in neon several simultaneous particle tracks of better quality could be seen. This was a most significant step.

In the air spark chamber primary ions are attached to O_2 molecules forming negative ions. A field of the order of 70 to 100 kv/cm is required to detach them. This is about three times the voltage needed in the neon spark chamber. The recovery time in air is much longer.

Subsequently, Cook (1961) Cronin (1961) and others constructed a variety of multiplate spark chambers and operated them successfully in accelerator beams.

1.2. Gaseous Processes.

Townsend first studied the spark breakdown phenomena in gases and gave a theoretical explanation which was later modified by Meek and Raether.

1.2.1 - Townsend theory of spark breakdown:-

Townsend studied the variation of the current in a gap between plane parallel electrodes, as a function of applied electric field. With increasing field the current increases and attains

/a

a maximum value corresponding to the number of primary electrons which are collected by anode. At higher fields the maximum current increases at a rate which increases rapidly with field. This is due to ionisation of gas by electron collision, and called gas amplification. The process is cumulative. The positive ions also produce secondary electrons by bombardment on the cathode. The current in the gap can be expressed as

$$i = i_o \exp(\alpha d) \qquad 1.1$$

where α is the number of secondary electrons produced by a single primary electron per unit length of its path, and is called Townsend's first ionisation coefficient; d is the gap width. Other inelastic collisions taking place are the formation of metastable atoms, and electron excitation resulting in the emission of photons which produce photo ionisation.

If the secondary process on the cathode is also considered the number of secondary electrons in the gap can be expressed as

$$n = \frac{n_o \exp(\alpha d)}{1-\gamma(\exp(\alpha d)-1)} \qquad 1.2$$

Where γ is the number of electrons released from the cathode per incident positive ion, and is called Townsend's second ionisation coefficient.

At low voltage gradients $\gamma(\exp(\alpha d)-1)$ is zero, and it increases with the gradient until it finally becomes unity.

$$\gamma(\exp(\alpha d)-1) = 1 \qquad 1.3$$

Thus n in expression 1.2 becomes indeterminate.

At breakdown α is such that $\exp(\alpha d) \gg 1$. Therefore the Townsend sparking criterion was

$$\gamma \exp(\alpha d) = 1 \qquad 1.4$$

Electron avalanches have been studied with a cloud chamber. The electron avalanche appears as a cone shaped cloud with apex towards the cathode, and the axis in the direction of the field.

The Townsend criterion for the formation of sparks has been found in general agreement with experiment for breakdown of gases at reduced pressures. On the basis of the gamma mechanism the formative time should correspond to the time of movement of positive ions across the gap. This is observed for small gaps at low gas pressures. But in oscillographic studies of the development of long sparks at atmospheric pressure, much higher speeds of formation are recorded, and these correspond to electron movement across the gap. These short formative times occur when the gap is subjected to impulse voltages of only 2 or 3% above the D.C. breakdown voltage. But with smaller over voltages longer formative times can occur, which correspond to the time of transit of positive ions across the gap. The impulse breakdown voltage of gaps between a positive point and a negative plane appears to be independent of the cathode material. Further, the cathode effect can hardly explain the growth of lightning discharge from a cloud. Thus, the Townsend theory cannot describe the mechanism of breakdown of large gaps at atmospheric pressure.

1.2.2. Streamer theory of spark formation:- This theory was proposed by Meek (1940) and independently by Raether (1940). It has been elaborated by Loeb, Meek, Raether, and now generally referred to as the streamer theory. Its basis is the consideration of individual electron avalanches, the transition from an avalanche into a streamer and the mechanism for the advance of streamers. The theory involves ionisation processes depending on the gas only, including ionisation by electron collision according to the Townsend, α-mechanism, photoionisation, the Penning effect and the space charge field effects caused by avalanches and streamers.

When a charged particle passes through the gas of the chamber, it leaves a trail of ions, i.e. electrons and positive ions. These primary electrons are accelerated in the applied field and cause further ionisation by collision. When one of the original electrons has moved in the direction of the applied field, a distance x, the number of electrons created is $\exp(\alpha x)$. The process is rapidly cummulative and is termed "electron avalanche". In a field of a magnitude required to cause breakdown, the electrons travel at a speed of the order of 10^7cm/sec., while positive ions move with a velocity of the order of 10^5cm/sec. Thus the positive ions may be considered stationary in comparison with rapidly moving electrons. The avalanche develops across the gap as a cloud of electrons, behind which is left a positive ion space charge. The space charge field distorts the external field. Outside the avalanche the space

/charge

charge augments the external field.

When the voltage applied is in excess of the minimum breakdown value, the space charge field within the avalanche attains a value of the order of the external field, before the avalanche reaches the anode. The densely ionised gas inside the avalanche emits photons which produce photoelectrons. These electrons initiate auxiliary avalanches outside the main avalanche. The greatest multiplication in these auxiliary avalanches occurs along the axis of the main avalanche where the space charge field supplements the external field. The positive ions left behind by these auxiliary avalanches effectively lengthen and intensify the space charge of the main avalanche. Thus the process develops as a self propogating streamer. The streamers proceed across the gap to form a conducting filament of highly ionised gas between the electrodes. This makes the initial stage of the spark channel through which the external circuit discharges.

In a small distance dx at the end of a path x, the number of ion pairs produced is $\alpha \exp(\alpha x)dx$, and these are contained in a volume $\pi r^2 dx$. The electron density is then given by

$$N_{-}(x) = \alpha \exp(\alpha x) / \pi r^2 \qquad 1.5$$

where r is the radius of the avalanche head which is assumed to be spherical.

The space charge field strength at a distance r is given by

$$E_s = \left(\frac{4}{3}\pi r^3 e / r^2\right) \alpha \exp(\alpha x) / \pi r^2$$

In m.k.s. units

$$E_s = e\alpha \exp(\alpha x) / 3\pi\epsilon_0 r \propto \alpha \exp(\alpha x)/r \qquad 1.6$$

where e is the electron charge and ϵ_0 is the permittivity constant.

The space charge field is of the order of applied field when

$$\exp(\alpha x_c) \simeq 10^8 \qquad 1.7$$

or $$\alpha x_c \simeq 20$$

Dickey (1952) indicated that the number of electrons which finally had to be formed to produce the observed current, and thus, a significant change in electrode potential should be of the order of 10^{13}.

Thus, it seems that the transition from avalanche to streamer takes place when the number of electrons in the avalanche reaches 10^8, but the collapse of voltage occurs when it is 10^{13}.

When an avalanche initiates streamer formation in midgap region, the streamers are both anode directed and cathode directed. (Fig.1.1). In the case of positive streamers or cathode directed streamers, photons produce photoelectrons ahead of streamers and these initiate avalanches which develop towards the tip of the streamer, because of the attraction of the positive space charge field surrounding the tip. Each auxiliary avalanche causes an extension of the streamer tip. In this way the streamer advances towards the cathode. The negative streamers grow as a result of auxiliary avalanches developing away from the streamer tip.

For successful operation of the spark chamber the magnitude of the electric field should be so chosen that the value of α in the gas used is sufficiently high to satisfy Meek's criterion before

/the

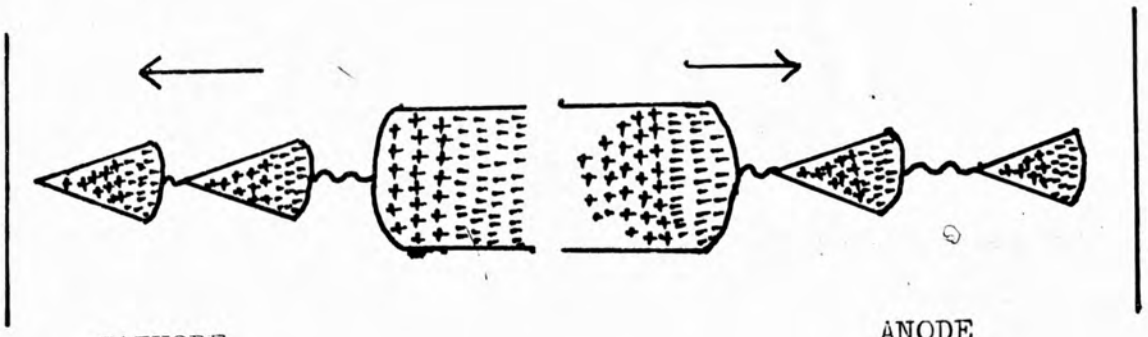

Fig. -11- Streamer Propogation

Gases	α, Ion Pairs / Cm.			Sp. Ion. Ion Pairs/Cm.
	5KV/Cm	10KV/CM	15/KV/cm	Atmo.Press.
He.	6	60	154	8
Ne.	23	68	180	25
Ar.	0.6	6	60	40
Ne+0.01% Ar.	114	170	380	25

Table-1.1-Townsend coefficient and specific ionisation in different gases.

the avalanche reaches the anode. α primarily depends upon the nature of the gas. Its value in a particular gas increases as the applied field is increased. Since the total number of electrons in an avalanche also depends upon the number of primary electrons, the gas should be so chosen that the number of primary ions and α are both high. Table 1.1. shows that neon with a very small admixture of argon is the most suitable gas. But neon is very dear, so it can be mixed with a certain proportion of helium without any harm. About 70% neon and 30% helium used in this work, is the most widely used gas. Commercially pure neon has always a small proportion of argon. The presence of a small proportion of argon in neon acts in the following way.

$$Ne^{*} + A_r \rightarrow A_r^{+} + e^{-} + Ne$$

In the case of pure neon, electrons, in addition to producing ionization, raise neon more frequently to an excited state, which then does not improve the production factor of the electron. When argon is present the excited neon collides with argon and ionizes it 'Druyvesteyn and Penning, 1940). This is called Penning effect. The table below shows the ionisation potentials and energy of metastable states of some gases (Meek and Craggs 1953).

Gas	Ionization poten.	metastable states
Argon	15.8 ev.	11.49 ev. and 11.66 ev.
Helium	24.6 ev.	19.8 ev.
Neon	21.6 ev.	16.53 ev. and 16.62 ev.

1.3. The Multiplate Spark Chamber.

When the spark formation is used for the detection of the tracks of charged particles, the electric field is applied in the form of a fast rising high voltage pulse on the electrodes. It is essential that this pulse should arrive within one microsecond of the passage of the particles through the chamber. The amplitude of the high voltage pulse should be well above the d.c. sparking voltage of the gap, and the rise time should be very small, otherwise most of the primary electrons might be swept out of the gap before the field reaches its peak value. In small gap chambers, a small clearing field is also essential to remove electrons produced by random processes. The clearing field is arranged in such a way that the transit time of an electron to cross the gap is twice the delay time between the passage of the particle and initial rise of the high voltage pulse. In wide gap chambers a small clearing field is not effective, and when a high clearing field is applied it produces a large lateral shift between the track and the spark (Brookes, 1965). The memory time and recovery time can be reduced by adding some organic gas or vapour.

In the multiplate chamber we get a series of sparks which define the track. Study of streamer density (chapter 4.2) shows that only two streamers per centimetre of the track develop fully and others are suppressed. Thus in multiplate chambers of gap width about 5 mms, only one avalanche in each gap would develop fully. The electric field near it would tend to be enhanced in the

/direction

direction of the applied field. The streamer propogation and the spark would then follow the direction of the applied field. This explains why the sparks in small gaps rarely follow the inclined tracks. Thus the multiplate spark chambers are actually track sampling devices. Thus to construct tracks from the sparks the mean alignment point of sparks with the track has to be found. From the process of the spark mechanism in small gaps, it is clear that the electrons nearest the cathode are most effective in forming avalanches. In agreement with this Rutherglen and Patterson (1961) have found that the mean alignment point is at about 0.2 of the electrode spacing from the cathode. This holds good for zero clearing field. In the presence of a clearing field, the electrons move in a direction normal to the plate, with the result that the mean alignment point of the sparks relative to the original track also moves. By examining a large number of angled tracks the mean alignment point for a particular track can be found.

The efficiency of such a chamber for a track making an angle more than 40° with the vertical is very small. The photograph of a typical track is shown in Fig. 1.2. (Mishra, 1966).

1.4. Discharge Chamber.

The discharge chamber which is also called the projection chamber was first made by Fukui and Miyamoto (1961). It is a delineating chamber of very simple operation. The chamber was a box with glass walls about 1 cm. wide. A conductive transparent

/(SnO_2)

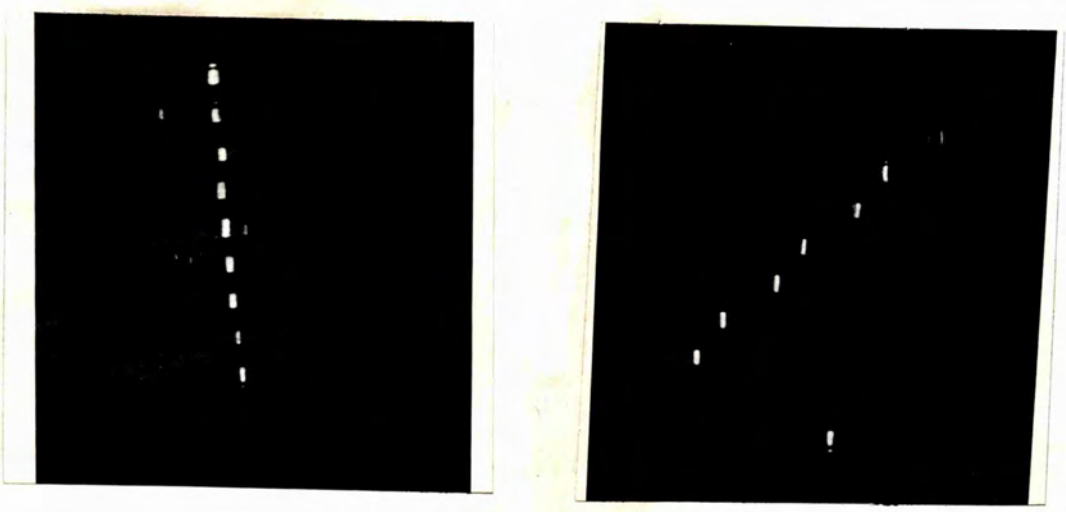

Fig.1.2--Typical cosmic ray tracks in a multigap spark chamber (Mishra, 1966)

(SnO_2) coating on two opposite surfaces forms the electrodes (Fig. 1.3.). The high voltage pulse is applied when the particle passes through the chamber parallel to the electrodes. The track is indicated by many streamers connecting the two electrodes and is viewed through the transparent electrodes. The length of the pulse is about 0.1 microsecond. The important property of such a chamber is that the energy of the discharge is shared by many partial discharges. The remarkable difference from the spark chamber with metallic electrodes is that the electric field in the gap does not drop rapidly as a consequence of the large surface resistivity of glass. The main limitation is that the chamber provides a plane projection of the trajectory. The recovery time is of the order of 0.1 or 0.2 sec. Stainless steel wire mesh has also been used as transparent electrodes. A discharge chamber with a 6 cm gap has been made by Charpak (1963). He used a helium-neon mixture, commonly known as "Penegal" saturated with Halogen vapours. The high voltage used was of the order of 2Kv/cm. The pulse length was very large, several microseconds. The addition of halogen reduces the working voltage by increasing the amplification, and lowers the recovery time, but on the other hand, it makes the quality of the tracks very poor.

1.5. Wide Gap Chamber

The wide gap spark chamber was first reported by Borisov (1962). He used gaps of 4.5 and 10 cm. and a field of 14 Kv/cm. He said that sparks traced the tracks up to an angle of incidence of 40^0 Alikhanian (1963) used a single gap of about 20 cm. gap width. High voltage pulses of amplitude 60-80 Kv and duration 10^{-7} sec.

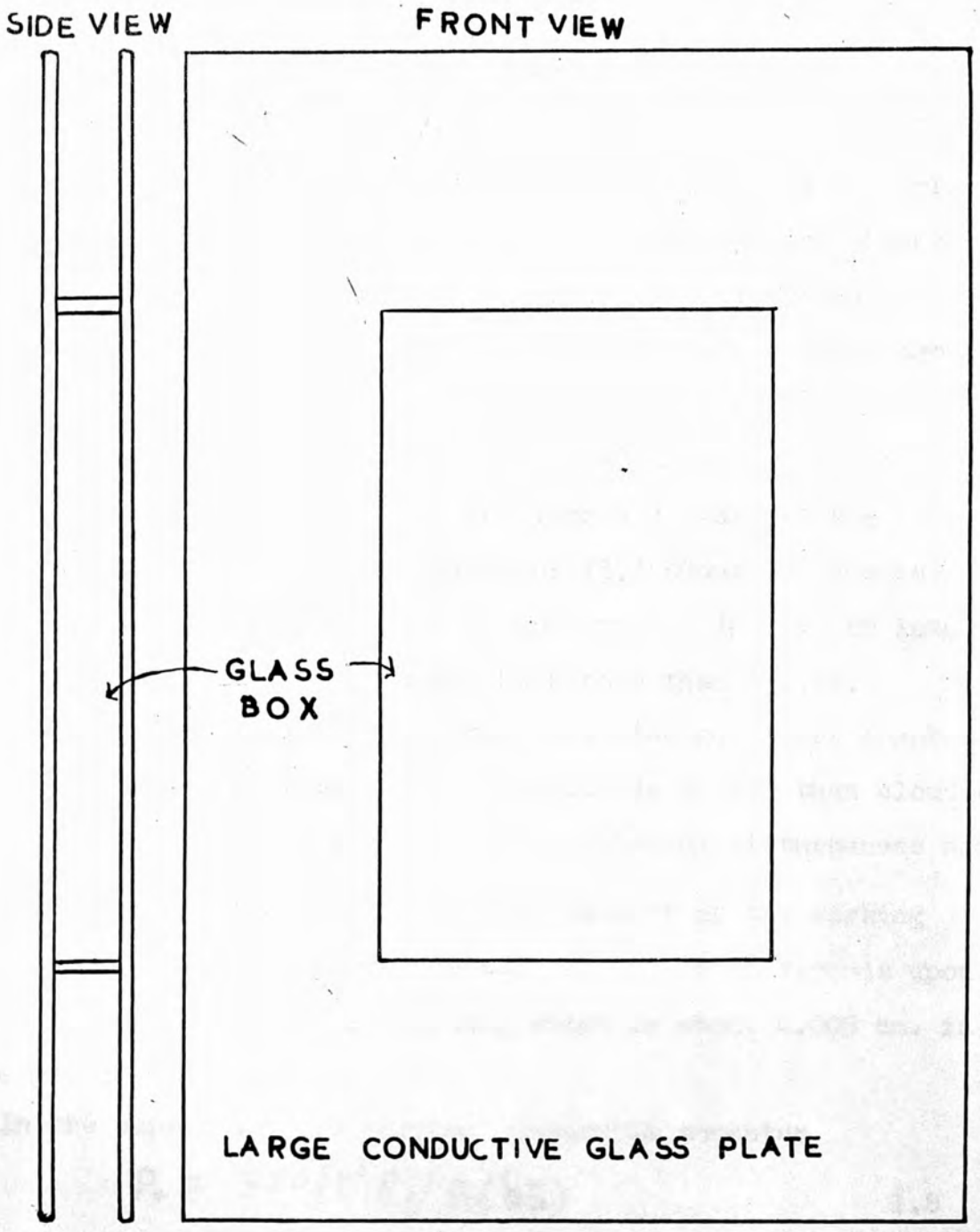

Fig. 1.3--Discharge (or Prpjection) chamber-- by Fukui and Miyamoto (1961).

were obtained with a Marx generator (chapter 2.4). Good quality tracks making an angle up to 40° with the vertical were observed. The chamber was placed in a magnetic field of 5 Kilogauss and curved trajectories were seen. The momentum measured was in good agreement with the momentum selected by means of absorbers and coincidence-anti-coincidence arrangement. Garron (1964) made a 40 cm wide gap chamber. He used a field of 10 Kv/cm and measured the momentum of cosmic rays. In a magnetic field of 13.3 KGauss an accuracy of $\pm$ 1.4% for a momentum of 1 Bev/c was obtained. In a 40 cm long bubble chamber the accuracy cannot be better than $\pm$ 2.4%.

The maximum detectable momentum is a wide gap spark chamber and streamer chamber is an order of magnitude better than cloud or bubble chamber. This is possible because thermal disturbances and distortions due to the mechanical displacement of the working medium are absent. The maximum detectable momentum depends upon the error in measurement of sagitta, which is about 0.005 cm. in a wide gap chamber.

In the expression for maximum measurable momentum

$$P_o = 300(\ell^2 B)/8(\delta s) \qquad 1.8$$

Po is the maximum momentum in ev/c, l is the track length in Cm, B is the magnetic field in gauss and δs is the error in sagitta. If a wide gap chamber track one metre in length is placed in a magnetic field of 10^4 Gauss,

$$P_o = 300 \frac{(100)^2 10^4}{8(0.005)} = 400 \text{ Gev/c} \qquad 1.9$$

The intensity of the spark decreases rapidly when the angle between the trajectory and the electric field increases beyond 35°. The mechanism describing how the spark follows the trajectory was proposed by Fukui and Miyamoto (1961). The enlargement of the neighbouring electron avalanches may cause geometrical merging. Then the space charge field is so large that the resultant field is almost along the trajectory, with the result that the streamer has a tendency to follow it. For this to happen the lateral distance between adjacent avalanches must be small so that the merger may occur. This distance is such that adjacent avalanches overlap each other. Something similar may happen when there is an electrical attraction between opposite ends of each pair of adjacent avalanches.

If d be the distance between the centre of adjacent avalanches, γ the radius defined by electron diffusion and θ the angle between the trajectory and the field, then the first of the above conditions would be satisfied when

$$\sin\theta \leq 2k_1\gamma/d \qquad 1.10$$

and the second condition when

$$\cos\theta \geq 2k_2\gamma/d \qquad 1.11$$

(Fig.1.4)

combining the two we get

$$\tan\theta \leq k_1/k_2$$

If k_1 and k_2 are of the order of unity, we have

$$\theta \leq 45^{\circ}$$

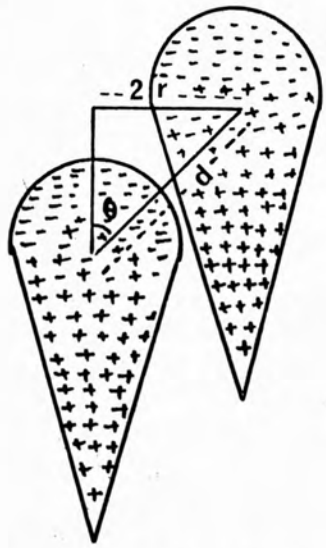

Fig.1.4(a) Geometrical merge of the adjacent avalanches.

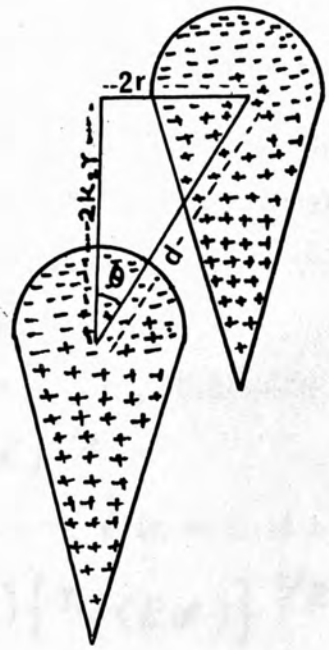

Fig. 1.4(b) Attraction between opposite ends of adjacent avalanches.

Bolotove et al. (1966) have shown that the first condition is the main condition for discharge development along the track. The avalanche radius can be expressed as

$$\gamma = (4Dt)^{1/2} = \left(4D\frac{x}{v}\right)^{1/2} = \left(4D\frac{x}{kE}\right)^{1/2} \qquad 1.13$$

where x is the distance through which the original electron has moved in the direction of electric field, D the diffusion coefficient and k the electron mobility.

From Meek's criterion we get

$$x = 20/\alpha \qquad 1.14$$

and from the expression for D (Kaye and Laby 1966)

$$D/k = \eta P/Ne \qquad 1.15$$

where, η is the ratio of the mean agitation energy of electron to that of gas molecules, P the normal pressure in dynes/cm^2, N the number of gas molecules per cm^3 of the gas and e the electronic charge.

Combining the equations 1.13, 1.14 and 1.15 we get

$$\gamma = (\eta/E\alpha)^{1/2}$$

and substituting this value of γ in equation 1.10 we get

$$\sin\theta_{max} = (2/d)\{\eta/(E\alpha)\}^{1/2} \qquad 1.16$$

This is not a quantitative relation, because of the lack of quantitative information about the effect of the space charge field and photoionisation on discharge development. In the case of high concentration of ions ambipolar diffusion might be more

/effective

The ambipolar diffusion $D_a = D_-/(K_+/K_-)$

where K_+ is the mobility of positive ions.

On considering this the equation 1.16 becomes

$$\sin\theta_{max} = (2/d)\{(K_+/K_-)\eta/(E\alpha)\}^{1/2} \qquad 1.17$$

A qualitative comparison can be made between calculated and experimental values of θmax.

If pressure is increased the only term on the right hand side altered significantly will be d (it will decrease) and therefore θmax should increase. Bolotove et al. (1966) have determined θmax in different gases for pressures up to 5 atmospheres, and have found that this prediction holds.

1.6. Streamer Chamber

In the streamer chamber which is a new and evolved form of spark chamber, the H.V. pulse is applied only for a very limited time (~ 20 ns.), with the result that only the gas amplification process is used and practically no current passes between the electrodes. In this mode the tracks are depicted just by the arrested streamers, with the result that tracks at all angles may be detected - i.e. complete isotropy is possible.

An important step in the development of streamer chamber was taken by Alikhanian et al. (1963) who studied the discharge mode in a wide gap chamber by applying pulses of 500 ns. length. They were able to obtain complete circular tracks for electrons of 34 Mev.

/when

when the chamber was placed in a magnetic field. The first genuine streamer chamber was reported by Chikovani et al. (1964). By using an H.V. pulse of very short length they were able to check the development of the streamers at a stage when they were just sufficiently luminous to be photographed. Tracks appeared as a series of luminous centres when the field was of the order of 10Kv/cm. It was found that as the field was increased, and the length of the pulse decreased, the streamer became smaller and more intense. Such a chamber is capable of registering tracks of the particles originating in the chamber itself.

The most recent addition to this family of instruments is the avalanche chamber reported by Gygi and Schneider (1966). Using an almost triangular pulse of 300 Kv amplitude and 5 ns base length across a chamber of 10 cm. gap width they were able to limit the discharges to single avalanches of about 1 mm. i.e. the growth into streamers was prevented. Since the avalanches cannot be seen they were only able to photograph them by means of image intensifier. This form of chamber does have the advantage, however, that ionisation measurements are possible.

C H A P T E R 2

THE DESIGN AND CONSTRUCTION OF STREAMER CHAMBER SYSTEM

2.1. General Principles.

The apparatus as a whole can be split up into two parts. First is the chamber itself and second the associated electronics including detectors, logic, trigger amplifier and high voltage switch (Fig. 2.1.).

Charged cosmic ray particles passing right through the chamber are detected by the scintillation counters placed above and below the chamber, and the resulting pulses are fed into a coincidence circuit. The output of the coincidence circuit operates the trigger amplifier. The very fast rising output pulse of the trigger amplifier, which is a few Kv in amplitude, makes the high voltage switch work. In the wide gap chamber the high voltage switch consists of a Marx generator which is an arrangement of low inductance rapid discharge condensers and spark gaps, which are so connected that they are charged in parallel, but discharged in series. The whole electronics system should be so fast that overall delay between the passage of the charged particle through the chamber and the initial rise of the high voltage pulse on the chamber must be less than a microsecond.

In the wide gap spark chamber the duration of the high voltage pulse (and hence the field) is adjusted by a shunt resistance connected between the earthed and high voltage plates. Its value is so chosen that the pulse length is between half a microsecond

/and

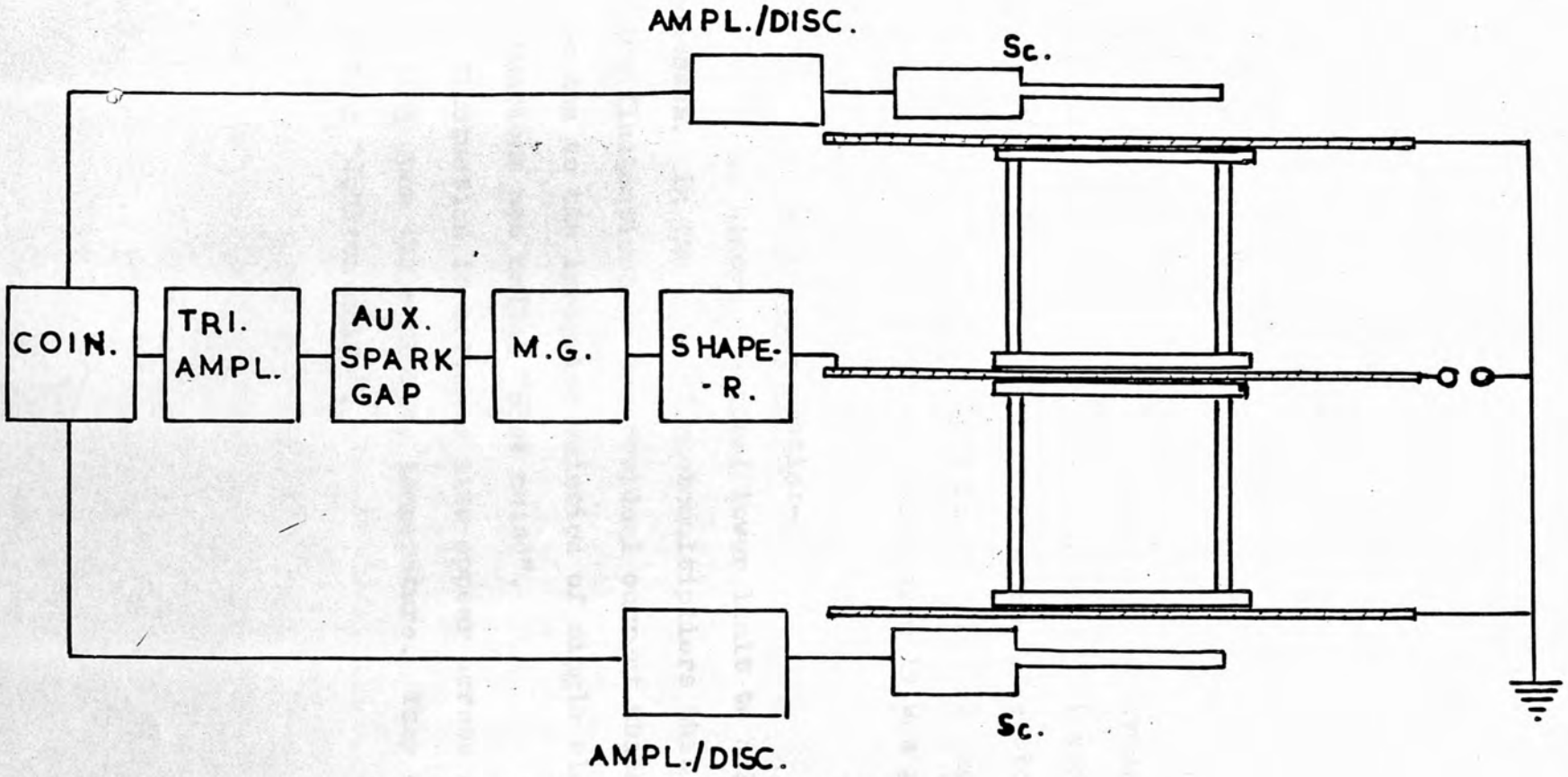

Fig. 2.1-Basic Components of Streamer Chamber.

and one microsecond. This arrangement is not found suitable for streamer chamber operation, where the length of the H.V. pulse must be less than 50 nanosec. To achieve such a pulse, a shaping circuit is included between the Marx generator and the chamber. By means of this circuit (chap.2.5.2.) the front of the pulse can be improved and its length can be adjusted to any value without affecting the amplitude.

2.2. Triggering Scintillation-Counters.

In the development and subsequent study of the streamer chamber, cosmic ray particles have been employed. They were detected with two scintillation counters that consisted of circular plastic (NE102A) phosphors of 10.5 inches diameter, and about 1 inch thick, coupled by a short light guide to eleven stage photo-multiplier tubes (EMI6097C). Each assembly was placed in a light tight metal casing.

Noise and signal to noise ratio:-

There is always a natural lower limit to all measuring processes. In the case of photomultipliers this limit is set by random fluctuations in the residual current which might be supposed to be due to the irregular emission of single electrons. Such fluctuations are called "shot noise".

Fluctuation in voltages also appear across coupling resistors depending upon their abolute temperature. They are called "thermal noise" or "Johnson noise".

If the random pulses are counted over an interval of time, the numbers will be found to vary about their average value. The standard deviation is a measure of the noise. If the number is very large

$$\sigma = (it/e)^{1/2} \qquad 2.1$$

where σ is the standard deviation, i, the current measured over a time t.

The root mean square value of the voltage fluctuation

$$\sigma e/c = (eit)^{1/2}/c \qquad 2.2$$

If this voltage appears across a resistor R, then

$$Ri = R(ei/t)^{1/2} \qquad 2.3$$

$t = 1/2\Delta f$, where Δf is the bandwidth.

Thus the r.m.s. fluctuation of the voltage

$$Ri = R(2ei\Delta f)^{1/2} \qquad 2.4$$

The value of i, the photocurrent is very small. So it is necessary to use a high value of R. Then the thermal fluctuations of charge density along the resister, which gives rise to "johnson noise" becomes important.

The r.m.s. value of "Johnson noise" is $(0.1eR\Delta f)^{\frac{1}{2}}$ at $300^{\circ}K$.

If G be the multiplication produced by the secondary emission process, the minimum output r.m.s. noise current would be $G(2ei\Delta f)^{\frac{1}{2}}$. The anode current $I = Gi$.

The total r.m.s. noise voltage is

$$(R^2G^2 2ei\Delta f + 0.1eR\Delta f)^{1/2}$$
$$= (eR\Delta f)^{1/2}(2G^2iR + 0.1)^{1/2} \qquad 2.5$$

If RI $\gg$ 0.05/G, "Johnson noise" will not predominate, which is easily achieved. (Sharpe, 1961).

In this scintillation counter, a peak signal of 2 volts was obtained. The anode load was 10 K and EHT, 2KV. Thus the peak anode current is 0.2mA and gain can be typically taken to be as 10^6, since maximum gain at 2400 volts has been quoted to be as 10^8. Using a bandwidth of 1 Mc/s, the r.m.s. noise voltage comes to be as 0.08 volt.

Noise level seen on the oscilloscope, after dissociating the photomultiplier from the crystal, was 0.1 volt. Therefore peak signal to noise ratio was 20.

Comparison of signal plus noise and noise distributions:-
The counter pulses were amplified by an I.D.L. amplifier to a maximum of about 8 volts and fed into a multichannel analyser which was set for 100 channels. The distribution of cosmic rays was first recorded, and then the crystal was removed, and the distribution of noise pulses only was recorded. The two distrubutions have been compared in Fig.2.2. The noise peak seems to have shifted slightly. At about channel number 10, the noise counts have dropped down to a negligibly small value. In the actual experiment the counter pulses were amplified to about 30 volts and the discriminator bias was fixed at $\frac{1}{2}$5 volts.

2.3. Electronics

The signals from the scintillation counters initiate a sequence of operations that culminate in the application of a 240 Kv pulse to the plates of the chamber. This is achieved with the /units

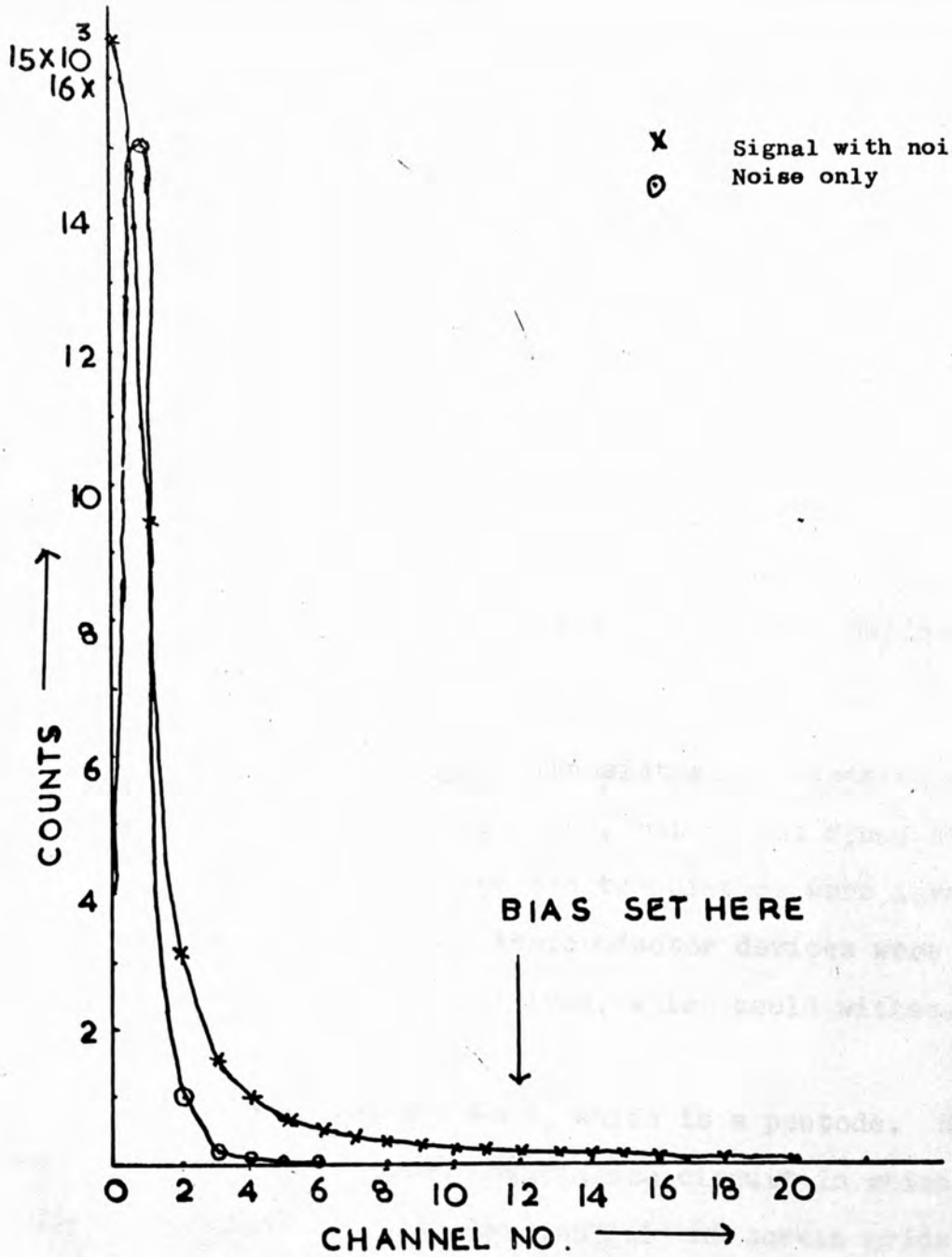

Fig. 2.2- Pulse height distribution of cosmic rays from plastic Scintillators compared with Photomultiplier noise.

units shown in Fig. 2.1, and these are described in detail in the following sections.

2.3.1. - Amplifier/Discriminator - I.D.L. wide band linear amplifiers which have built in voltage discriminators, were used.

The 2 volt pulses were amplified to about 30 volts, and the square 15 volt output pulses from the discriminator were further reduced to 4 volts with a potentiometer before entering the coincidence circuit. The time of transit of the pulse through the amplifier was measured to be 60 ns.

2.3.2. - Coincidence circuit - Transistor and diode coincidence circuits were used in the beginning, but it was found that after firing the chamber a few times the transistors were invariably destroyed. Accordingly, the semiconductor devices were removed and the circuit re-designed with valves, which could withstand the pick-up and feed-back pulses.

The valve used was the 6BN6, which is a pentode. Neilson and James (1955) used a pentode coincidence circuit in which they applied the input pulses to the control and screen grids which were negatively biased to keep the valve normally cut off. The valve conducts only during the time of overlap. In the writer's experience this arrangement gave a very small output. It seems that in this case the anode current was very small.

In the circuit used in this work (Fig.2.3) the input signals were applied to the control and suppressor grids which were negatively biased. For two properly coincident pulses, a negative output of about three volts amplitude was obtained. An advantage

/of

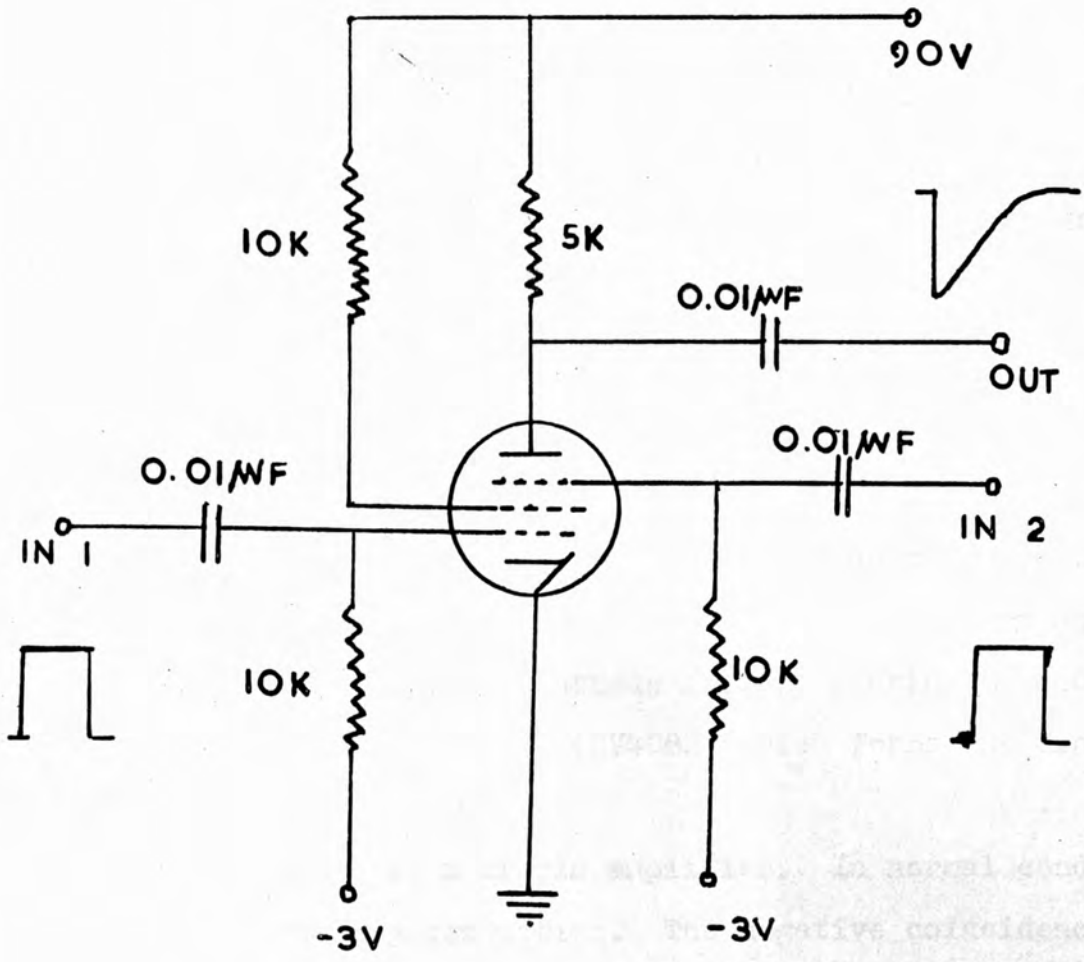

Fig.-2.3- Coincidence Circuit

of this circuit was that there was no signal at all in the absence of a coincidence.

For Cosmic rays, the coincidence counting rate was found to be about 2 to 4 per minute, over the goemetry of the apparatus.

The chance coincidence was found to be about one in four hours.

The time of transit of the pulse through this circuit was measured to be about 10 nanosecond.

2.3.3. - Trigger amplifier - It consists of four stages. The first is a pentode (E 180 F) amplifier, the second a secondary emission pentode (EFP60), the third a cathode follower, using EL 360 and the fourth is a beam power tetrode (CV4082) which forms the final amplifying stage, (Fig.2.4).

The first stage is a simple amplifier. In normal conditions the valve is partially conducting. The negative coincidence output cuts the valve off, giving a positive output. The amplitude is about 20 volts. Such a big pulse is entirely necessary for the successful operation of the next stage, the EFP60.

The EFP60 is a radio frequency pentode which contains an extra electrode (dynode) placed between the anode and the suppressor grid.

The dynode is kept positive with respect to the cathode. The electrons strike it after emerging from the cathode grid structure. The dynode surface is sensitised to emit a copious number of secondary electrons, on the average about four for each incident electron. Almost all the secondary electrons leaving the dynode are attracted to the anode which is at a higher potential.

/There

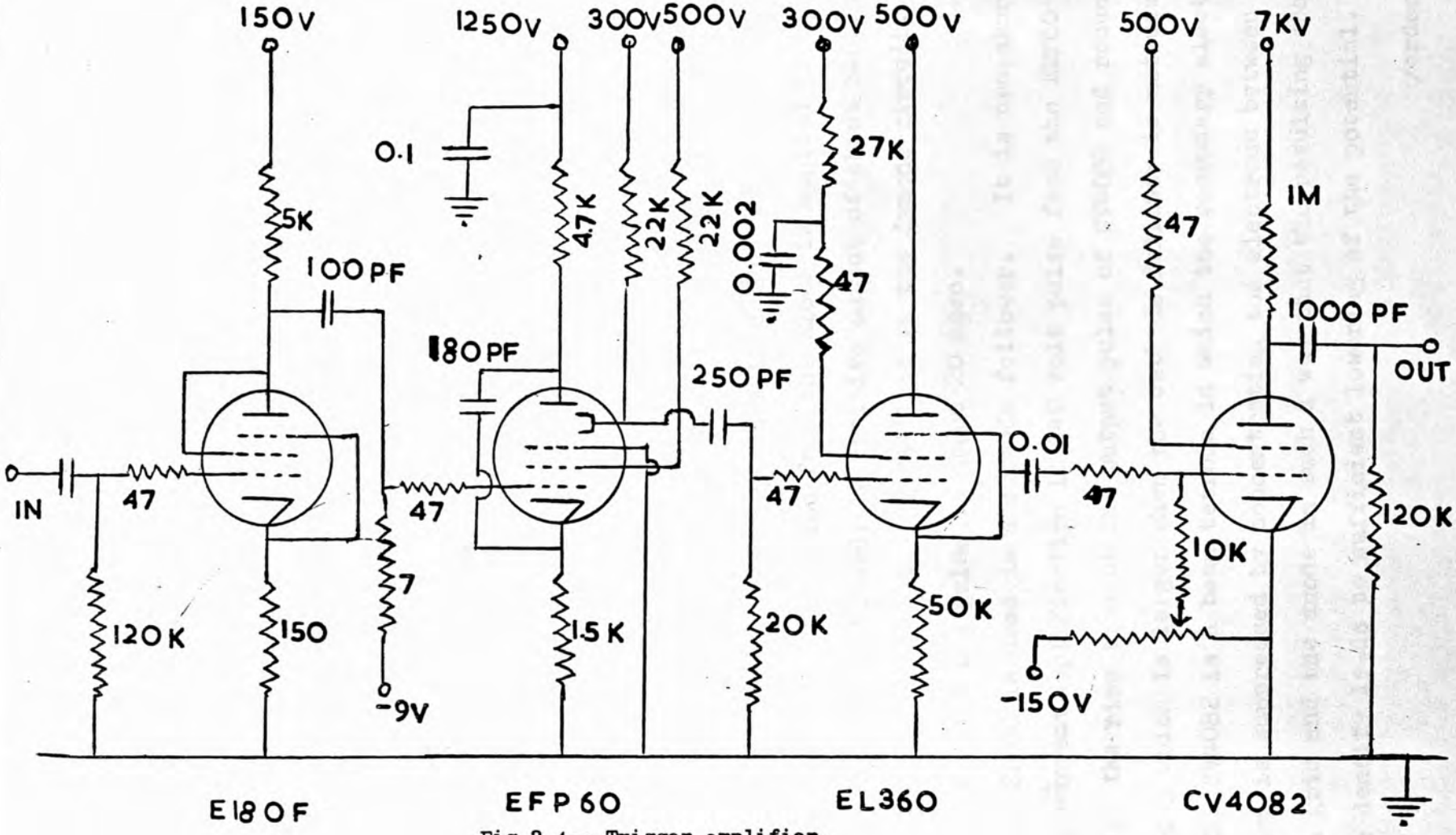

Fig.2.4-- Trigger amplifier.

There are three special features of this valve.

i) The ratio of the mutual conductance (between control grid and anode) to the total anode capacitance is between two and three times that found in the case of ordinary r.f. pentodes. This is particularly useful when the valve is used as a linear amplifier.

ii) A net current flows out of the dynode into the external circuit and it increases in magnitude when the central grid potential is raised. Therefore the signal appearing across a load resistor placed in the dynode circuit is in phase with the grid signal, and amplification can be obtained without phase inversion.

iii) Since the anode current is several times the cathode current, regeneration by feed-back from anode to cathode can be obtained.

A 20 volt positive pulse from the E180F is applied to the grid which is negatively biased. A positive output of about 140 volts amplitude appears across a 22 KΩ load in the dynode circuit. The rise time of the pulse is about 20 nsec.

The EL360 is used as a cathode follower. It is necessary because current amplification in 140 volt pulse from the EFP60 improves the rise time of the output pulse of CV4082 and reduces the delay which is larger when the cathode follower is not used.

The CV4082 is a beam tetrode in which the secondary electron emission is suppressed by concentrating the electrons between the screen grid and the anode in such a way that the resulting space charge density leads to sufficient lowering of the potential. In

/order

order to make the potential drop large for complete suppression the space-charge density and therefore also the current density must be large enough. This is why beam tetrodes are mainly used in power amplifiers where large currents are needed. A beam tetrode has a larger anode to screen current ratio than an equivalent pentode, and this ratio is constant over a larger range of anode currents. This is obtained by the use of an electron optic technique in its construction. The control grid and the screen grid are aligned. The resulting field then forces the electrons to pass between the screen grid wires, reducing the screen current. The electron paths in the screen anode region diverge less than in o ordinary pentodes. This leads to a higher space charge density, which is further enhanced by the use of beam plates. The beam plates concentrate the electrons in a limited region between g_2 and a. The distance between anode and screen is made large so that a sufficient potential drop may occur.

Normally this valve remains cut off. When 140v positive pulse from EL360 is applied to the control grid, the valve conducts, giving rise to a 6Kv negative pulse rising in about 10 nsec. This pulse is used to trigger a 28 Kv pulse which fires the Marx generator. The delay over the whole trigger amplifier was 60 nsec.

2.4. Auxiliary spark gap giving 28 Kv pulse.-

The 6Kv pulse from the trigger amplifier was not sufficient to fire 60 Kv, the charging voltage of the Marx generator. Therefore an intermediate switch working at 28 Kv was included.

This switch consisted of a storage capacitor and a spark gap (Fig.2.5 b&c). Two rapid discharge condensers (each 5000 pF and 15 Kv working) of very low inductance, were connected in series. The spark gap was made up of two stainless steel electrodes, each about one inch in diameter. The earthed electrode is hollow with a 3 mm hole on the top. The hollow space is packed up with Tufnol having a central hole through which passes the 1 mm diameter tungsten trigger electrode. In the space between the electrode and the tungsten wire was placed a barium titanate annulus with an inner diameter of about 1 mm and an outer of about 3 mm. The tip of the tungsten wire was level with the surfaces of the barium titanate annulus, and the earthed electrode. The $BaTiO_3$ did not fit tightly into the hole in the electrode, i.e. there was a small air gap.

By the use of the $BaTiO_3$, the electrical field was intensified. Advantage was taken of the effect that:- "the reduction of electric field in an insulator due to its dielectric constant causes overvolting of an adjacent air gap (Lavoi et al. 1964).

If a cylinder of dielectric constant k, inner radius r_2 and outer radius r_3 is inserted in a cylindrical gap of inner radius r_1 and outer radius r_4, the field at either electrode is intensified by the ratio

$$R = \log \frac{r_4}{r_1} \Big/ \left(\log \frac{r_2}{r_1} + \frac{1}{k} \log \frac{r_3}{r_1} + \log \frac{r_4}{r_3} \right) \qquad 2.6$$

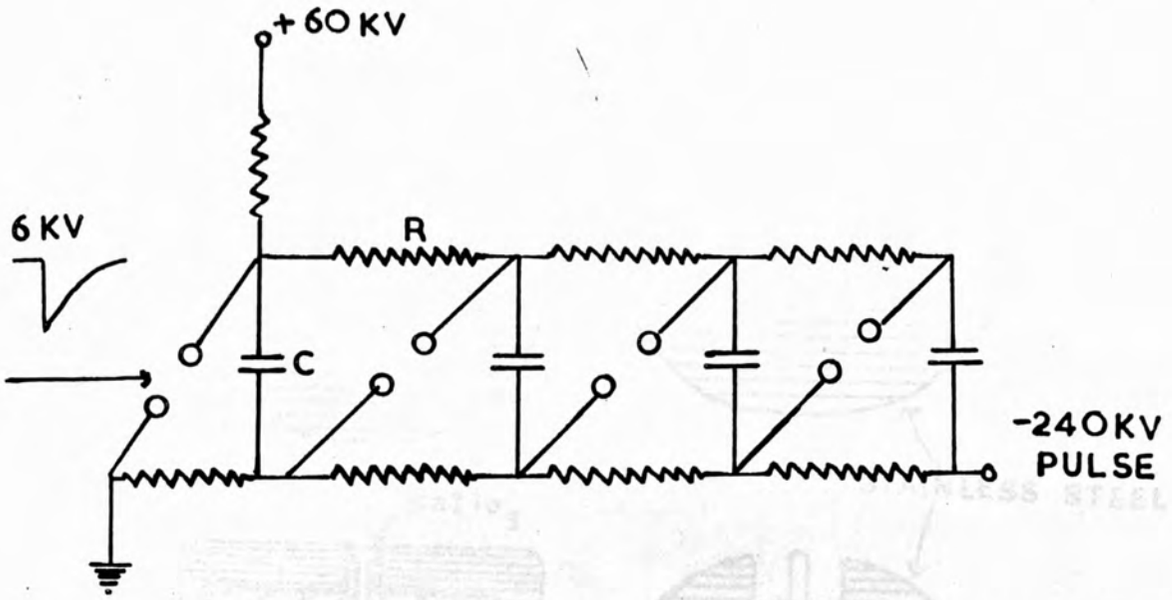

Fig, 2.5a-- Basic circuit of the MARX GENERATOR.

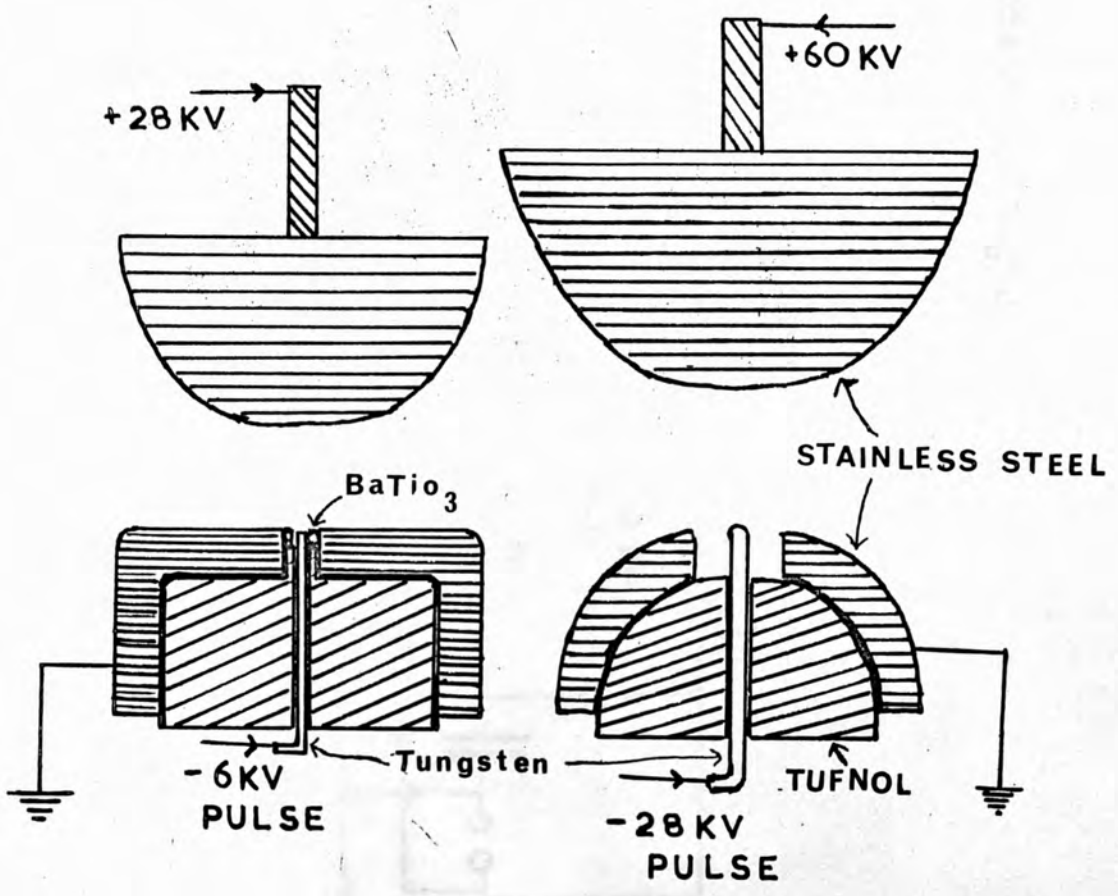

--Double the actual size --

Fig.2.5b--Design of the Intermidiate spark gap and the First spark gap of the Marx Generator.

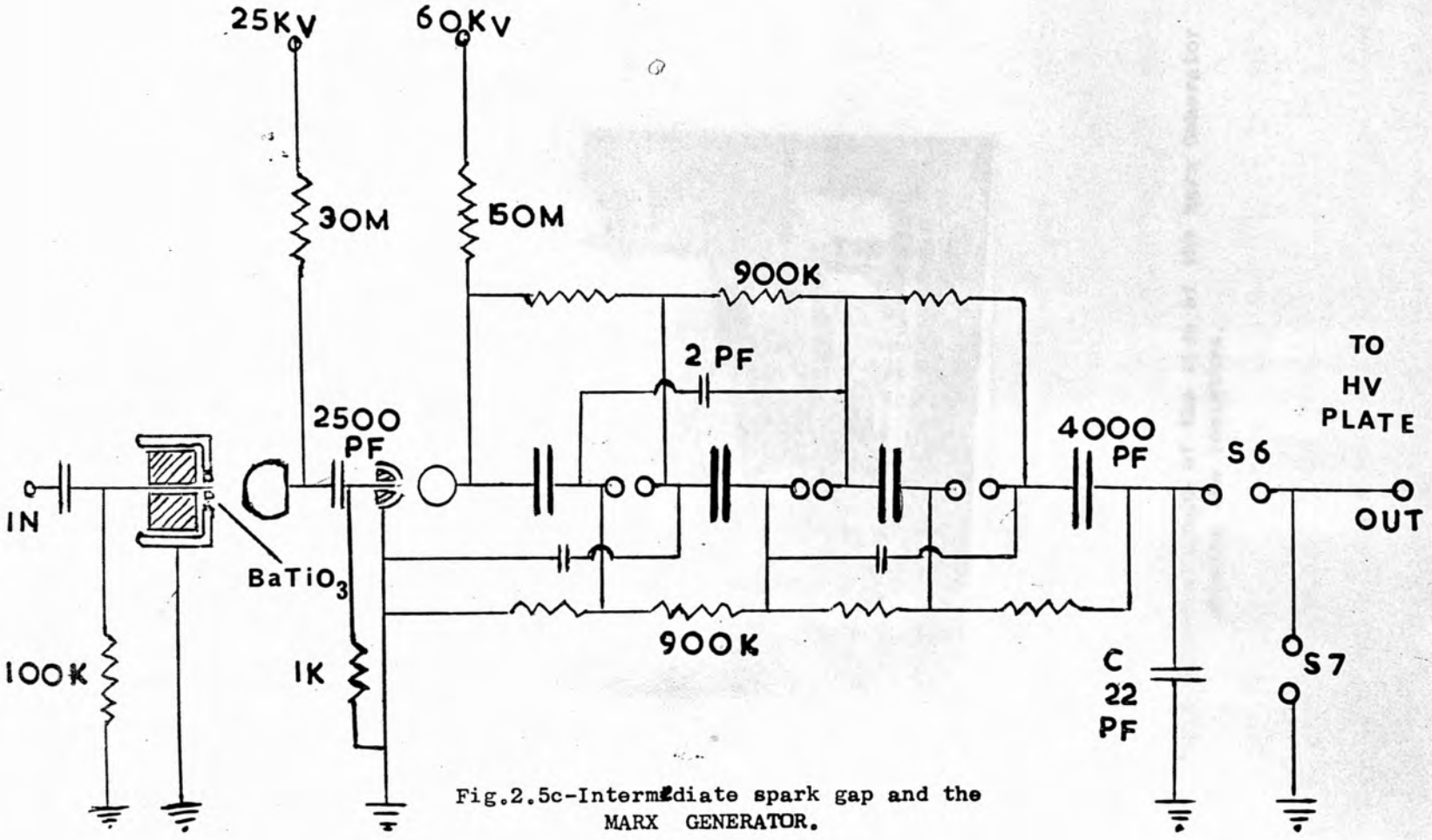

Fig.2.5c-Intermediate spark gap and the MARX GENERATOR.

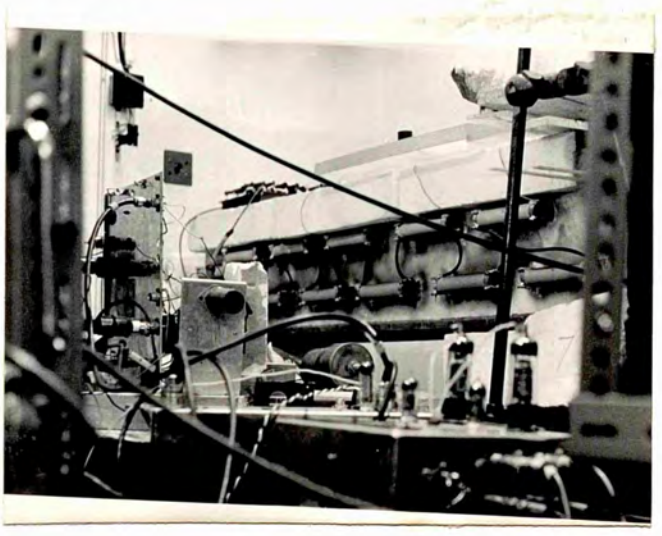

Fig.2.5(d)-Photograph of the side of the Marx Generator showing the resistors.

Despite the end effects present in the actual spark gap, this equation gives a good estimation of the ratio. In the present case R = 3. The $BaTiO_3$ has dielectric constant of over 1000, and being ceramic it is strongly resistant to spark heating. It lasts for over 5 million sparks.

The 6Kv pulse from the trigger amplifier produces a spark between the tungsten wire and the earthed electrode. Photons from this spark ionise the air gap above the third H.V. electrode and cause a very rapid breakdown. Since the storage capacitors have been charged to +28 Kv, a negative pulse of amplitude about 28 Kv and rise time 8 ns. is created. This pulse is used to fire the Marx generator.

By the use of barium titanate, the delay over the high voltage switch is reduced to 10 ns.

2.5. Marx Generator

2.5.1. - Working principle:- In the work that has been described so far, Marx Generators (M.G) have been preferred for the production of the high voltages that have to be applied to the streamer chamber.

The basic principle of these devices (Fig.2.5a) is the multiplication of voltage, when a number of condensers are charged in parallel and discharged in series. If there are n condensers, each charged to a voltage V, then on being suddenly connected in series, the effective capacitance would be 1/n of each capacitance

/and

and therefore the nominal voltage $V_o = nV$. However, because of the voltage drop over the internal impedance of the M.G., the actual output voltage across a resistive load is somewhat smaller than the nominal. This mechanism of switching over from parallel to series is provided by spark gaps. When the first gap is made to fire by the trigger pulse, there is sudden application of over-voltage across the second gap which soon breaks down. In the same way the successive gaps break down in turn. When there is no spark in the chamber the pulse decays with a time constant C_oR, where C_o is the effective capacitance of the M.G. and R is the shunt resistance.

A number of techniques have been employed to achieve the optimum performance of these generators; one of these is the use of small value condensers (Fig. 2.5c), to couple the adjacent stages. The effect is to improve the pulse front and reduce the time of transit of the pulse. They act in the following way.

The time lag between the breakdown of successive spark gaps depends upon the magnitude of overvoltage, which in the case of a particular gap depends upon the number of gaps already fired. Therefore, when many gaps have sparked, larger would become the overvoltage for the remaining gaps, with the result that the time lag between successive breakdowns would become shorter and shorter. This time lag is mainly due to the inductances of the condensers and spark gaps. Due to the small overvoltage and time lag, the output pulse rises slowly in the beginning. The overvoltage can

/be

be increased and time lag reduced, by using coupling condensers. Their introduction allows one to apply a hundred per cent, over-voltage on the second gap independently of the number of stages, if the first gap has already fired. After the $(n-1)^{th}$ breakdown, the n^{th} gap receives an overvoltage of (n-1)V. The capacitance of coupling condensers should be very very small in comparison to that of the M.G. This gives much faster rising pulse with small delay.

The properties which a M.G. must possess are low internal impedance, rapid rise-time, and short delay. A M.G. can have these properties only when the condensers have low inductances, of the order of a fraction of a microhenery, when the spark gaps are ionised by the photons from the previous gaps, and when they are rapidly overvoltaged. As the number of stages increases the effective inductance also increases, which makes the rise-time of the pulse worse. The M.G. used by Garron (1964) had 15 stages and a rise-time of about 15 to 20 n.s. Chikovani (1965) found it was possible even if the inductances were considerable, to improve the rise-time by incorporating a pulse-shaping arrangement after the M.G. Gygi and Schneider (1964) built a M.G. with $BaTiO_3$ capacitors, and low value coupling capacitors, and were able to produce pulses rising in 2 nanoseconds.

2.5.2. Design of the Marx-Generator - In the present M.G. very large paper condensers have been used. The total inductance of the four capacitors used is 0.8 nicrhenery (0.2 microhenery each),

/but

but with the use of coupling capacitors and a pulse shaping circuit pulses of up to 240 Kv in amplitude and rising in about 5-6 nanoseconds have been obtained.

This M.G. consists of four rapid discharge capacitors, 4000 PF each (60 Kv working), and four spark gaps. There are three coupling capacitors, 2 PF each, having polystyrene as dielectric (Fig. 2.5c).

Coaxial design has been preferred because it is easier to make and the internal inductance is minimum, (Keller, 1966). The condensers were fixed on a 6 feet x 1 foot perspex board, and enclosed on two sides by 6 feet x 1½ foot perspex held by means of nylon screws. The resistors were placed outside on the vertical walls. They are all Dubillier, 20 watts, 25 Kv working. The spark electrodes were screwed directly on to the capacitors. The first 60 Kv spark gap electrodes were made of stainless steel. The high voltage electrode was a hemisphere of an inch and a quarter in diameter, and the earthed electrode was a one inch diameter hollow hemisphere with 3 mm thick wall. Its top surface had a 6 mm diameter hole in the centre, (Fig. 2.5b). The inside was packed up with Tufnol having a 2 mm diameter central hole through which passed the tungsten trigger electrode. The other spark gaps were made up of hard steel spheres, half an inch in diameter. The upper open face was covered by polystyrene foam, and the coupling capacitors were placed on the top. The top could be opened for gap adjustment. The coupling condensers have

/aluminium

aluminium electrodes, which are 2 inches in diameter and 1/8 inch thick. Their surfaces are well polished and edges rounded off. 2.8 cm thick polystyrene slab serves as dielectric, which is projecting out in all directions to prevent the breakdown of the edges. Connecting cables are push fitted into the holes in the sides of the electrodes.

There are two very important requirements for rapid breakdown of spark gaps - one, quick application of overvoltage across them and the other, the presence of some electrons in the gaps. 2 PF coupling capacitors help in the fulfilment of the first requirement. The second can be obtained if the photons from the sparks in the first gap are reflected from the side walls and thus brought into the gaps. This was achieved by painting the entire inside surface with Dulux (I.C.I.) Brilliant White Emulsion which is a plastic paint. This provides an optical path linkage for photons between successive gaps.

2.5.3. Circuit Analysis - The M.G. circuit can be regarded as an LCR network, and the shape and size of the high voltage pulse, generated by it can be theoretically obtained using a Laplace transform of the equation representing the potential drop across the different components of the network, at a particular instant of time after the first gap has been fired.

In the equivalent circuit of the M.G. (Fig.2.6), C_1 is the effective total capacitance, L_1 the total inductance of the capacitors (the inductance of the spark gaps has been neglected here),

/C_2,

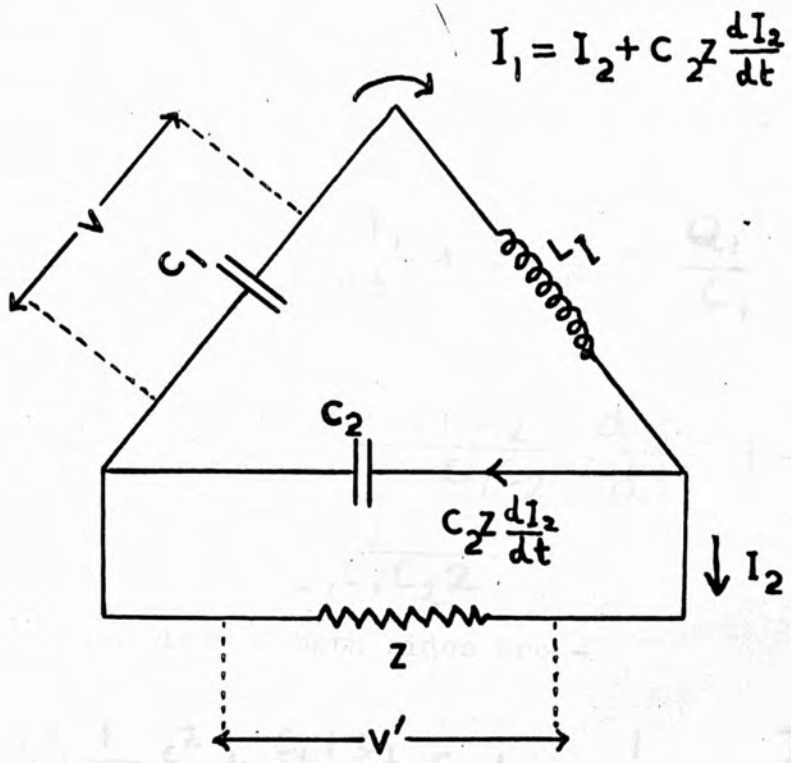

Fig. 2.6--Equivalent circuit of the Marx Generator.

C_2, the capacity introduced by output electrodes plus any stray capacitances, Z, either the terminating ohmic resistor parallel to C_2, or the characteristic impedance of the line.

Let the first gap fire at t = o, then at any instant of time, t, the potential drop over different parts of the circuit must satisfy the relation -

$$\frac{Q_2 + C_2 Z I_2}{C_1} + L_1 \frac{dI_1}{dt} + Z I_2 = \frac{Q_1}{C_1} \qquad 2.7$$

which can be written as

$$\frac{d^3Q_2}{dt^3} + \frac{1}{C_2 Z}\frac{d^2Q_2}{dt^2} + \frac{C_1 + C_2}{L_1 C_1 C_2}\frac{dQ_2}{dt} + \frac{Q_2}{L_1 C_1 C_2 Z} = \frac{Q_1}{L_1 C_1 C_2 Z} \qquad 2.8$$

Laplace transforms of both sides are -

$$q(s)\left\{S^3 + \frac{1}{C_2 Z}S^2 + \frac{C_1 + C_2}{L_1 C_1 C_2}S + \frac{1}{L_1 C_1 C_2 Z}\right\} = \frac{Q_1}{S L_1 C_1 C_2 Z} \qquad 2.9$$

or

$$v\left(S^3 + \frac{1}{C_2 Z}S^2 + \frac{C_1 + C_2}{L_1 C_1 C_2}S + \frac{1}{L_1 C_1 C_2 Z}\right) = \frac{V}{L_1 C_2} \qquad 2.10$$

Let the roots of the expression under bracket be

$$S = w,\ S = x + iy,\ S = x - iy \qquad 2.11$$

/Thus

Thus

$$(S-w)(S-x-iy)(S-x+iy) = S^3 + \frac{1}{C_2 Z}S^2 + \frac{C_1+C_2}{L_1C_1C_2}S + \frac{1}{L_1C_1C_2Z} \qquad 2.12$$

comparing the coefficients on both sides we have

$-(2x + w) = 1/C_2Z$, $x^2 + y^2 + 2xw = (C_1 + C_2)/L_1C_1C_2$

and $-a(x^2 + y^2) = 1/L_1C_1C_2Z.$ 2.13

Now

$$\frac{1}{(S-w)\{(S-x)^2+y^2\}} = \frac{1}{w^2-2wx+x^2+y^2}\left\{\frac{1}{S-a} - \frac{w-x}{y}\frac{y}{(S-x)^2+y^2} - \frac{S-x}{(S-x)^2+y^2}\right\} \qquad 2.14$$

Using the values of Laplace integrals we have

$$= \frac{\exp(wt) - (\exp(xt))\left(\frac{w-x}{y}\sin yt + \cos yt\right)}{L_1C_2(w^2-2wx+x^2+y^2)} \qquad 2.15$$

This equation has been solved for some of our typical values L_1, C_1, C_2 and Z. The shape of the pulse appears in Fig.27, which shows that the pulse rises to its maximum in 8 nanoseconds and the rise time is 4.7 nanoseconds.

The operation of the Marx generator was tested and the output pulse was observed with a Tektronix 581 A oscilloscope, after attenuation first by a resistance dividing (1:10) chain /and

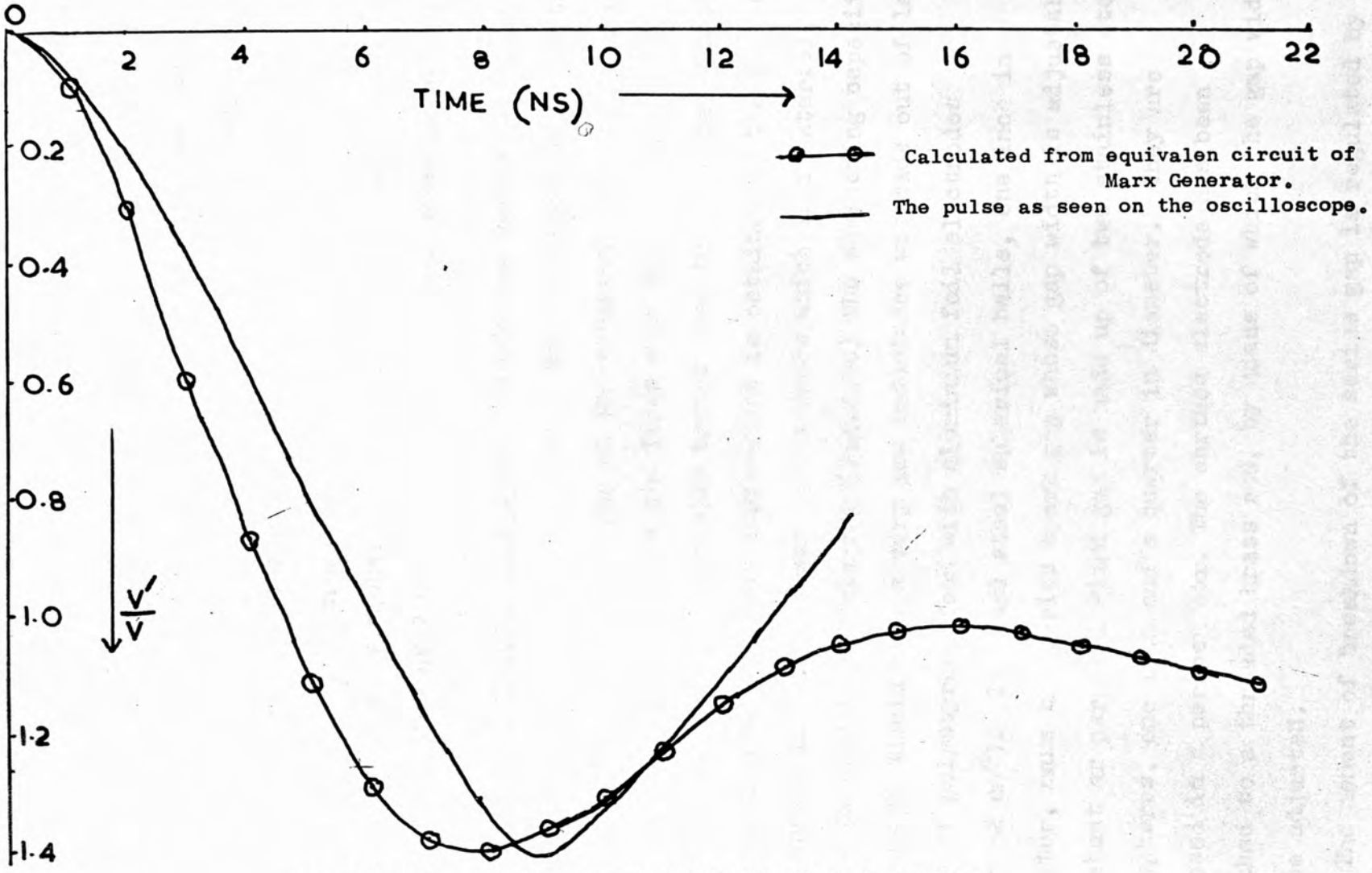

Fig.2.7--Shape of the HV pulse from the Marx Generator.

and then by a 1000 x HV probe (P6015). Noise and both mains borne and radiated interference prevented the whole pulse being seen, but the rising edge was clearly visible. After corrections for the 3.9 nanoseconds rise time of the oscilloscope and 4 nanoseconds rise time of the HV probe, the Marx output pulse was found to have a rise time of 7 nanoseconds and has been shown inFig.2.7.

2.5.4. - Pulse-shaping circuit:- After the Marx generator the high voltage pulse was improved with the spark gap arrangements shown in Fig. 2.5c. The charge on the enhanced stray capacitance builds up before the series gap fires with the result that the rise time of the pulse actually transferred to the chamber plates is further reduced. This improvement is obtained at the cost of an increase in delay by some nanoseconds which is immaterial.

Referring to the diagram (Fig.2.5c) the sharpening capacitor C_6, which should have a very low inductance was made out of large slabs of polystyrene foam with aluminium foil electrodes (58 x 32 cm^2). Two hard steel spherical balls, one inch in diameter, make the series spark gap whose gap width is adjustable. The shunt or parallel spark gap is made up of two stainless steel hemispheres, one inch and a quarter in diameter. They are enclosed in a perspex box. The earthed electrode has been attached to a threaded brass rod, by means of which the gap width can be adjusted.

The moment of breakdown of the series gap is regulated by adjusting the gap width, so that breakdown would occur when the

/full

voltage is reached across the gap. In some cases this gap has been pressurised with the advantages that the delay will be smaller and the moment of breakdown can be adjusted by changing the pressure. With this circuit the rise-time of the pulse was found to be 5-6 nanoseconds. In fact, this might have been even better, but the measurement was limited by the rise-time of the oscilloscope.

The length of the pulse and hence the duration of the field in the chamber was adjusted by changing the width of the shunt gap. All the spark gaps were operated in air at atmospheric pressure.

2.5.5. The operation of the Marx Generator:- The Marx generator has been operated at the charging voltages ranging from 30 Kv to 60 Kv. As the operating voltage increases the gap width has to be increased. The operating voltages of the Marx generators used by other workers have been between 20 and 30 Kv. At these voltages to get a pulse of about 240 Kv, 8 stages would be required. With the size of the condensers available a Marx generator of 8 stages would have been unmanagably long. Therefore, it was decided to increase the operative voltage and reduce the number of stages. The disadvantages are corona and some increase in delay. The corona problem was solved by using "Silastoner cold cure Rubber", the electrical breakdown strength of which is about 500v/mil.

For + 60 Kv operating voltage, a 28 Kv trigger pulse was used. Smaller pulses were found to give unreliable performance. The adjustment of the width of the gaps was found to be very important. All thefour spark gaps were individually adjusted for

/each

each operating voltage. The effect of the change in atmospheric conditions was found to be considerable. A slight change in operating voltage was required when there was a considerable change in atmospheric pressure. The operating voltage was kept about 500 volts lower than the static breakdown voltage of the gaps to prevent random triggering.

2.6. Design of the Chamber

2.6.1. An early unsuccessful Chamber:- A small prototype self triggered chamber was designed, as shown in Fig.2.8. Two wire grid planes, separated by a 1/4 inch perspex frame, were placed on the lower electrode of the chamber. The lower wire plane was located on 1/8" above the lower electrode. The chamber was placed inside a 5½ inch diameter perspex cylinder with 1/4 inch thick wall. The electrodes were 3½ inches square aluminium plates. The high voltage plate was attached to a metal rod passing through a central hole in the top perspex plate marked A, which closed the upper end of the perspex cylinder. With this arrangement, the gap width could be adjusted easily.

The lower electrode and the wire grid just above it formed a spark counter.

The chamber was expected to work as a self triggered chamber with the spark counter as a triggering counter, but on operating the edges of the electrodes were found to break down. Later, the upper electrode was removed, and the perspex plate marked A was

/replaced

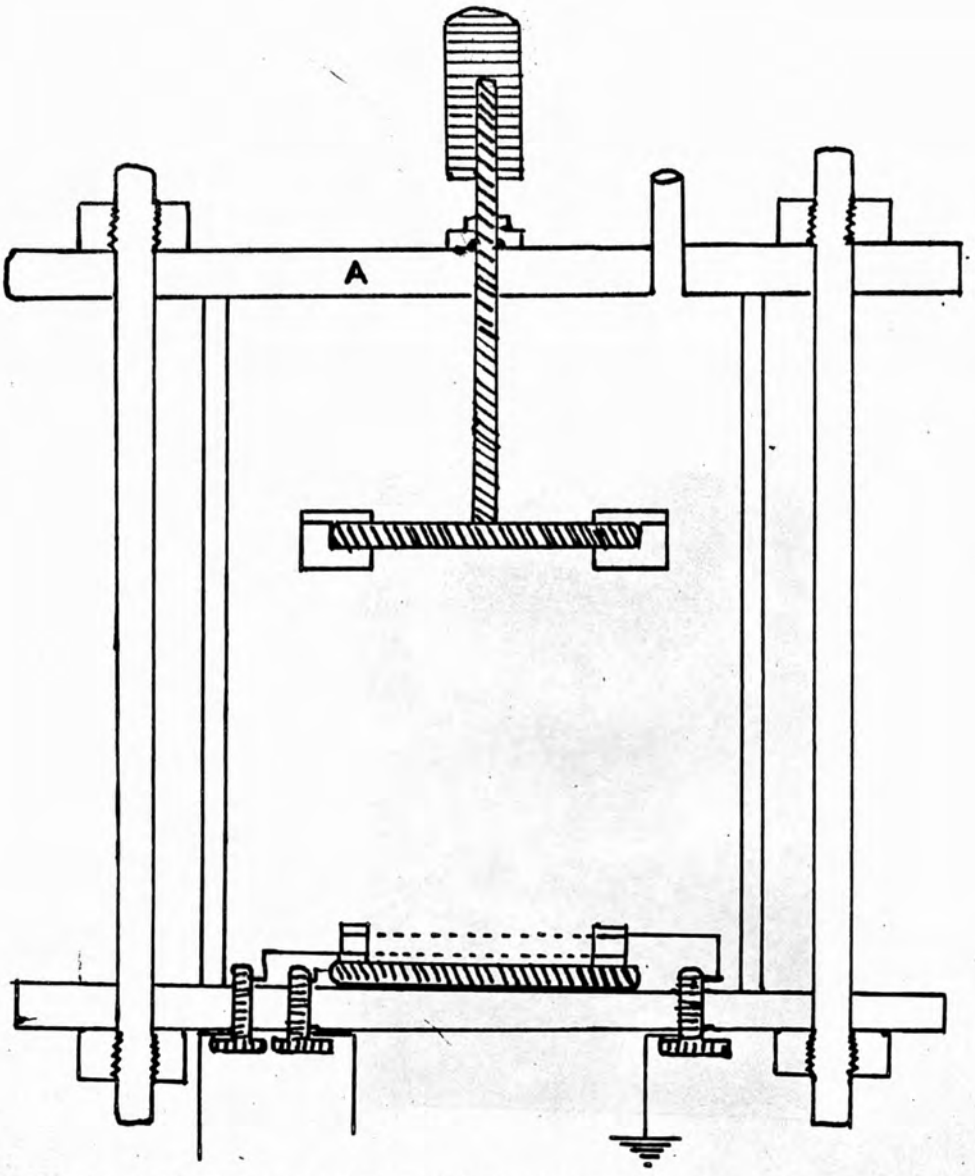

Fig.2.8--Unsuccessful prototype chamber.

Fig.2.9-The photograph of the spurious discharge produced in the prototype chamber shown in the fig.2.8.

replaced by a circular brass plate of the same size. The inside surface of the plate was polished. A circular perspex plate of diameter equal to the internal diameter of the perspex cylinder was placed over the grid system. A 2 inch square hole was cut in the centre of this plate to expose the grids. Silastomer rubber was placed round the outer edges of the circular plate. But even then the spurious breakdown could not be prevented.

It was inferred from this that the edges of the electrodes had to be kept out of the sensitive volume. This was kept in mind while designing the next chamber.

2.6.2. Final Chamber:-

The sensitive volume of the chamber is 20 x 20 x 20 cm^3. It is made up of a half inch thick perspex box with two sides open. The perspex walls have been cemented with "Tensol cement No.7". The open ends of the box have 1/8 inch 'O' ring grooving. The boxes, each have a small hole on the side wall, in which perspex tubing has been cemented to allow evacuating and filling of the chambers. Another box with sensitive volume 20 x 20 x 10 cm^3 has been made in the similar way. 9 inches square and 1/2 inch thick perspex plates have been used to seal the open ends and to screen the electrodes. The inner surface opposite the side through which the photographs were taken was painted black with Rustin black paint to minimise the back reflected light.

The electrodes were 2 ft. square, 1/4 inch thick Duraluminium plates, with their edges rounded off. The plate which was used as

/the

the high voltage electrode had both the surfaces polished. The high voltage cable was soldered to a copper rod which was a push fit into one of its sides. The earth electrodes have the inside surfaces polished, the outsides just smoothed to remove any sharp points. There are blind screw holes on the outside surfaces, and screws with rounded tops for earth connections. The chamber is shown in Fig.2.10.

The transparent electrode consisted of a wire grid mounted on a frame (2 ft. square, 1/4 inch thick) of perspex, with 8 inch square hole in the centre. Along the two opposite edges strips $\frac{1}{2}$ inch wide and 1/16 inch deep were milled on both sides in which copper strips were fixed with Araldite epoxy resin.

The grid consisted of 0.1 mm stainless steel wires wound on the perspex frame at a spacing corresponding to 4 wires per cm. During winding the wire was always kept under tension. The wire was made to pass over two fixed pulleys (Fig.2.11). A third pulley in between them was resting on the wire with a 300 gms weight hanging from it. The frame itself was rotated slowly about a horizontal axis. The wires were first fixed on to the copper strips with Araldite. The copper strips were then silvered and the wires were soldered on to them, using "Tinman's" solder and Baker's fluid. When the soldering was over the whole frame was washed immediately with soap and water to avoid corrosion - otherwise the stainless steel wire broke.

Four (2 x 3 x 37 inches^3) wooden joists with $\frac{1}{2}$ inch diameter holes at 3 inches from either end were used for clamping the

/perspex

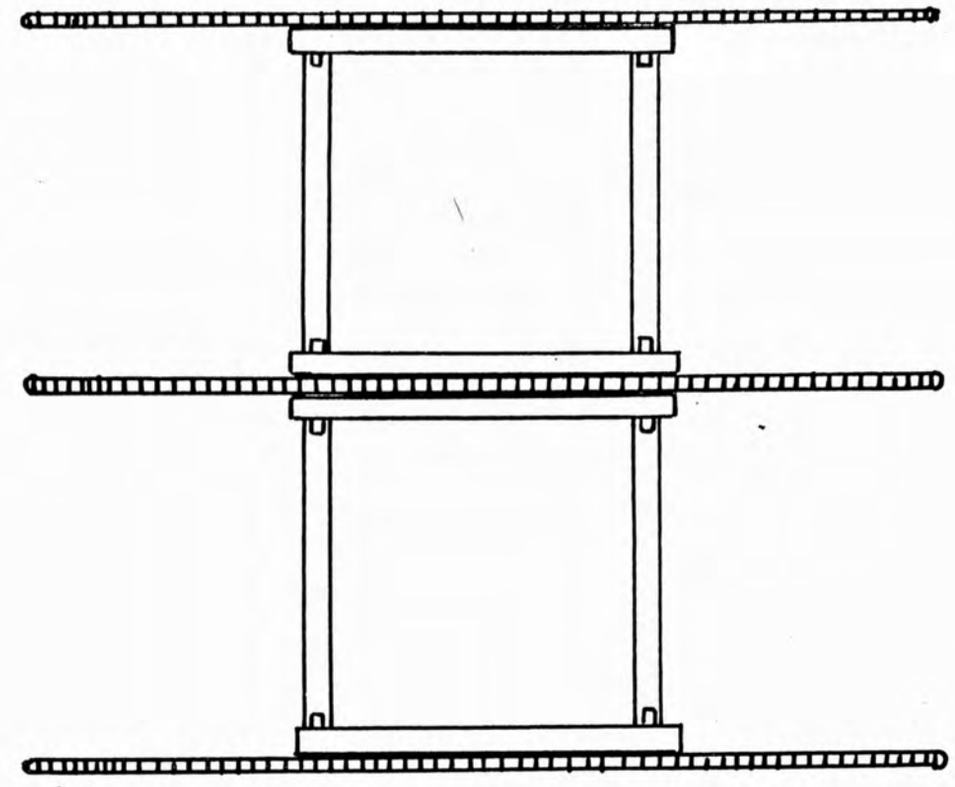

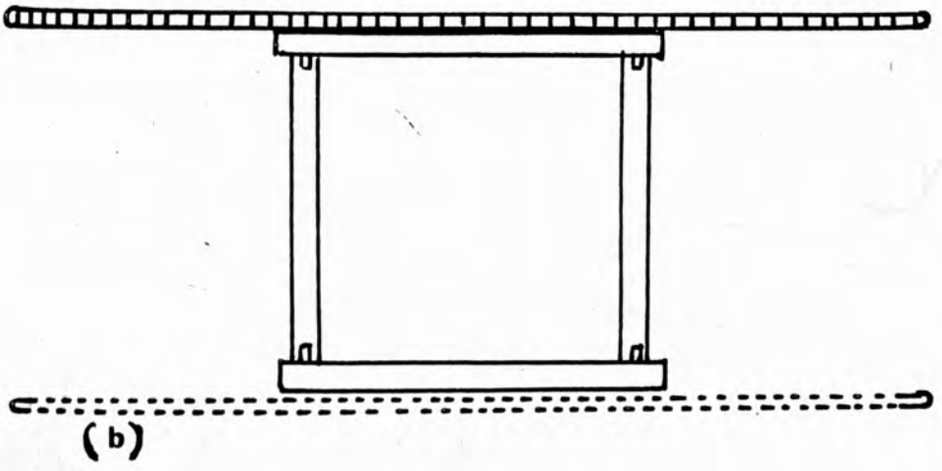

Fig.2.10 (a) Double gap chamber with Aluminium plate electrodes
(b) Streamer chamber with transparent earthed electrode.

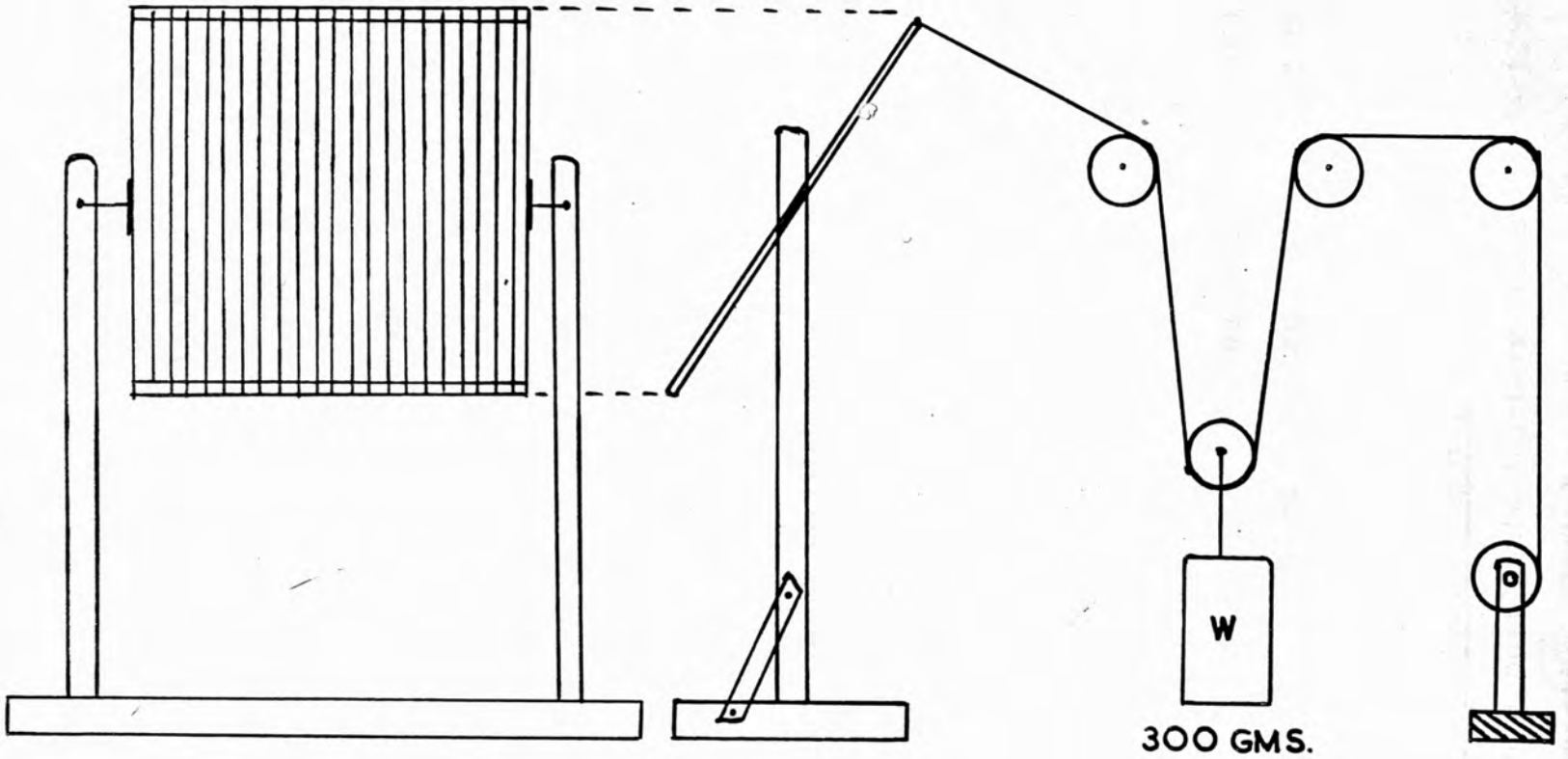

Fig. 2.11-- Grid winding arrangement.

perspex boxes and electrodes together. This was achieved by four 30 inches long ¼ inch diameter nylon rods threaded at either end to receive Tufnol nuts.

An advantage of this method of clamping was that the entire assembly could be manipulated and oriented at will.

In the initial experiments with the final chamber an attempt was made to work in the spark mode - that is the electrodes were not insulated from the Ne-He gas.

In the later experiment employing the streamer mode the electrodes were always insulated from the gas with a half inch thick perspex plate. In the double-gap experiments the central electrode was used as the high voltage plate and the outer electrodes were earthed. To reduce the damage to neighbouring electronics a braided earth loop was arranged to connect the Marx generator to the chamber. The electrodes had been designed to be much larger than the chamber to ensure that the applied electric field inside the chamber would be reasonably uniform. The particular arrangements of the electrodes etc. for the different modes are described in the sections on the operation of the chamber.

2.7. Evacuating and Filling system:-

In conventional multiplate chambers and in projection chambers the most common practice adopted has been to keep the gas flowing through the chamber and out into the air. At the start a lot of

/gas

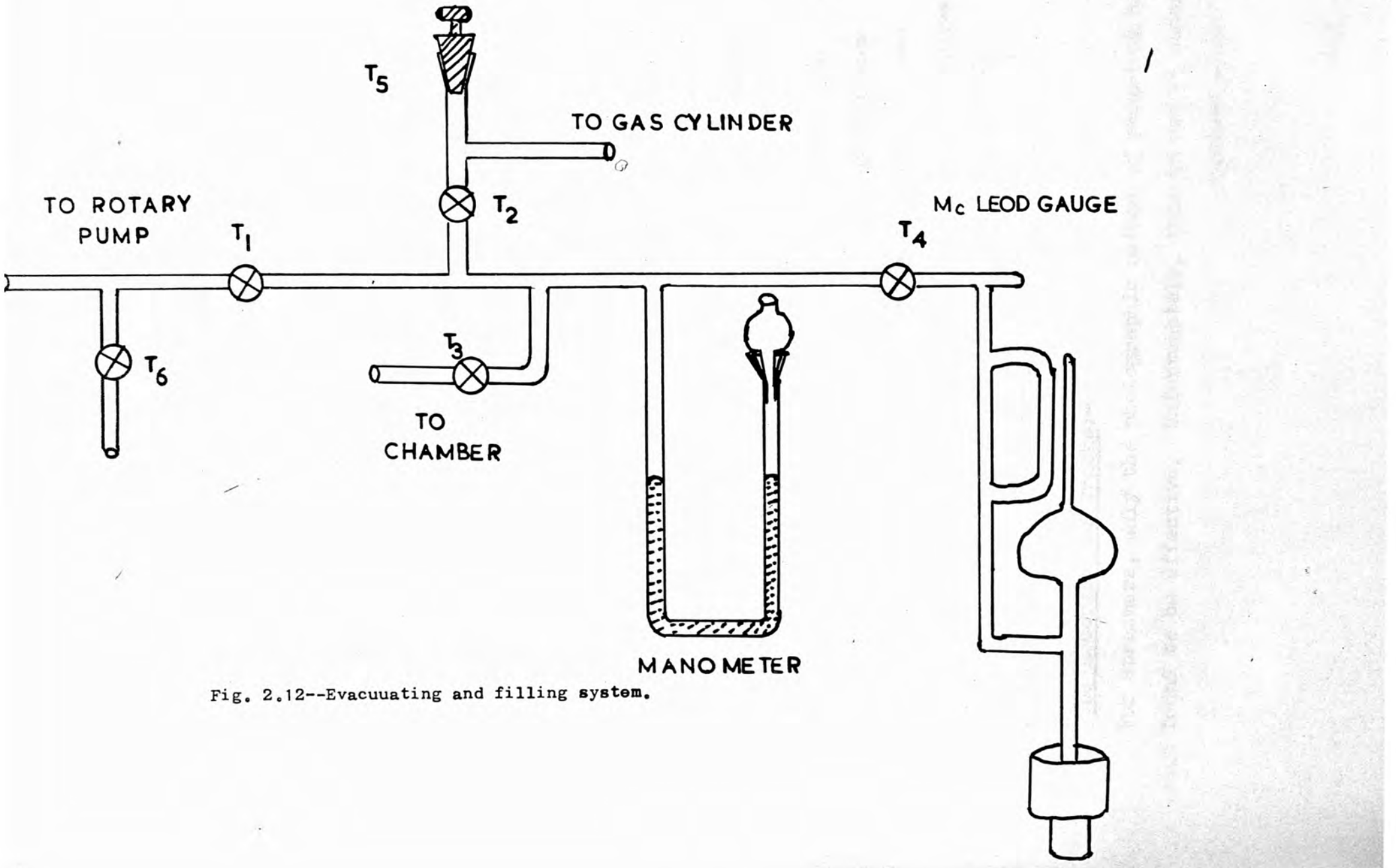

Fig. 2.12--Evacuuating and filling system.

gas is wasted in flushing the air out of the chamber, and the large number of gaps makes evacuation rather difficult. A purifying system can be used, but in this case the whole system would become very complicated.

In wide gap spark and streamer chambers the most common system adopted has been to evacuate the chamber to about 0.1 mm of Hg. before filling. If the chamber is quite gas right then once evacuated and filled it can work for a long time.

The system adopted in the present work, therefore, is the evacuation and filling the chamber as indicated in Fig.2.12.

Two precautions were taken: the tap T_5 which opens up when the gas pressure inside the tube becomes more than 2 atmospheres was included to prevent explosion, and a reservoir was inserted into the manometer to prevent the loss of mercury when by any chance the gas rushes into the chamber at a high speed during filling.

With a rotary pump it was found possible to reduce the pressure inside the chamber to 40 micron of Hg. and this was considered sufficient. The leakage rage at this pressure was found to be 64×10^{-3} micron litre/sec. The chamber was always filled directly from the gas cylinder to a pressure of 2 cm of Hg. above atmospheric pressure.

2.8. The Recording of Tracks:-

For streamers, only the photographic method of recording has been found to be effective. Unfortunately, this is not an automatic

/process -

process - but other methods such as vidicon scanning have proved impractical because of very low light output of the streamers. This may soon be overcome with the new English Electric "image isocon", which can respond to a light level of 10^{-6} foot candles.

In the present work tracks have been photographed with a 35 mm camera that has a 50 mm focal length and stop numbers from 1.9 to 16.

The clear perspex of the chamber will transmit about 90% of the visible light, the slight loss being almost entirely due to surface reflections. This transparency is unimpared by heating or by long exposure to moisture or ultraviolet light, and thus a great help in successful photography of the streamers.

Before photography, the chamber was surrounded by black cloth to cut off the background light from valves, indicator lamps and spark gaps. The camera was focused in the middle of the chamber from the distance of about 5 feet for the continuous streamer mode (double gap) and 3.5 feet for the streamer projection and streamer side view modes. The photography was done in darkness using the time exposure. In this way the shutter remained open and when the chamber had sparked, the shutter was closed and the film advanced manually.

The aperture and depth of focus play a very important role in photography.

Stops and f-numbers generally describe the aperture of the lens in a camera. The worst aberration produced is by the rays

/of

of light traversing the peripherial parts of the lens. Therefore for better performance of the lens, the path of thelight should be restricted to the axial or near axial region. The astigmatism, the chromatic aberration, the curvature and the spherical aberration are proportional to the size, the size, the square and the cube of the size of the stop respectively.

Stops and f-numbers:-

The amount of light passing through the lens is proportional to the area of its aperture which is proportional to the square of its diameter, and the area of the image is proportional to the square of the focal length. Therefore, the intensity of an image is proportional to D^2/f^2, where D is the aperture diameter and f the focal length of the lens. If D is expressed as a fraction of f, then the intensity is proportional to f^2/n^2f^2 or $1/n^2$ where n is called the stop or the f-number.

Different method of choosing the values of n have been adopted in different cameras.

In the continuous streamer mode the spark intensity was sufficiently high for a small aperture to be safely used, and f/8 was found to be suitable. The necessary apertures for side view streamer and projection streamer modes were f/2.8 and F/4 respectively.

Depth of focus:- The problem of depth of focus is illustrated in Fig.213 - it is seen that unless precautions be taken, out of focus points will appear as discs. When the image is viewed

/as

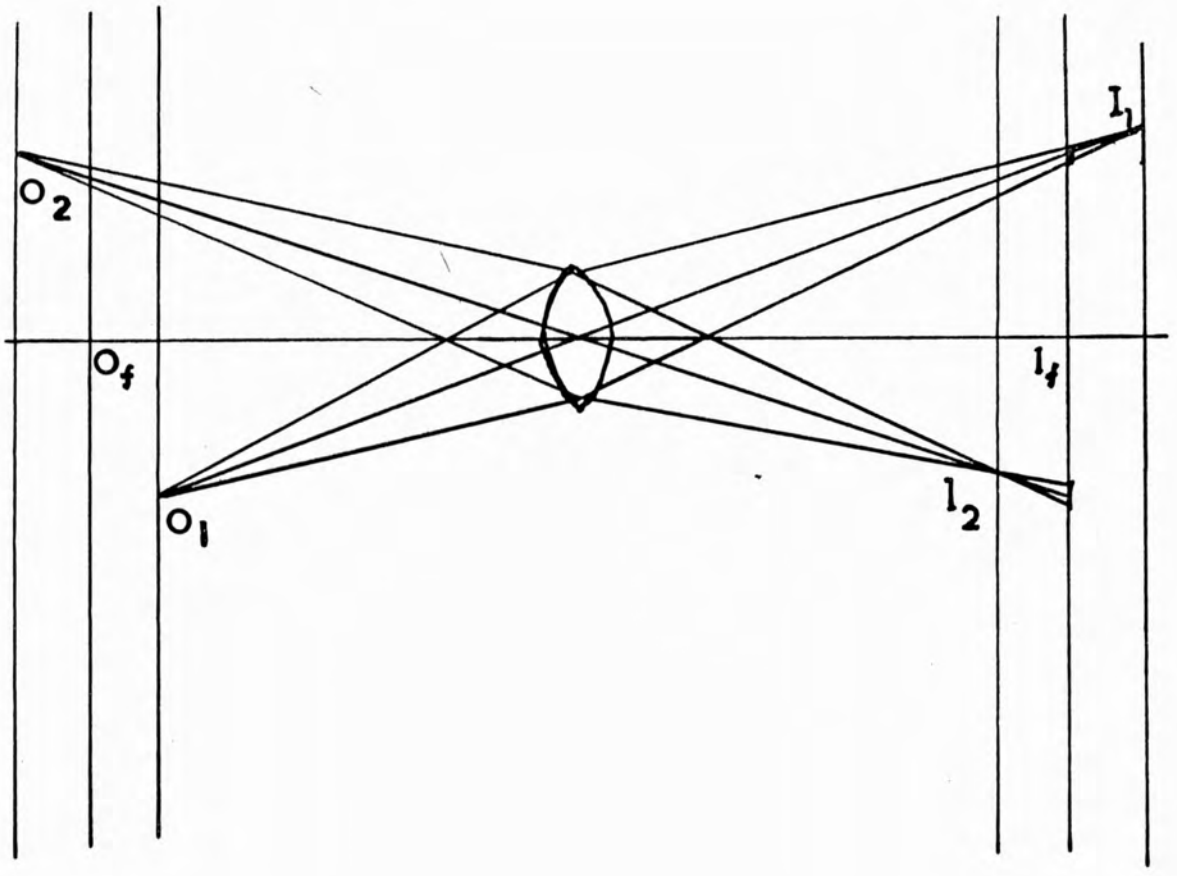

Fig. 2.13--Illustration of the Depth of focus.

as long as it subtends an angle less than 0.29 m rad at the eye, the disc is seen as a point. In this limit to the proper perspective, the disc is called the "circle of confusion", and has a diameter of about 0.01 inch and 0.25 mm.

In photography it is known that for a particular size of print the magnification required for different sizes of negative is inversely proportional to their size and hence to the focal length of the lenses used. As a consequence it can be shown that a value of f/1000 can be taken for the "circle of confusion"(6).

From Lawrence (1941):

$$\text{Depth of focus} = \frac{2n\delta d(d-f)}{f^2} \qquad 2.16$$

where d is the object distance

substituting for δ, we have

$$\text{Depth of focus} = \frac{2nd(d-f)}{1000f} = \frac{2nd^2}{f}\ 10^3 \qquad 2.17$$

if $f \ll d$

In photographing continuous streamer tracks, the stop used was 8, the distance was 150 cm, and the focal length of the lens was 5 cms - giving a value of the depth of focus of 70 cm, which is considerably larger than the depth of the chamber.

For the other two modes, the stops used were 2.8 and 4 at a distance of 120 cm. The corresponding depth of focus were 16 cm and 23 cm respectively i.e. greater than the depth of the chamber.

Because of the very low light emission of the streamers, very

/fast

fast film is required to record the .. Throughout this work "Ilford HP_4" film has been used. This film has a speed of 400 ASA when developed in "Ilford ID-11" developer at a temperature of 20°C and 650 when developed in"Ilford Microphen" for 5½ minutes at 20°C, this giving a contrast gradient of 0.55. The speed can be further increased to 1250 ASA (with a contrast gradient of 0.9) if the development in "microphen" be for 16 minutes at 20°C.

In the continuous streamer mode a speed of 400 ASA was found to be sufficient but for streamer (projection and side view) photography a speed of 1250 ASA was necessary.

For high resolution, the speed of the emulsion should be rather low. Fortunately however, HP_4 film has an excellent speed/grain ratio, and further, the grain size is checked by the use of fine grain developer like "ID-11" and "Microphen".
The resolution can also be affected by halation (i.e. reflection effects of the back surface of the film) but in our case the intensity was low enough for these effects to be minimal.

The printing has been done with a tungsten light enlarger, and Ilford "document" and "Ilfobrom 5" printing papers have been found satisfactory. These are extra hard contrast papers and Ilford "copyphen" developer has been found to be quite suitable for them. The Ilford "hypan" fixer was satisfactory, both for the films and prints. Considerable care had to be taken in preparing the prints as the exposure and development times varied with the quality of the negative and the size of the prints.

C H A P T E R III

PERFORMANCE OF THE CHAMBER

3.1. Initial operation in the Spark Mode

In the initial experiments the double gap chamber was operated in spark mode. The electrodes were not insulated from the sensitive gas, and the high voltage pulse was allowed to remain on the plates for a time long enough for the plasma channel to bridge the gap, and for the spark current to flow. The results are shown in the Fig. 3.1a, and it is seen that the tracks although obviously straight and true are nevertheless very broad. This is probably due to a large flow of current from the external circuit. When an attempt was made to check this current flow by reducing the pulse length (decreasing the shunt resistance) - although finer tracks were produced it was seen that the track efficiency of the chamber was affected, and robbing became probable. This relative lack of success lead to the adoption of the arrested streamer technique, which was made possible by insulating the electrodes and improving the pulse shaping circuit. As a first step towards this the electrodes of the top gap only were insulated from the sensitive volume. The result was quite encouraging, as seen in theFig. 3.1b.

3.2. Track formation by Streamers

If immediately after the passage of an energetic ionising particle through the sensitive gas a high voltage field is applied,

/each

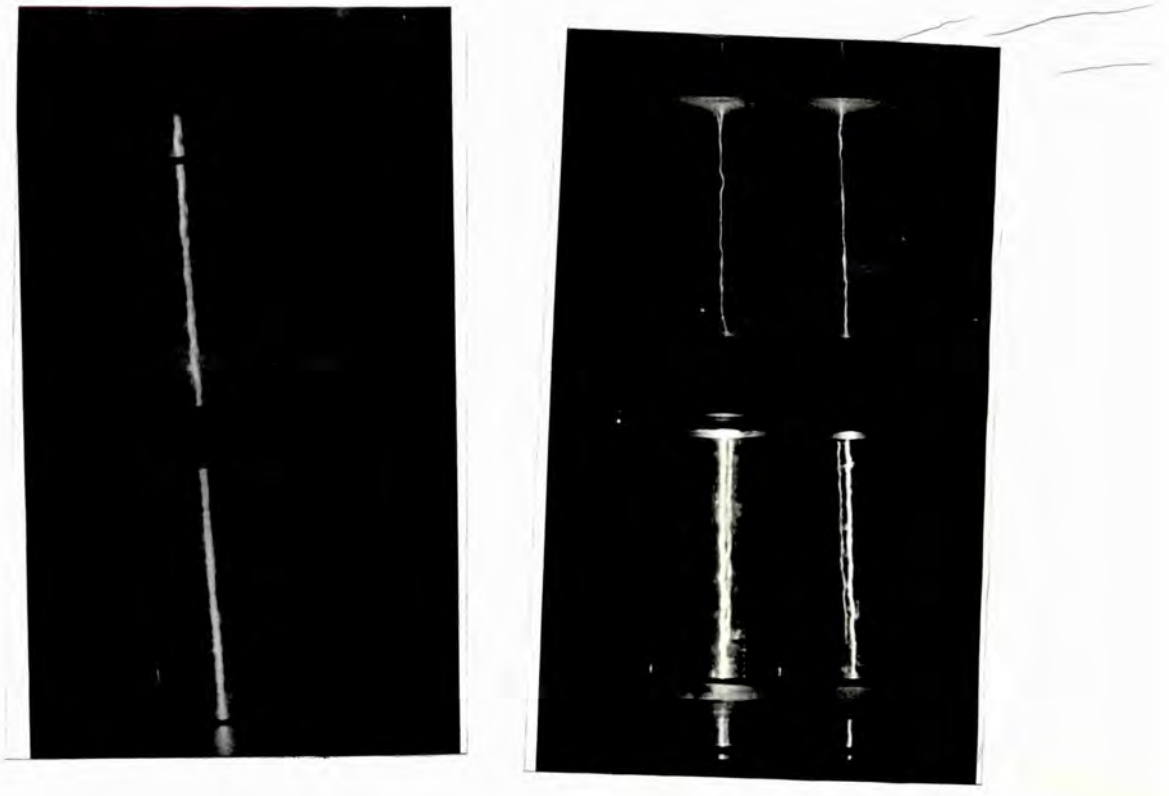

Fig. 3.1--Cosmic ray tracks in double gap spark chamber--(a) all the electrodes were unshielded --(b) electrodes of the top gap only were shielded.

each resulting primary electron initiates the growth of an avalanche. The rate of growth is statistical and large fluctuations occur. Thus at a particular instant of time the avalanches have developed to different sizes. This means that some of them would be able to satisfy Meek's criterion before others. The earliest streamers inhibit the growth of the adjacent slow developing avalanches by reducing the external field. It is these early streamers that give sufficient light intensity to be recorded. Getting streamers of requisite size can be achieved by controlling the length of the high voltage pulse. The minimum size of the streamer necessary to give sufficient light output depends upon the amplitude of the high voltage pulse.

During the time interval between the passage of the particle and application of the high voltage to the chamber, there is a tendency for the primary electrons to diffuse away from the trajectory especially if there are no electronegative gases and vapours in the chamber. If the high voltage pulse is applied within one microsecond of the passage of the particle, most of the primary electrons are within a fraction of a millimetre of the trajectory. During the formative time the electrons move towards the anode, so the resulting chain of streamers in the form of luminous centres may be slightly displaced laterally. The direction of the track, however, still indicates the trajectory of the particles.

/If

If the streamers are made very small by adjusting the pulse parameters, the chamber can be made completely isotropic. Even complex events can be easily recorded. The tracks of the particles originating in the chamber itself can also be made visible. Because the high voltage plate does not discharge itself, the multitrack efficiency of such a chamber is very high. It is this fact that makes the instrument ideal for studying complex events and cosmic ray showers.

In the present work two distinct modes of operation have been employed. In the first the streamers were made to grow almost parallel to trajectories which were themselves almost in the field direction and they were seen and photographed in a plane parallel to the electric field. The arrangement is similar to the wide gap spark chamber and has been called the "continuous streamer mode". In the second mode the particles passed in a direction almost perpendicular to the elctric field and the streamers grew in a direction normal to the trajectory. These streamers can be viewed in two ways: (a) through the side walls of the chamber box in which case (called the "side view") tracks appear as a number of short parallel dashes one above the other (b) through a transparent electrode in a direction parallel to the electric field. This mode has been called "the streamer projection mode".

3.3. The continuous streamer mode

Two 20 cm gaps have been used in this mode as shown in the

/figures

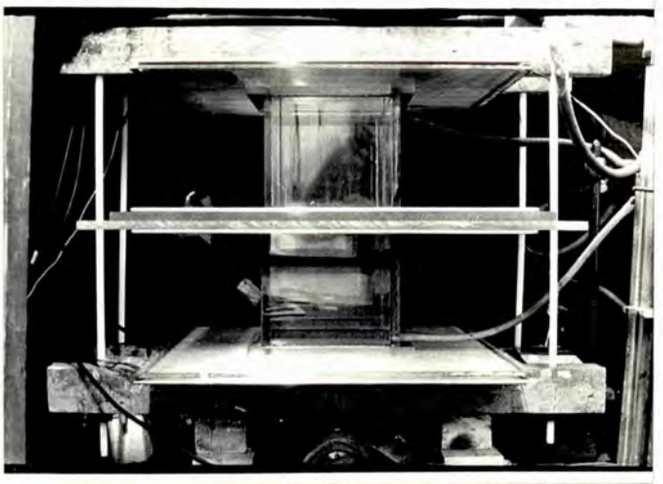

Fig.3.2--Photographs of the double gap chamber.

2.10 and 3.2. The electrodes were insulated from the working gas by half inch perspex plates. The electric field was nominally 11 KV/cm and the shunting spark gap width was of the order of 4 cm, which corresponds to a pulse length of about 30 nanoseconds. Very thin bright tracks were recorded as shown in Figure 3.3a, and the efficiency appeared to be very high. In some cases difference in the intensity of the tracks in the two gaps has been observed, which is due to the statistical fluctuations in the development of streamers. The second side track in the second gap in figure 3.3b might probably have been made by a knock on electron. The quality of the tracks as a whole is a lot better than that of spark tracks.

The mechanism of formation of these spark-like tracks must be the same as that for the true sparks (described earlier in Chapter I Section 5) but of course the plasma carries no current from the external circuit. That is the space charge field is so large that the streamers grow in the direction of the track rather than the direction of the applied field.

At some stage shunting resistances were used in place of the shunting spark gap but they were not found to be very satisfactory. For a value of 220 Ω, the chamber was found to work with rather low efficiency. Any decrease in this resistance reduced the efficiency still further, but any increase made the tracks too bright and broad. The trouble seems to be that the high voltage pulse starts decreasing as soon as it is applied,

/that

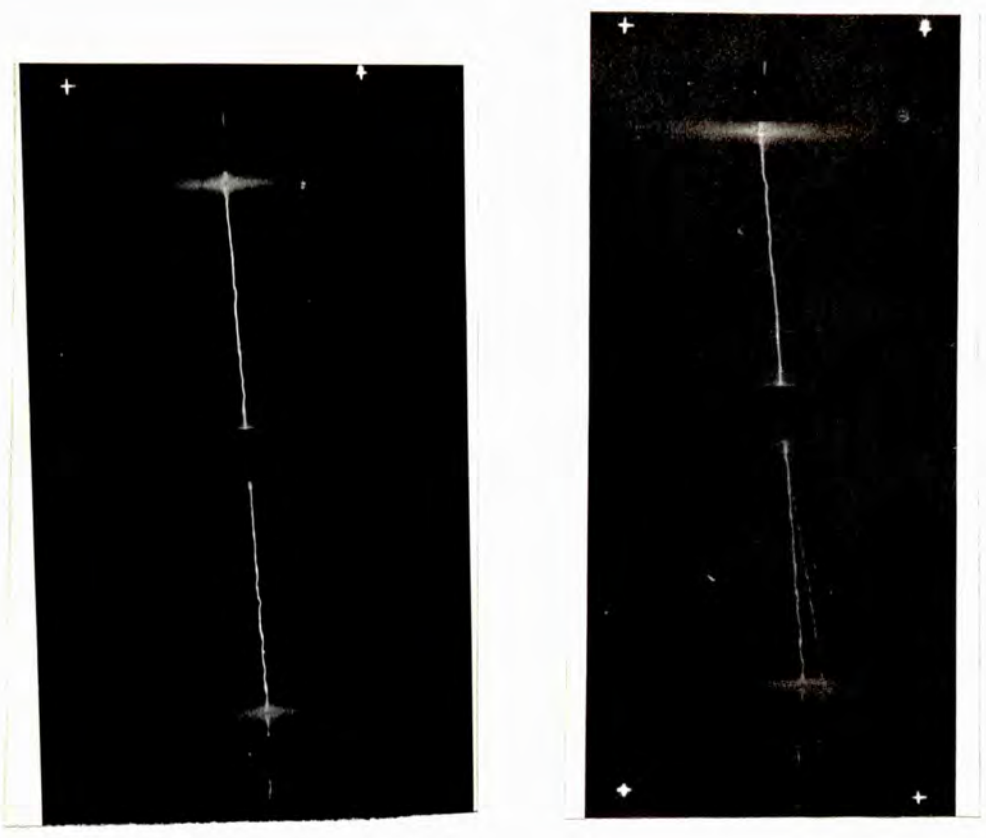

(a) (b)

Fig.3.3-Tracks of cosmic rays in double gap continuous streamer chamber--(a) a particle coming almost vertically (b) an angled track with probably a knock electron track in the second gap.

t at is the uncertainty in the moment of streamer formation is too large when compared with the full time of the pulse. The multiple track efficiency was also found to be poor. These troubles were completely absent in the case of a shunt spark gap. The amplitude of the high voltage pulse remains constant until the gap breaks down. The duration of the field depends upon the delay in the breakdown of the shunt gap and the time required for development of the spark. These time intervals depend upon the form and the amplitude of the high voltage pulse, and on the pressure and nature of the gas in the gap. In air the development time of the spark is about 7 to 10 nanoseconds. The delay time decreases as the gap width decreases. A chamber with shunt spark gap works with equal efficiency both for single and multiple tracks.

3.4. The streamer side-view mode.

The electrodes were arranged to be in vertical plane and the cosmic ray particles moving downwards entered the chamber through the top, and were photographed from the side. The streamers grew horizontally in both directions, towards cathode and anode.

When the shunt gap was widened to give a pulse length 200 nanoseconds or more, the streamers were so long that they bridged the space between the electrodes, and neighbouring streamers merged together to make the whole chamber glow as shown in Figure 3.4a. On decreasing the gap width so that the

/pulse

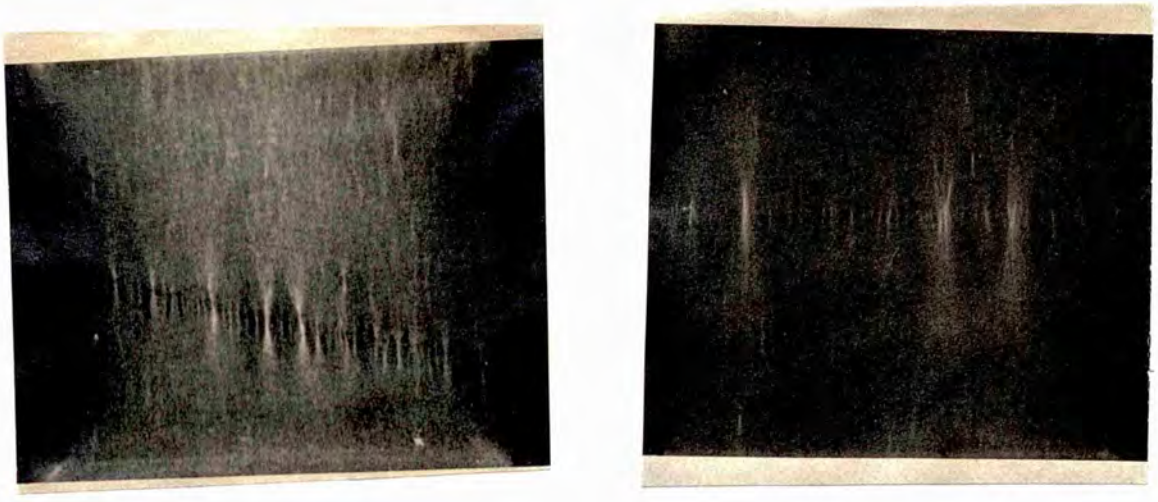

(a)

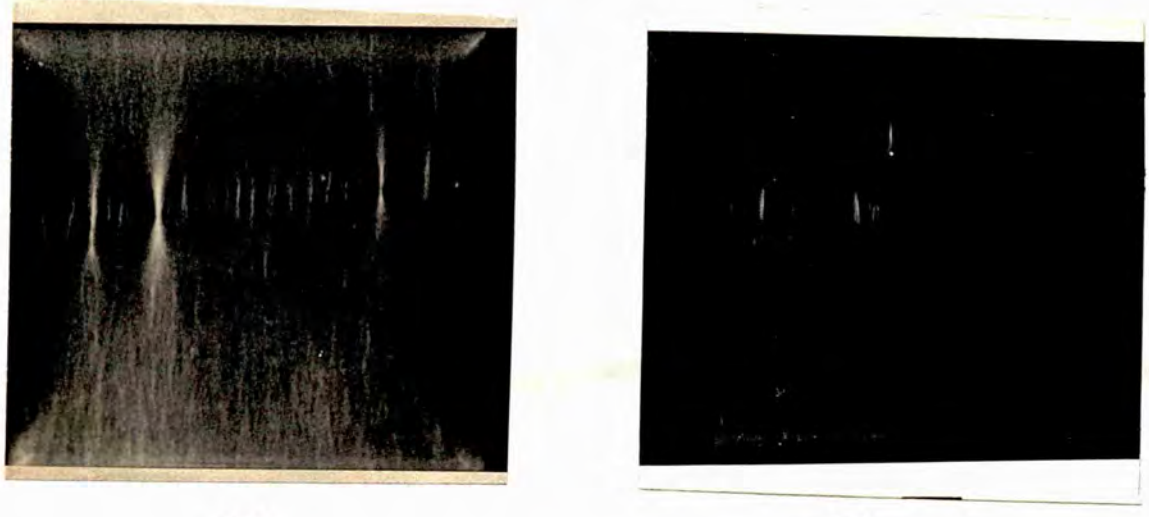

(b) (c)

Fig.3.4-Cosmic ray tracks in streamer side view mode
(a) very long streamers covering almost the whole gap (b) smaller streamers (some cms in length) (c)very small streamers (average length 7mm)

pulse length was about 100 nanoseconds, the discharges were not allowed to develop to this extent and the particles path could be seen more clearly (Figure 3.4b). Further reduction of the gap to yield a pulse of 30 nanoseconds resulted in short streamers as shown in Figure 3.4c.

The average length of the streamers corresponding to 100 nanoseconds pulse was several centimetres, whereas that corresponding to 30 nanoseconds was about 7 mm. On reducing the gap further the intensity of the streamers decreased so much that they could not be recorded. The tracks appeared as a number of stripes differing in intensity and length due to fluctuation in the development of the streamers.

3.5. The streamer projection mode

In this mode the streamers were viewed end on through the wire grid earthed electrode. The tracks appeared as a series of luminous centres. The size of the luminous centre was found to depend upon the amplitude and the length of the high voltage pulse. For a nominal value of the field of 11 KV/cm the best tracks were found for the shunt gap width of about 4 cm. For a pulse amplitude of 60 to 100 KV, Dologoshein (1964) found the most suitable gap width to be 15 to 18 mm, in air at atmospheric pressure.

The gap width of 4 cm was required to be changed slightly with the change in atmospheric pressure. For a considerable increase in this pressure, the delay in breakdown of the gap

/increases

increases which makes the high voltage pulse longer, resulting in an increase in the size of the streamers. On the other hand for a considerable decrease in atmospheric pressure, the pulse length is shortened and the streamers become too faint to be photographed.

The light output in this mode was found to be much better than that of the side view mode. Bulos and others (1967) have made an estimate of the light emitted by streamers in these two modes for different field parameters by photography. They found the (cut-off) f-number for which the light intensity became too low to affect the film. They assumed that the intensity was proportional to the square of the f-number at cut off. The following relations were given:-

Brightness in projection mode α $E^{2.8 \pm 1.2}$ 3.1

Brightness in side view mode α $E^{1.0 \pm 2.3}$

When the applied electric field was almost doubled by reducing the electrode separation to 10 cm the quality of the streamers improved. The pulse length had to be correspondingly reduced to approximately 20 nanoseconds. The streamers were more uniform in size and much brighter. The average width was found to be 2.16 ± 0.07 mm. At this nominal field of 22KV/cm, sometimes the whole chamber was found to glow. The reasons might be residual electrons and the delayed breakdown of the shunt gap due to fluctuations.

/Single

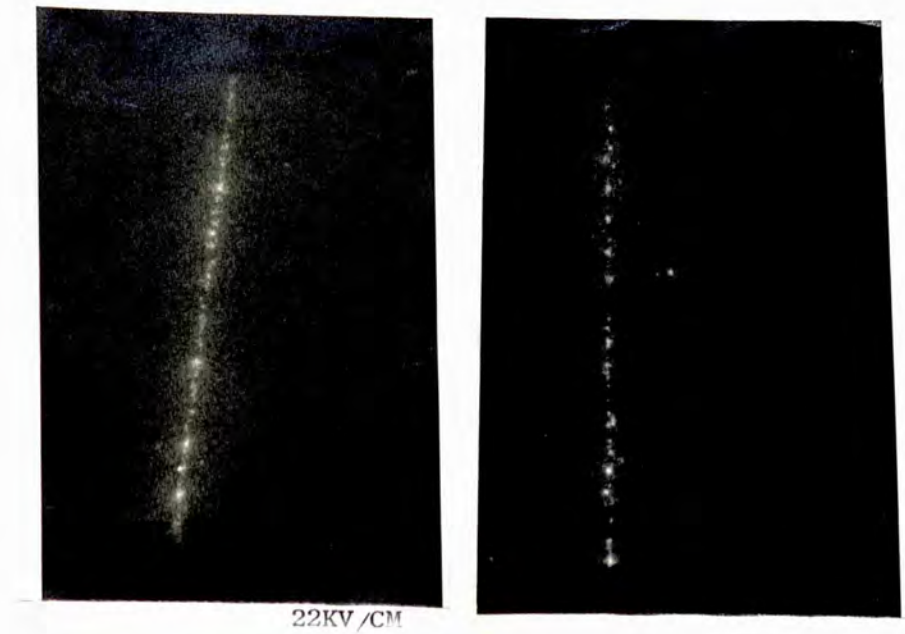

22KV/CM

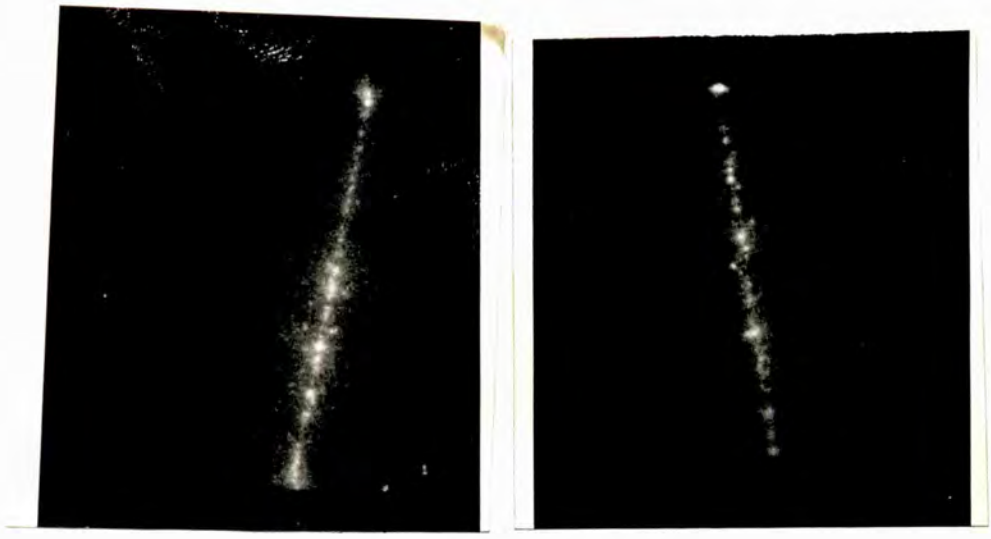

11KV/CM

Fig.3.5--Cosmic ray tracks in streamer projection mode at the fields (nominal) of 22 and 11KV/CM.

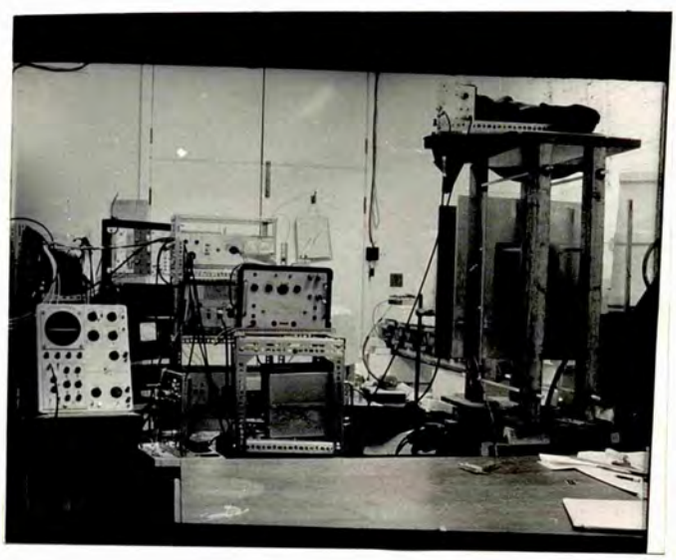

Fig.3.5(a)--Photograph of the streamer chamber arranged for operation in the projection mode.

Single tracks at 22KV/cm are shown in Figure 3.5 and a comparison with the tracks at 11KV/cm shows the superiority of high fields. The isotropy and capability of the chamber to record complex events have been shown and discussed in the next chapter.

The background light from reflections from the perspex walls was reduced to a great extent by using black paint. This paint although on the inside wall did not appear to give any trouble in the performance of the chamber.

The scintillation counters on the top and bottom of the chamber were about 1 1/4 metre apart, and the crystal area was 500 cm^2. This made the solid angle rather small. Thus, the geometry allowed only 2 cosmic ray particles per minute on the average to pass right across the chamber. This gave sufficient time to wind the film and open the shutter. The manual handling of the camera does not allow one to take more than about six pictures per minute, which was achieved while recording α's and β's in the self triggered chamber (Chapter VI).

3.6. Operation at reduced pressure

3.6.1. The continuous streamer mode:- In the case of the continuous streamer mode the pressure was varied from 200 mm to 743 mm. The amplitude of the high voltage pulse was kept constant. At 200 mm of Hg the efficiency was very low and the whole chamber was found to glow. As the shunt gap was reduced, the background glow decreased, but there was no appreciable

/improvement

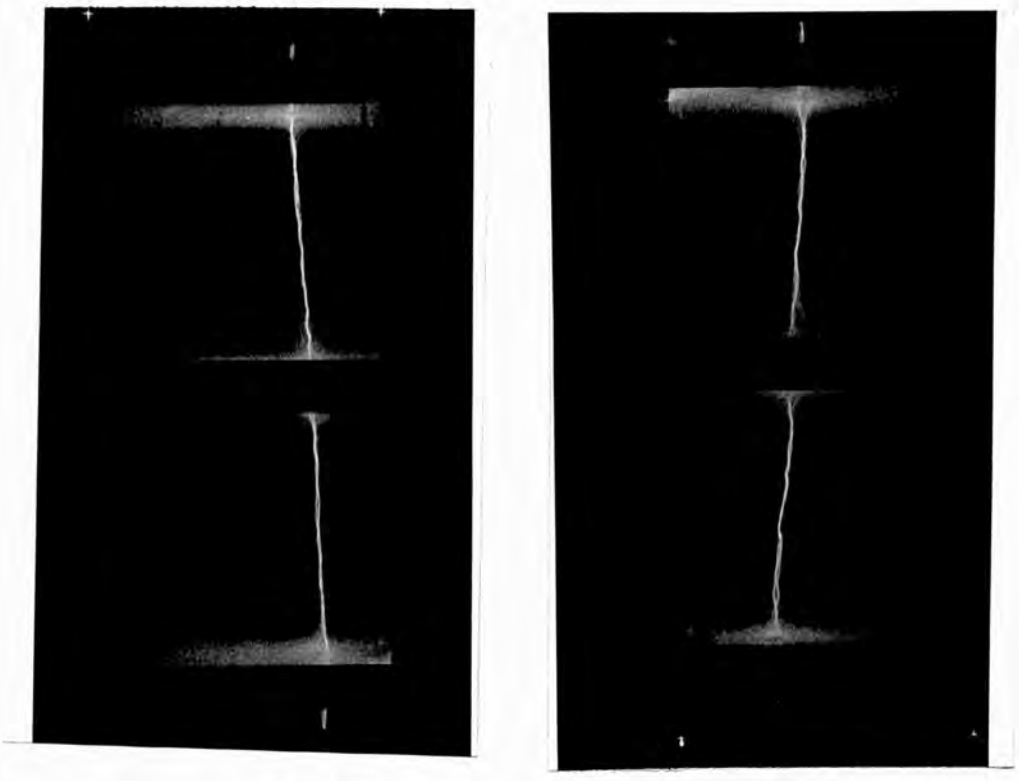

397mm.Hg 255mm.Hg

Fig.3.6--Cosmic ray tracks at reduced pressure of the gas (Ne+He) in the chambers (continuous streamer mode).

improvement in the efficiency. The glow is probably connected with the reduction of the breakdown voltage with pressure. An appreciable decrease in the number of primary electrons, and in the gas multiplication, might be the reason for the low efficiency. As the pressure was increased the efficiency improved. At a pressure of 255 mm of Hg and above the background glow reduced to a minimum and the quality of tracks was quite good. The tracks have been shown in Figure 3.6, where the improvement in the track quality with the increase in pressure can be marked. At these pressures the tracks were a little wider than those at atmospheric pressure - most probably due to the increase in the electron diffusion at low pressure.

Bunaciu and Kullander (1967) used a 1.6 cm wide spark chamber with helium and alcohol at 100 mm pressure for 5.3 Mev alpha particles and 0.5 Mev beta particles. No tracks were shown but they say that the lowest pressure at which one can get well defined tracks depends upon the chamber field and the alcohol concentration. For a 1.6 cm gap and an alcohol concentration of 20%, the minimum working pressure was 30 mm. How low energy particles (particularly alphas) cause a large number of primary ions. This probably explains the successful operation at such a low pressure. The requirement of an increase in alcohol concentration as the pressure decreases was to control the discharge mechanism and make the sparks thinner.

/3.6.2

3.6.2. Streamer projection mode:- In the streamer projection mode, the pressure was varied from 400 mm Hg to 767 mm Hg. At a pressure of about 400 mm of Hg, tracks were seen, but the whole sensitive volume was found to glow for a shunt spark gap width of 3.8cm. As the gap was reduced, the background glow was fainter. For a 3 cm gap width the glow was significantly reduced, and completely absent for 2 cm but the tracks became too faint to be photographed. The streamer density was found to be about 1.5/ cm. When the pressure was raised to 531 mm Hg, the efficiency was still too low with the 2 cm shunt gap, but the background glow was absent. When the shunt was opened to about 3.5 cm, the efficiency went up to 90%. The streamer density was found to be almost the same, 1.6/Cm. The opening of the shunt gap did not increase the background glow. The tracks at these pressures are shown in Figure 3.7.

Dologoshein (1964) used a 10 cm chamber at pressures in the range of 300-760 mm Hg. The streamer density ($\sim$2/cm) was found to be constant in this interval of pressure, but he found a decrease in this density when the pressure was below 300 mm Hg.

It can be seen from the present work that a chamber can be made to work well in the pressure range 500 to 760 mm Hg, without reducing the electric field ($\sim$ 11KV/cm). To work below this pressure, the field will have to be decreased, but this may affect the gas multiplication and thereby the quality of streamers.

/The

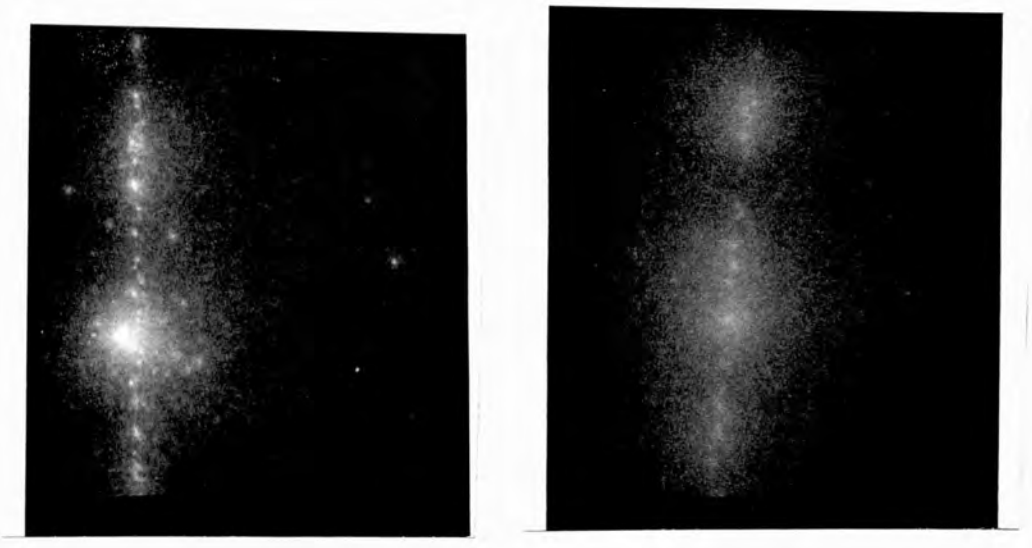

531mm.Hg 400mm.Hg

Fig.3.7--Cosmic ray tracks at reduced pressure in streamer projection mode.

The reason for the continuous streamer chamber working down to 200 mm Hg might be the greater light output.

It is thought that it is the time fluctuation in the development of neighbouring avalanches, and not the number of primary ions, that determines the streamer density. This must explain the observed constant density in the range 500 to 767 mm Hg.

C H A P T E R IV

CHARACTERISTICS: RESULTS AND DISCUSSION

4.1.1. Continuous mode Tracks (width, robbing and inclination

The average width of the tracks in this mode was (2.2 ± 0.15) mm. This value is almost the same as the width of the streamers (∿2 mm) in a field of 14 KV/cm obtained by Chikovani and others (1964). The present observations showed very little change of width when the length of the high voltage pulse was increased. This was to be expected as the width of the streamers is governed by the lateral diffusion of electrons and this in turn is determined mainly by the total delay between the passage of the particle through the chamber and the initial rise of the high voltage pulse (∿ 500 nanoseconds) and not the pulse length (∿30 nanoseconds). A greater pulse length causes an increased number of ions to exist in the continuous streamer tracks, and thus brightens the track.

In the case of conventional spark chambers the phenomenon of robbing occurs i.e. sometimes plasma channel is formed in one gap earlier than the others due to fluctuations in the streamer development, and the current available for sparking passes through only that gap thus reducing the intensity of the other tracks in the chamber. The robbing was quite frequent

/in

in the double gap chamber operated in spark mode, but almost absent when the electrodes of the top gap were shielded. In continuous streamer mode this effect cannot occur, but variations in the relative brightness of the tracks may still happen due to fluctuations in the streamer development. These effects have been shown in Figure 4.1. Only when the fluctuation is so large that the intensity of one of the tracks is too weak to be photographed does one of the tracks disappear. But this is expected to be very rare. The photograph of the shower in the Figure 4.1 shows this effect.

The maximum inclination of the tracks, considering both gaps was only 17° from the vertical (Figure 4.2). This geometrical limitation was due to the large size of the chambers which kept the two scintillation counters about four feet apart. But in some cases, odd tracks in one gap have been found to make a maximum angle of 25°. This has been shown in Figure 4.2. The property of the streamers following the trajectory depends upon the number of streamers in the gap. The maximum number of streamers per centimetre of the gap width has been found to be two. Thus, it can be seen that in the conventional multi-gap chambers (maximum width 1 cm) only two streamers would develop in each gap. The field between the head of one avalanche and the tail of other would be weaker than the external field and therefore the streamer would develop along the direction of the external field. But in the wide gap chamber, 20 cm wide,

/there

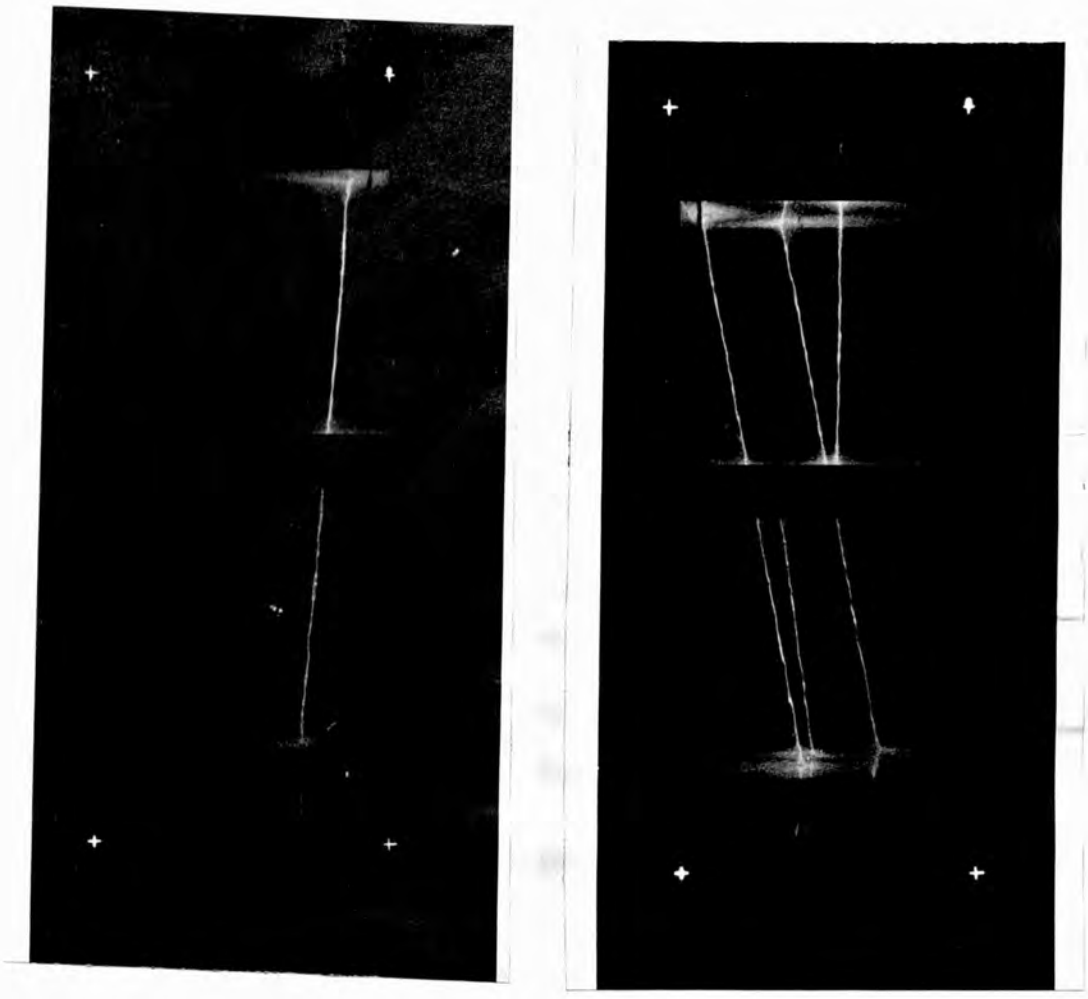

Fig. 4.1--Photographs of cosmic ray tracks showing the effects of robbing in the double gap continuous streamer chamber.

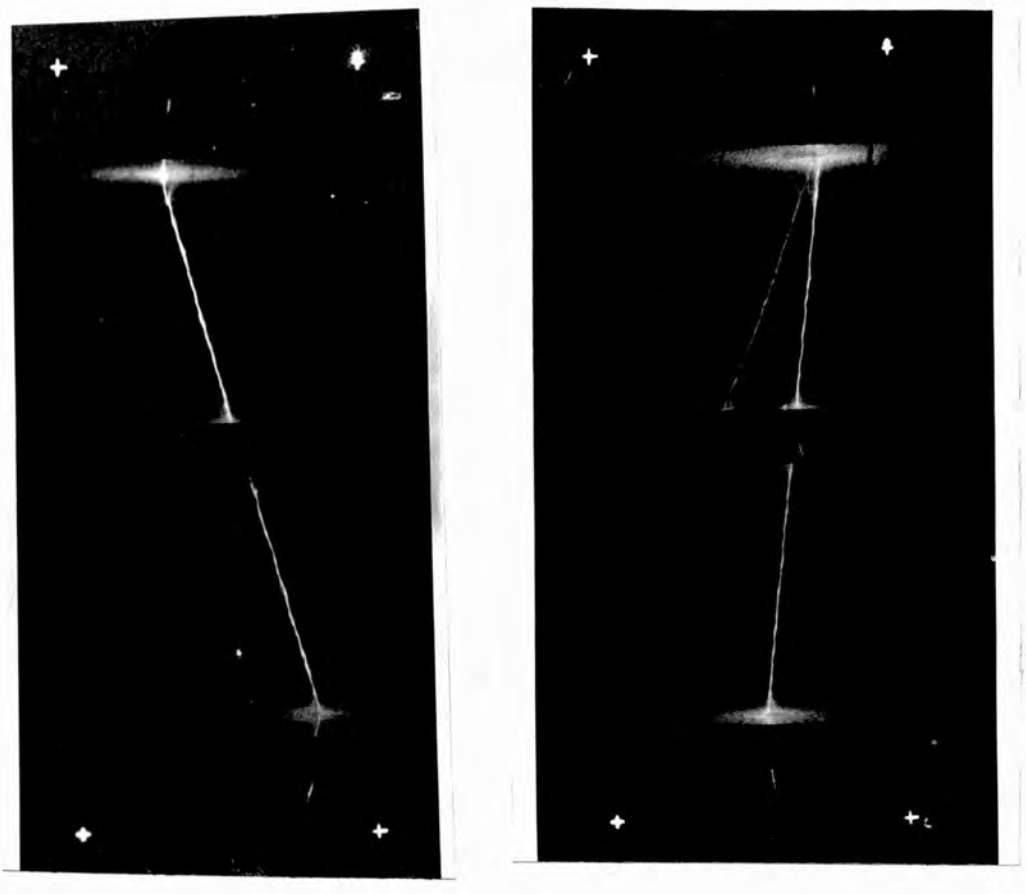

Fig. 4.2--Inclined tracks in the double gap chamber - the track in the first photograph makes an angle of 17° from the vertical (direction of electric field)--the odd track in the top gap of the second photograph makes an angle of 25.°

there would be about 30 to 40 streamers. The inter avalanche space charge field combines with the external field and the streamers propagate in the direction of the resultant field. As has been discussed in Chapter one, the conditions for the geometric merge of the neighbouring avalanches are such that the maximum angle of inclination is 45° at atmospheric pressure (Fukui and Miyamoto 1961). But in practice the efficiency starts to decrease significantly above 30°.

4.1.2. Track distortion:- Apart from distortion in the form of small differences of intensity and in the width of the continuous streamer track, there was another type of distortion in which the track extremities had a tendency to be perpendicular to cathode. Similar distortions have also been found in wide gap spark chambers (Garron 1965). The reason might be that the ionisation electrons near the cathode have been swept away by the rising edge of the high voltage pulse which could result in the extreme streamers merely following the applied field. It was also observed in all cases. Its maximum value was about a centimetre. There was a distortion near anode as well, in which the tracks looked diffused. It was very rare suggesting that the process was statistical in which case the local streamers might have propagated direct to the electrode so as to obtain a path of least resistance. The cathode and anode distortions have been shown in Figure 4.3.

/4.1.3.

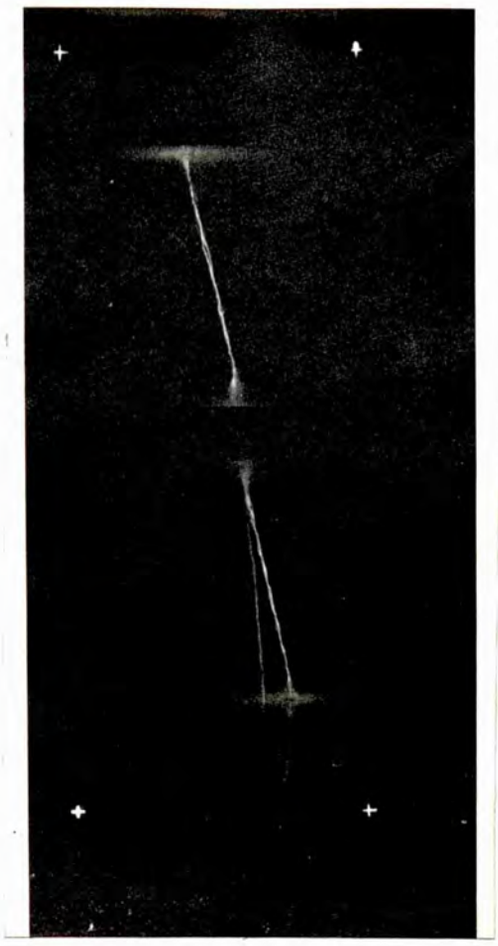

Fig. 4.3--Showing the cathode and anode distortions - the very thin side track in the second gap might have been made by a knock on electron.

4.1.3. Small angle scattering:- The analysis of the tracks described in sections 5 and 6 of this chapter showed that a small error might arise due to small angle scattering in the central electrode assembly. This will be due to multiple scattering and the largest angle observed was 2° (Figure 4.4). By reducing the thickness of the electrodes and the walls of the chamber, the multiple scattering can be minimised, but in that case evacuation of the chamber cannot be done, and hence the arrangement of flushing the air out of the chamber by the gas will have to be adopted.

4.1.4. Rejection of tracks from analysis:-

Some of the tracks were not included in the analysis. A few were too faint and others were diffused because they passed too near a chamber wall. This effect may be seen in Figure 4.4b where in the top gap the proximity of the trajectory to side wall of the chamber is clearly visible. In the multiple scattering experiment it was found that about 12% of the tracks had to be rejected for these reasons.

4.2. STREAMERS

4.2.1. Sizes and linear density of streamers in side view and projection modes.

In the side view mode the average length of the streamers (which could be photographed) in a field of about 11 Kv/cm,

/(nominal),

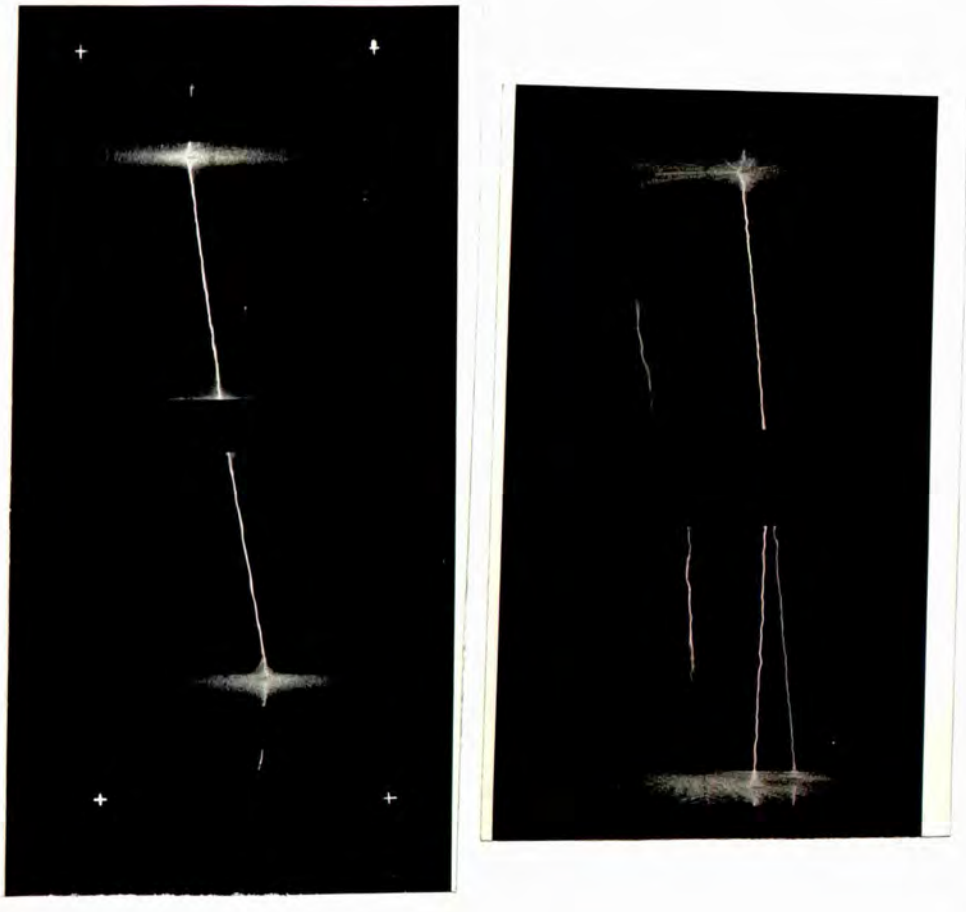

(a) (b)

Fig. 4.4 (a)-A double gap track showing multiple scattering in central electrode,
(b)-an example of diffused tracks which were rejected from the analysis.

(nominal) was 7 mm. Although smaller streamers were visible it was found that they were too faint to be photographed with the 1200 a.s.a. film. When the field was doubled, that is to 22Kv/cm, the average size was reduced to 4 mm. Again the low light emission from smaller streamers prevented photography. However, fluctuations in the shunt breakdown result in variations in the length of the streamers between different exposures.

The streamer density was found to increase from about 1.6 to 2 per cm., when the field was raised from 11 to 22Kv/cm - which was to be expected in view of the shorter development times.

The tracks in the projection mode were found to be brighter than those in the side view mode, because the projected area of the streamers (2 mm in diameter) was much smaller. The tracl were in the form of luminous centres with linear density of about 2/cm. The brightness and width were more uniform than they were in side-view.

4.2.2. Fine structure of a steamer -

The operation of the chamber in this mode offers a good opportunity to study the development of the streamer in some detail. For example in the photograph of a single streamer shown in Figure 4.5. the fine structure is clearly visible, but it should be added that the applied pulse had to be lengthened and reduced in amplitude in order to obtain such

/a

Fig. 4.5--Photograph of a single streamer showing its fine structure.

a large (a few centimetres) streamer. It may be seen that the evolution is indeed symmetrical - the extremities appear to advance equally towards the anode and cathode.

There has been some uncertainty in the interpretation of the narrow neck. In the figure 4.5. the interesting feature is that the intensity of light emitted from the neck - presumably where the initial avalanche was created - is less than that emitted at its extremities. This is to be compared with the photos shown in Figure 3.4. where the streamers were created in a much larger field, and in which there is no appreciable variation in intensity.

According to our model of streamer mechanism it is to be expected that the field just beyond the extremities of the initial avalanche will be greater than the applied field in which this avalanche grew. It is thus reasonable to imagine that the auxiliary avalanches will be smaller and hence brighter than the original. It is also reasonable to accept the broadening of the advancing fronts on this model.

In the case of the streamer developing in the higher field, the primary avalanche will be much shorter and brighter and will not present the contrast with the later avalanches. However, this is merely a hypothesis and confirms the fact that no satisfactory quantitative explanation of the spark mechanism has yet been given.

/4.3.

4.3. Isotropic properties of streamer chamber.

Ideally for many experiments a chamber that responds isotropically is desired. In addition, it is an asset if the chamber is capable of registering many simultaneous tracks. Inevitably, as a result of the asymmetric nature of the electric field, these ideals are only approximately realised.

The conventional multigap spark chambers reproduce only the sample of the track that lies within an angle of 35° with respect to the electric field. For an angle greater than that, efficiency falls sharply. The tracks originating in the chamber will not be recorded unless they pass through several gaps. In general simple narrow gap chambers do not have a high multitrack efficiency - although precautions can be taken to overcome some of the difficulties.

In wide gap spark chambers the sparks follow the trajectory up to an angle of 35° from the field, i.e. they are by no means isotropic. The multiple track efficiency is better than the case of the multigap chambers.

Streamer chambers, on the other hand, are potentially isotropic. The primary avalanches which produce the luminous centres along the track develop independently from each other, and as long as they are arrested while still small they may record any direction (Figure 4.6). This operating condition depends upon the length and amplitude of the high voltage pulse. For a field of the order of 10 Kv/cm, the optimum

/length

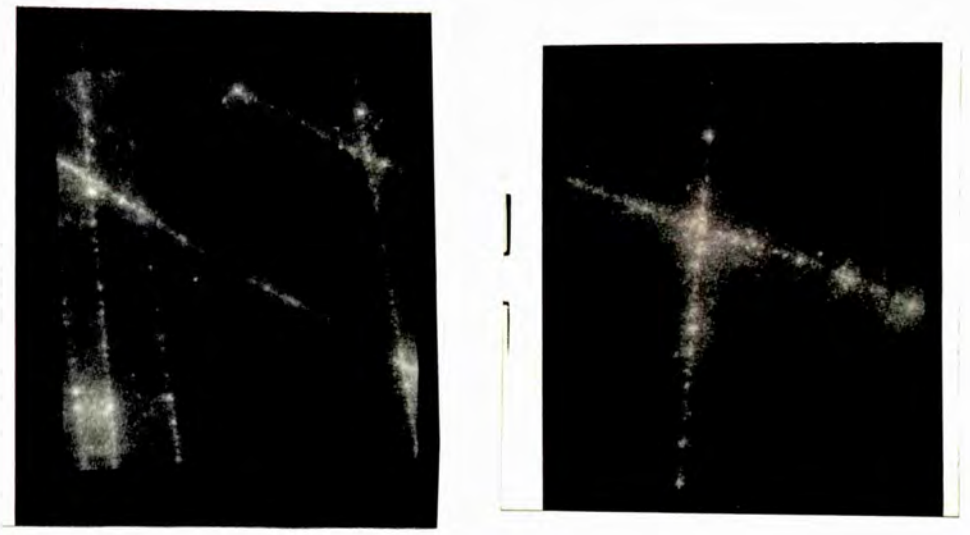

Fig. 4.6--Streamer projection tracks showing the recording of any direction.

length of the pulse is about 30 nanoseconds. A longer pulse of this amplitude makes the track overdeveloped and a shorter makes it disappear. The pulse length can be changed within a very small margin of about 5 to 10% of the time required for the development of an electron avalanche into a streamer. If the amplitude of the pulse is smaller, its length has to be increased, and if the amplitude is higher the length has to be decreased. The shunt spark gap controls the length of the high voltage pulse quite efficiently. The chamber is equally efficient for single tracks and for groups of tracks, such as cosmic ray showers. For example, in figure 4.7a, an axis of a cosmic ray extensive air shower happened to pass through the chamber. There are about 20 detectable tracks including a number of trajectories originating in the chamber itself. In another exposure (Figure 4.7b) the edge of a cosmic ray shower seems to have been recorded, with low energy electrons and photons moving randomly in all directions. Both these photographs show the isotropy of the chamber and also the remarkable efficiency for many simultaneous tracks.

To realise the full potential of the isotropic response it is necessary to take stereo photographs - i.e. at least two exposures of the same event from different angles. In the present work a mirror was arranged as shown in Figure 4.8a, which enabled two 90° views to be recorded on a single frame.

/The

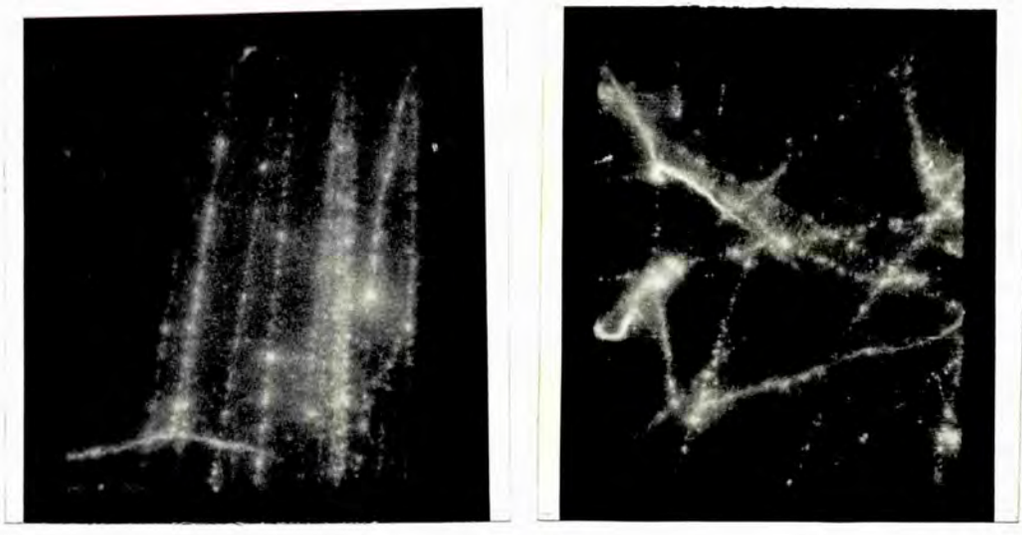

(a) (b)

Fig. 4.7--Cosmic ray showers in projection mode--(a) axis of a shower , (b) probably the periphery of a shower containing mainly electrons and photons.

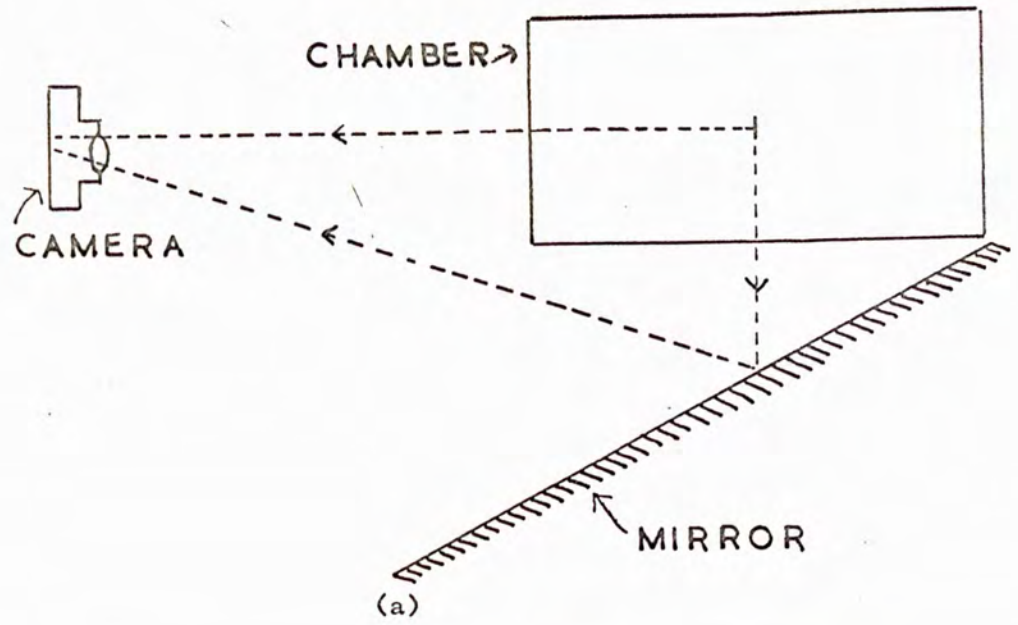

(a)

(b)

Fig.4.8(a)-Arrangement of mirror for stereo photography of streamers,
(b)-stereo photographs of cosmic ray tracks.

camera was focused directly for the streamer viewed perpendicular to the electrical field (side-view). The projected streamers which are brighter were viewed with the help of a mirror placed near the transparent grid earthed electrode. Typical photographs are shown in Figure 4.8b. The tracks parallel to the electric field (projection) seem to be slightly out of focus, due to the limitations of the depth of focus. The aperture used was f/1.9, for which the depth of focus was about 15 cm. The tracks viewed in projection were just out of this depth of focus. The minimum depth of focus required to bring both the views in focus was about 30 cm. This could have been achieved by increasing the length of streamers and decreasing the aperture, but slight defocussing was thought to be acceptable.

In Figure 4.9 are shown some complex events produced by cosmic rays, and in Figure 4.10 various trajectories with small side tracks may be seen. The latter were probably made by knock-on electrons.

One obvious way to control the length of the pulse applied to the chamber is to use a shunt resistance to enable the high voltage electrode to discharge with a certain time constant. However, it is found to be very difficult to select a value that gives high recording efficiency both for single and for multiple tracks. If the value of the shunt resistance is adjusted for single tracks, multiple

/tracks

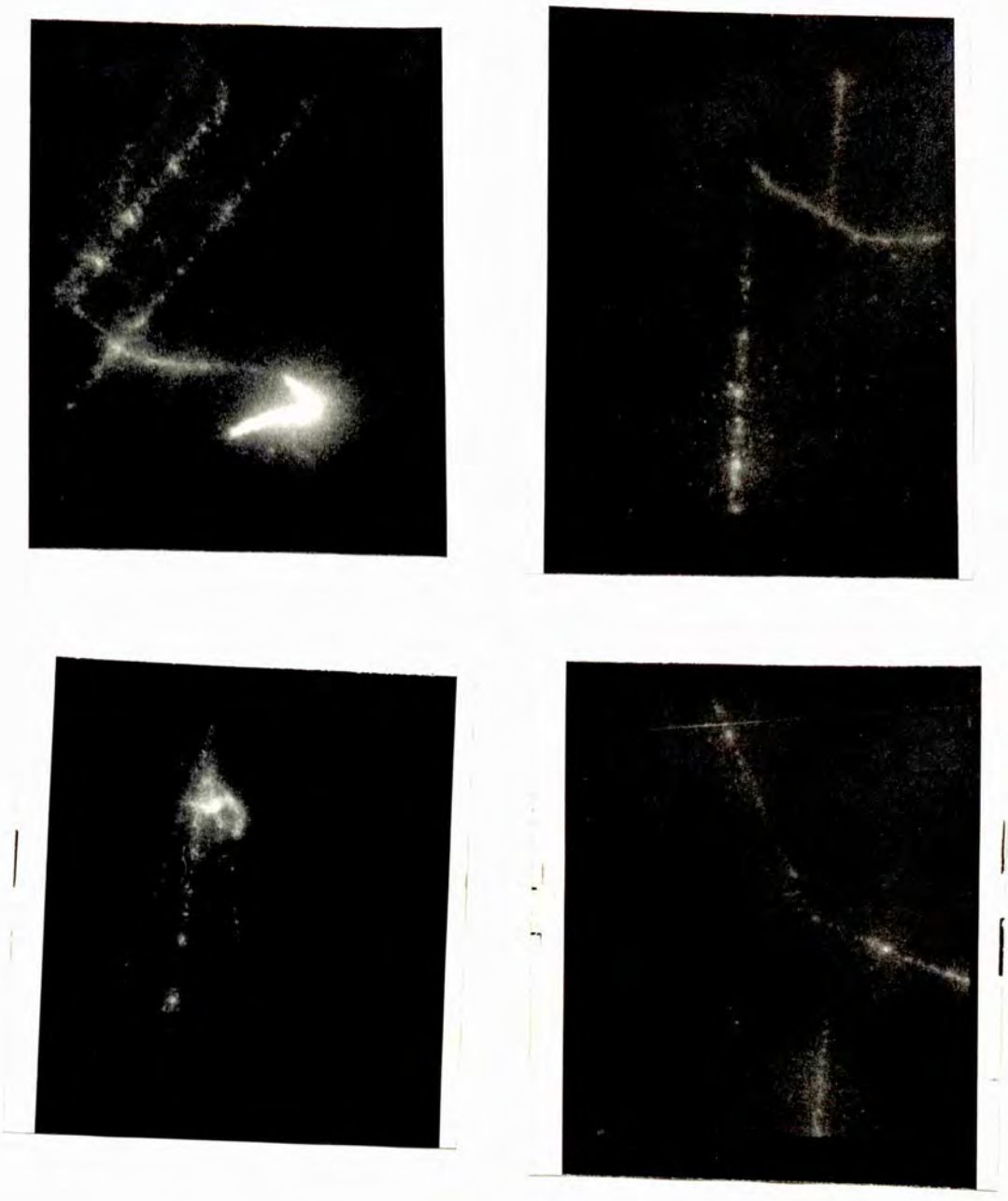

Fig. 4.9-Some complex events produced by cosmic rays in the streamer projection mode.

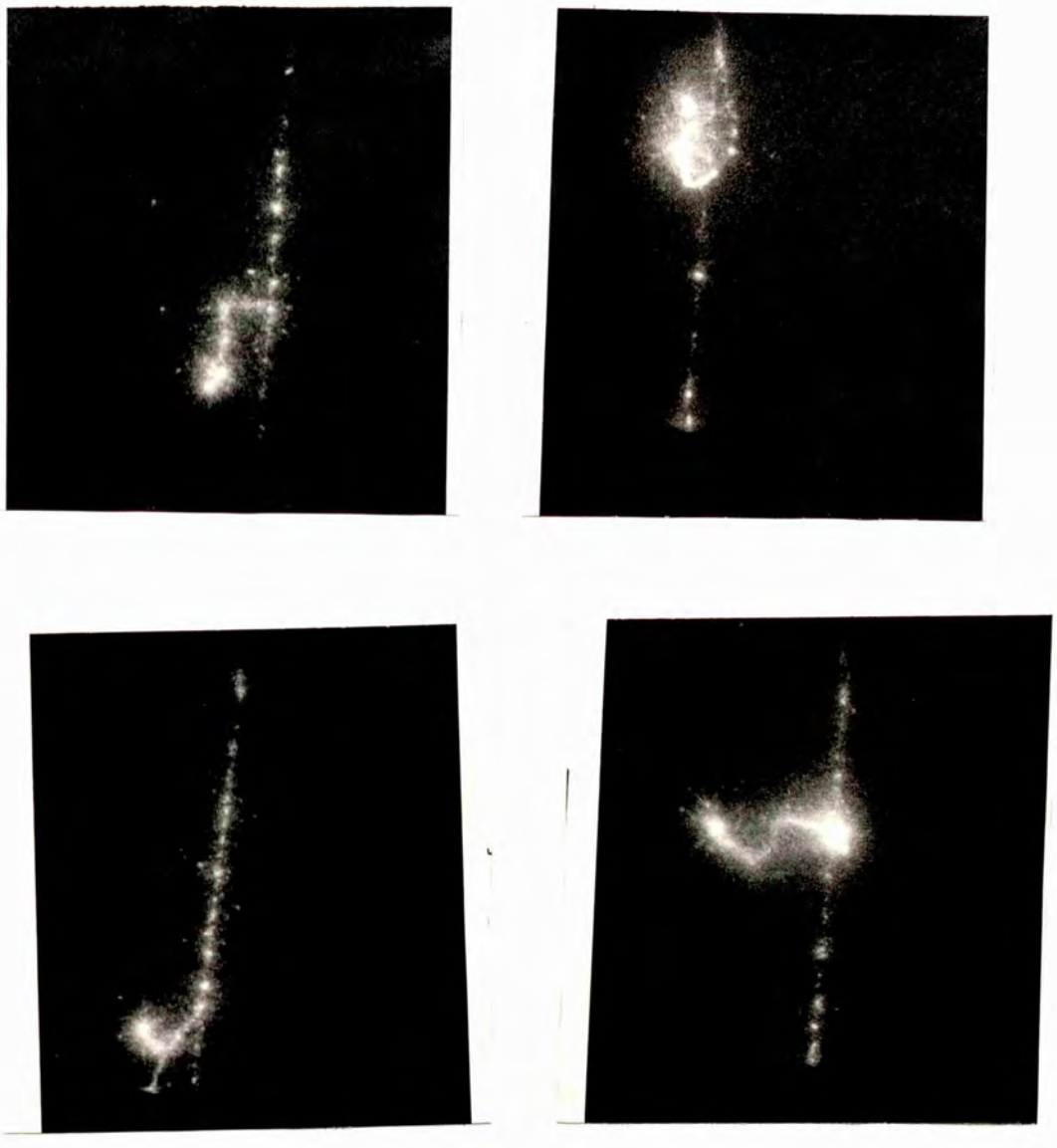

Fig. 4.10 - Cosmic ray tracks (projection mode) with small side tracks made probably by knock on electrons.

tracks become very very feeble. On the other hand, if it is adjusted for multiple tracks, the streamers for a single track are overdeveloped. A shunt spark gap is free from these defects. When a group of particles passes through the chamber, the effective amplitude of the high voltage pulse is somewhat smaller (due to parasitic inductances), which is compensated by a corresponding delay in the breakdown of the shunt gap.

For a field of about 11 Kv/cm, the isotropy obtained can be said to be of the first approximation, because the dimensions of the streamers along the electric field and perpendicular to it are different. The length of the streamers along the electric field should be about one centimetre to obtain good photographs, whereas the diameter of the luminous centre in a direction perpendicular to the electric field is about 2 mm. When the electric field was increased to about 22 Kv/cm smaller side view streamers could be detected, i.e. about 4 mm. This, of course, results in a closer approximation to isotropy.

4.4. Sensitive time of the chamber

The sensitive time is the time interval, at the end of which, if the high voltage is applied, the chamber can still reproduce the track. It is measured in terms of delay introduced between the passage of the charged particle through the chamber and application of high voltage pulse so that the

/chamber

chamber efficiency may become almost zero. The memory time of the chamber used in this work was found to be about 6 microseconds. The delay of the circuit was about 0.5 microseconds. The table below shows the value of the memory time found by various authors.

Authors	Memory time (microsecond)	sensitive volume (cm^3)	gas used
Lyubimov, et al (1964)	15	40 x 50 x 30	He
Lyubimov et al.(1964)	.5	40 x 50 x 30	He + 1% Air
Garron, et al.(1965)	5	35 x 35 x 40	90% Ne + 10% He
Keller et al (1966)	5	Double gap (10 cm each)	90% Ne + 10% He
Chikovani et al (1966)	10	40 x 40 x 20	70% Ne + 30% He
Eschstruth et al (1968)	30	66 x 33 x 11	90% Ne + 10% He
Present work (1968)	6	20 x 20 x 20	70% Ne + 30% He

An electronic delay device based on sharp differentiation of a square pulse from a multivibrator, was used between the coincidence circuit and the trigger amplifier. The efficiency of the chamber to reproduce the tracks was determined for various delays. The graphical relation between delay and efficiency is shown in Figure 4.11. At a delay of 10 micro-

/second

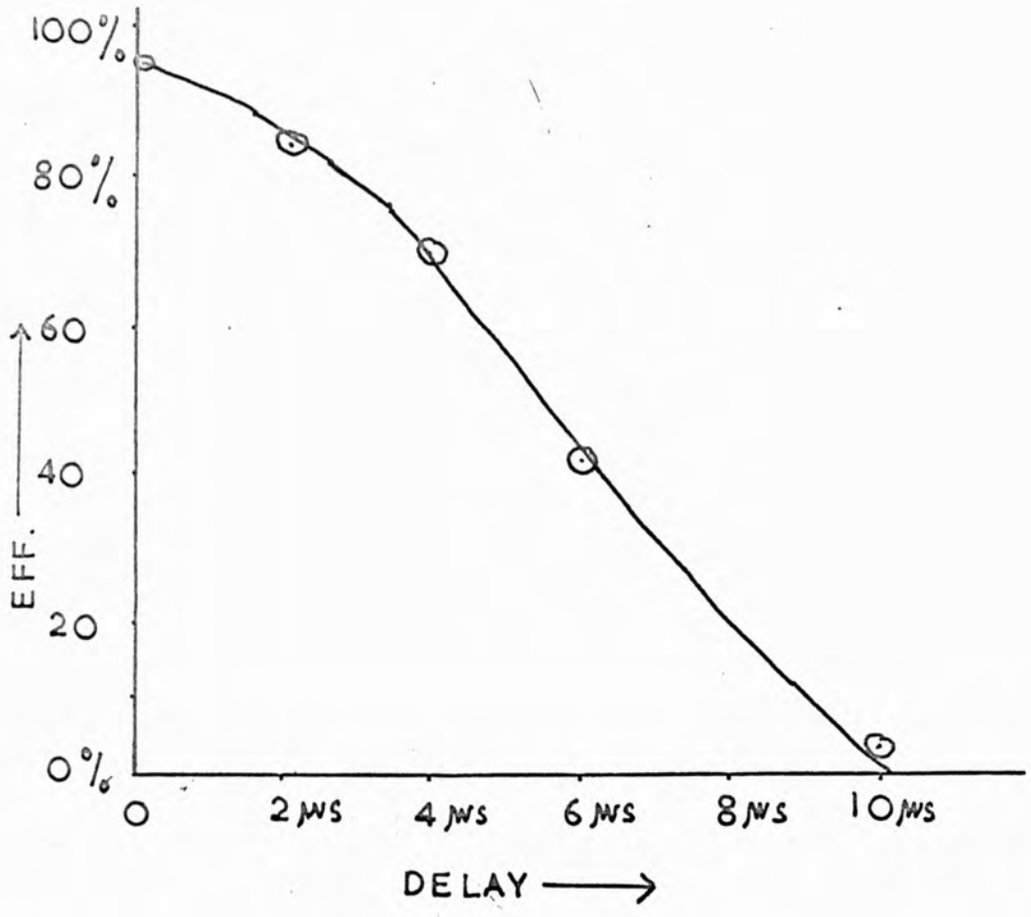

Fig. 4.11 - The dependence of the efficiency of the chamber on the delay before application of the HV pulse.

second no track was seen in the chamber. For delays more than two microseconds, the tracks looked diffused.

The sensitive time of the chamber depends upon the life of the electrons ejected by the incident charged particle. The reasons for the loss of electrons from the trajectory are diffusion and the electron attachment by molecules of electronegative gases that are present as small impurities in the working gas.

The diffusion radius can be calculated by the relation $r = (2Dt)^{\frac{1}{2}}$, where D is the diffusion coefficient ($2 \times 10^3 cm^2/sec$ for electrons in Ne + He). In 10 microsecond the diffusion radius of the electrons would be 2 mm only. The tracks should not have disappeared for such a low diffusion. The loss of electrons appears to be due to the presence of some electronegative gas in the chamber along with the filling gas. As the experiment was done after a few hours of filling, probably helium might have diffused out and air diffused in. The second possibility might be that as the gas is only commercially pure, it may contain some electronegative gases. It can be seen from Lyubimov's experiment (1964) that the addition of 1% of air to helium reduced the memory time from 15 to 5 microseconds.

In extremely pure noble gases the memory time should be of the order of 1 millisecond. Chikovani et al (1964) and Dologoshein et al (1964) have found tracks in their streamer chambers filled with pure neon, even with delays of 200 microseconds.

In certain experiments, chambers with a small memory time ($\sim$1 microsecond) are required. In such cases the natural memory time of the chamber has to be reduced by artificial means, without affecting the performance of the chamber.

In small gap chambers a clearing field is used to regulate the memory time. In a wide gap chamber (>10 cm) however, a clearing field is insufficient to remove the electrons from the tracks in the desired time of a few microseconds. Thus, the memory time of the wide gap chamber can only be effectively regulated by adding to the working gas various small admixtures of electronegative gases. Lyubimov and Pavlovsky (1964) were able to reduce the memory time to about 2 microseconds by adding 0.1% of propane to the neon filling the chamber. Chikovani et al (1966) used 5% of Argon and 6×10^{-3}% of freon-12 to achieve a high number of primary electrons and a very steep decrease in memory time.

Bulos et al (1967) studied the effect of admixtures of several promising gases on memory time reduction. Freon-12, ethylene and methane were all found to be effective in reducing the chamber memory to less than 5 microseconds without decreasing the light output appreciably. Sulphur dioxide could reduce the memory time but had undesirable side effects.

In the present work no attempt was made to reduce the memory time by admixture of electronegative gases, since this was not necessary for the satisfactory operation.

/the

The admixture of electronegative gases causes a reduction in the number of free primary ions, during the delay before the application of the high voltage pulse. But the effect of the admixture of polyatomic gases is rather to extinguish the photon mechanism of the avalanche to streamer development.

4.5. Spatial accuracy.

In any experiment it is important to know the precision with which the direction of a trajectory may be stated. A good measure of this precision is given by (a) the spatial accuracy and (b) the probable angular error.

The spatial accuracy of a track is the root mean square deviation of the measured points about the reconstructed trajectory.

The process consists of measuring the coordinates of a number of points on the track, constructing the straight line by least square method, which represents the actual trajectory and then determining the standard deviation of the measured points in a direction normal to the constructed track.

The measurements of the coordinate points were made on the digitised microscope at the University College, London. The digital accuracy of the microscope was two micron. The scanning can be done quite quickly and the values of the coordinate points are typed and punched on a five hole paper tape, by means of the teleprinter attached to the microscope.

/All

All the films containing the tracks in the three modes and the tracks of the multiple scattering experiments (chapter V) were scanned by this instrument.

For the determination of the spatial accuracy and the angular spread, representative tracks were selected and the films were oriented with respect to the microscope to give a slope of about unity, so that the changes in the values of x and y coordinates were large.

For the continuous streamer mode, ten frames each having tracks in both the gaps were taken. Ten arbitrary points on each track were chosen and their coordinates measured. For the construction of straight lines the tracks in the two gaps were considered independent. In the streamer side-view mode ten tracks were selected and the coordinates of 15 points on each of them were measured. In streamer projection mode, ten tracks were again selected but the coordinates of 20 points on each of them were measured. All the points were taken arbitrarily.

The straight lines were constructed by the method of least squares.

$$y_i - m x_i = \delta_i + c \qquad 4.1$$

$$\sum_{i=1}^{N} (\delta_i)^2 = R \qquad 4.2$$

$$\frac{dR}{dc} = \sum_{i=1}^{N} (y_i - m x_i - c) = 0 \qquad 4.3.$$

$$\frac{dR}{dm} = \sum_{i=1}^{N} -x(y_i - mx_i - c) = 0 \qquad 4.4.$$

Solving equations 4.3 and 4.4, we have

$$m = \frac{N\sum x_i y_i - \sum x_i \sum y_i}{N\sum x_i^2 - (\sum x_i)^2} \qquad 4.5.$$

and

$$c = \{\sum x_i \sum x_i y_i - \sum x_i^2 \sum y_i\} / \{(\sum x_i)^2 - N\sum x_i^2\} \qquad 4.6.$$

$$\text{The S.D.} = \left\{\sum_{i=1}^{N} (\delta_i)^2/(N-1)\right\}^{1/2} = \sigma \quad \text{(say)} \qquad 4.7.$$

Each of the selected tracks were scanned ten times. This was done in order to determine the angular spread, which is discussed in the next section.

All the calculations for the standard deviation were done by the Atlas computer. The standard deviation for each track was actually the mean of the values each computed of ten fifteen and twenty measured points in the respective modes.

The value of the standard deviation given in the table 4.1 for each mode is the mean of the standard deviation for the tracks. The error indicates the standard deviation of the mean. The values obtained, ((0.34$\pm$ 0.02) mm for the tracks in continuous streamer mode (0.41$\pm$ 0.03) mm and (0.44 $\pm$ 0.02) mm in streamer projection mode with the field strengths of 11 kv/cm and 22 kv/cm respectively, and (0.9$\pm$ 0.07) mm in streamer side view mode, are all in good agreement with the values obtained by other authors.

/Eschstruth

Mode	Field strength KV/Cm (nominal)	Angular error mrad.	Standard Deviation (mm.)
Continuous streamer Fig.3.3	11	1.5 ±0.1	0.34± 0.02
Streamer projection Fig.3.5	11	2.2±0.24	0.41 ± 0.03
Streamer projection Fig.3.5	22	1.5 ± 0.08	0.44 ± 0.02
Streamer side-view Fig.3.4	11	4.2 ± 0.6	0.9 ± 0.07

Table 4.1--The values of the standard deviation and angular error of the tracks in different modes.

Eschstruth et al (1968) have found a value of 0.5 mm for standard deviation which they call streamer scatter. This value is for the streamer projection mode in a 11 cm wide chamber with a field of 18.5 Kv/cm. The value in the side view mode is 0.7 mm. Bulos and others (1967) have quoted a value $\pm$ 0.5 mm for the spatial resolution with their 2 metre long streamer chamber, being operated with an electric field of 20 Kv/cm. Chikovani et al (1964) have found the standard deviation, σ = 0.3 mm in a 19 cm streamer chamber with 200 Kv high voltage pulse. Bolotov (1964) used a computer to fit a least square straight line to 100 points on a spark in 20 cm gap. The root mean square deviation laterally parallel to the electrodes was 0.3 mm. Alikhanian et al (1965) measured tracks in a gap of 35 cm and found that the spark straggled the fitted line with a root mean square error of 0.3 mm.

Thus it appears that the present values compare favourably with other estimates.

Chikovani et al (1964) studied the root mean square deviation with respect to the delay between the passage of the particles and the application of the high voltage pulse. For a delay of about one microsecond, the value of σ found (0.3 mm) was much less than the diffusion radius of the electrons, but for a delay of 100 microseconds or more, σ has been found to be of the same order as the diffusion radius. They

/explained

explained this by a model illustrating the mechanism of streamer tracks. The model is based on the supposition that clusters of electrons, rather than isolated track electrons, are mainly responsible for the production of luminous centres. Due to fluctuations in the development of avalanches, one avalanche may develop faster than the other neighbouring ones. This particular faster developing avalanche will meet Meek's criterion earlier, and so the external field in a small region in its neighbourhood will be reduced. This will inhibit the growth of the adjacent avalanches. Thus there must exist a certain distance, d_0, such that only one of the several developing avalanches would become a streamer. Now according to the cluster model, there also exists a distance $d_1 < d_0$ such that the avalanches initiated by several electrons within d_1, would join together to make a single streamer. Due to diffusion the electrons are distributed across the track by the normal law, with a root mean square deviation $\sigma_{d.f} = (2Dt)^{\frac{1}{2}}$. Therefore the middle of the track would contain more electrons than the peripheral ones, and as a result, the avalanche streamer transition would occur with a higher probability. The fluctuation in the position of this cluster of electrons is less than that in a single electron. These two factors narrow the track width. The root mean square deviation is

$$\sigma = (2tD/m)^{1/2} \qquad 4.8$$

/where

where M is the number of electrons in the cluster.

For a small value of delay (1 microsecond) $M \simeq 4$, but for large delay $M \simeq 1$. When calculations are made with this formula agreement is obtained with the experimental values.

In a chamber having a small memory time due to the presence of some electronegative gas, the electron density along the trajectory would be smaller, and hence the value of M also would be a bit smaller than if it were in a pure noble gas. This would increase the value of σ. The chambers having small natural memory times are most likely to contain some electronegative gas as impurity in the working gas, which may well explain their slightly higher value of σ. The table below shows a relation between the value of σ and memory time.

Authors	Memory time (microsecond)	(side-view)	(projection)
Eschstruth et al.(1968)	30	0.7 mm	0.35 mm
Chikovani et al (1964)	200	-	0.3 mm
Present work	6	0.9 mm	0.44 mm

The value of the spatial resolution in the streamer side view mode was (0.9 + 0.07) mm. These streamers were

/about

7 mm in length, which was the reason of the high value.

The standard deviation in streamer continuous mode tracks was 0.34 mm. The reason for this low value was perhaps that in this mode there is a more effective clustering of electrons, due to their smaller lateral displacement.

4.6. Angular accuracy

The angular accuracy was estimated as the average of the standard deviations of a number of determinations of the angles of tracks, computed by the method of least square.

As stated in the previous section, each track was scanned ten times, and so for each track ten values of the gradient "m" were obtained. For a particular track the standard deviation of these ten values of "m" was given by

$$\sigma_\theta = \left\{ \sum_{i=1}^{n} (m_i - \bar{m}) / (n-1) \right\}^{1/2} \qquad 4.9.$$

where n = 10.

The scanning with the digitised microscope and the calculations on a computer, made the analysis fairly rapid, and thus suitable for a large number of tracks.

The error in σ_θ is the standard deviation of mean. The angular error of the tracks in the continuous streamer and streamer projection modes (22 Kv/cm) were quite low, 1.5 m rad. The value for the side view streamers (11Kv/cm) was

/rather

rather high (4.2 $\pm$ 0.6)m rad. The explanation is probably that they are about 7 mm long making it difficult to determine their centres. The analysis of similar tracks in the chamber described by Eschstrutt, et al (1968) gave a value of 7.5 m rad. Their chamber was placed in a magnetic field to study the decay $K_L^0 \rightarrow \pi^+ \pi^- \pi^0$. The length of the streamers was adjusted to be about 1 cm to give sufficient light output for good photography, which may be the reason for the high value. Cargi and Schneider (1966) studied the streamers in their 10 cm wide chamber with a field of 30 Kv/cm. The angular error (viewed perpendicular to the field) was found to be 3 m rad for a 10 cm long track.

It is of interest to note that Alikhanian et al (1963) studied the accuracy of spark tracks in their 21 cm gap spark chamber. They found that the trajectory of a straight track was established with an accuracy of up to 10^{-5} radian which is comparable with the value we have obtained in the continuous streamer mode.

We conclude from this analysis that the present streamer chamber compares favourably with other chambers that have been described so far.

C H A P T E R V

APPLICATION OF STREAMER CHAMBER TO THE STUDY OF MULTIPLE SCATTERING

5.1. Theories of multiple scattering.

By 1939 physicists had observed that energetic charged particles passing through matter were frequently deviated through small angles. In that year Williams suggested that this small angle scattering could be accounted for in terms of multiple Rutherford scattering.

When the impact parameter is greater than the nuclear radius, the scattering occurs in the coulomb field of the nucleus. The net scattering would be the accumulated effect of the successive nuclei encountered. The probability of any one deflection is given by in real the Rutherford scattering law. Most of the scattering observed arises from this. In his theory Williams assigned two limits for the extreme collision distances. The upper limit is determined by the shielding of the orbital electrons, and the lower limit r_0 (nuclear radius), by the modification of the electrostatic field within the nuclear radius. When the impact parameter is less than the nuclear radius, the incoming particle approaches closer to the centre of the nucleus, and is likely to be scattered through a large angle. These single large angle scatters are easily recognisable and may be ignored in any investigation of multiple scattering.

/The

The main simplifying approximations are:-

(i) the average deflection is mainly contributed by scattering through small angles;

(ii) the distribution of the observed scattering angles should be Gaussian and is expected to be unaffected by single scattering which in general would lie at larger angles. This large angle scattering is rare, and is unlikely to occur more than once for any one particle in the scatterer. It is clear that is is the lower limit of the impact parameter that determines the upper limit of the angles that are included in the theory.

(iii) The scattering measured is the projection of the deflection on a plane perpendicular to the line of sight and containing the initial direction - that is the usual plane of a photograph.

In a field free space a particle moving with a velocity v parallel to a direction x may be represented by the infinite plane wave - $A \exp(ix/\lambda)$. In the presence of an electrostatic scattering field in which the potential of the particle is $V(r)$ the solution is of the form

$$\psi = A \exp(ix/\lambda) + \psi_1 \qquad 5.1.$$

where ψ_1 represents the effect of the field. For low velocities ψ_1 is determined by the non-relativistic wave equation of Schrodinger.

$$\nabla^2\psi_1 + (2M/\hbar^2) E \psi_1 = (2M/\hbar^2) V(A e^{ix/\lambda} + \psi_1) \qquad 5.2.$$

If the scattering field is sufficiently weak, then the term $V\psi_1$ may be neglected (Born approximation). The solution for ψ_1 at large distances R from the scattering field is given by

$$\psi_1(R) = \frac{A}{R}\frac{M}{2\pi\hbar^2}\int V(\tau)\, e^{i(x+|R-\tau|)/\hbar}\, d\tau_\tau \qquad 5.3.$$

This means that the scattered wave at R may be obtained by supposing that every element of volume $d\tau_\tau$ of the field scatters waves of amplitude $(M/2\pi\hbar^2)Vd\tau r/R$, the phase of the secondary wave being the same as that of the primary wave at the point of scattering τ. For a field that is spherically symmetrical the probability $I(\theta)$ of scattering through an angle θ per unit solid angle (per incident particle per unit area), according to (5.3.) is

$$I(\theta) = |\psi_1(R,\theta)|^2 R^2/A^2 = (2M/\mu\hbar^2)^2 f^2$$

$$f = \int V(\tau)\,\tau \sin\mu r\, d\tau\,, \quad \mu = 2\sin\tfrac{1}{2}\theta/\hbar \qquad 5.4.$$

For the scattering of a particle of charge e by a nucleus of charge ze, the probability

$$I(\theta) = z^2e^4/4M^2v^4\sin^4\tfrac{1}{2}\theta \qquad 5.5$$

which is the Rutherford scattering

If the field deviates from coulombian, the modified scattering may be obtained by evaluating (5.4.) for the modified field.

For the requirements of relativistic theory, where small angle scattering is concerned, the same equation may be used, if a relativistic expression for mass is inserted. In Dirac's relativistic theory of electrons there is a term representing the effect of spin, which is negligibly small. This makes the theory of small angle scattering simple.

The probability of a particle being scattered through an angle between $\bar{\Phi}$ and $\bar{\Phi} + d\bar{\Phi}$ can be expressed as a sum of two probabilities.

$$P(\bar{\Phi})d\bar{\Phi} = G(\bar{\Phi})d\bar{\Phi} + S(\bar{\Phi})d\bar{\Phi} \qquad 5.6.$$

$G(\bar{\Phi})$ represents the Gaussian distribution and $S(\bar{\Phi})$ the Rutherford distribution of single scattering.

The mean square value of projected deflections has been found using Rutherford's expression for the probability of single scattering and integrating over the limit $\bar{\Phi}_{min}$ and $\bar{\Phi}_{max}$. For angles less than $\bar{\Phi}_{max}$ Gaussian curve is predominant and for angles greater than $\bar{\Phi}_{max}$ the Rutherford distrubution.

The mean absolute deviation

$$\langle \Phi \rangle = \frac{2e^2 (Nt)^{1/2} Z}{p v} \left(\log \frac{\bar{\Phi}^2_{max}}{\bar{\Phi}^2_{min}} \right)^{\frac{1}{2}} = \delta L \qquad 5.7.$$

where $\delta = 2e^2 (Nt)^{1/2} Z / p v$ and $L = (\log \bar{\Phi}^2_{max} / \bar{\Phi}^2_{min})^{1/2}$

N, t, z = the number of atoms per c.c., the thickness in cm and the atomic number of the material of the scatterer.

The angle Φ max is the greatest single angle scattering which can contribute to the observed deflection. Physically it is determined by the finite size of the nucleus. As a first approximation to Φ max, Williams takes the angle Φ_1, which is such that in traversing the thickness t, a particle will suffer on the average just one deflection greater than Φ_1

The theory shows that

$$\Phi = \delta(\pi/2)^{1/2} \qquad 5.8$$

Φ min is the effective minimum angle. Its magnitude is determined by the screening of the field by the orbital electron. In deriving the basic single angle scattering formula using the Fermi-Thomas statistical model of the atom to allow for the effect of screening, Williams considers separately the cases: $\gamma = Z/137\beta \ll 1$ (when the Born approximation is valid) and $\gamma \gg 1$ (classical)

For $\gamma \ll 1$ $\quad \Phi_{min} = 1.75\, mc\, Z^{1/3}/137P$ $\qquad$ 5.9

Thus $\left(\log \dfrac{\Phi^2_{max}}{\Phi^2_{min}}\right)^{1/2} = \left\{\log\left(\dfrac{2\pi Z^{4/3} N t \hbar^2 z^2}{3.1\, m^2c^2\beta^2}\right)\right\}^{1/2} = (\log M)^{1/2}$ $\qquad$ 5.10

For $\gamma \gg 1$

$$M_{cl} = 0.20\,\pi N t Z^{-2/3}(\hbar^2/mc^2)^2 \qquad 5.11$$

M is the average number of collisions. These assumptions give the mean deviation $\bar{\Theta} = \delta(\log M)^{1/2}$ $\qquad$ 5.12

when deflections greater than Φ_1 are taken into account, the mean deflection due to all Φ's is expressed by

$$\bar{\theta}_1 = (1.45\delta + 0.80\bar{\theta}) \qquad 5.13$$

$\bar{\theta}_1$ is actually the root mean square scattering angle.

For lead as scatterer the product of the mean total energy of the particles and the mean angle of scattering can be expressed as

$$[E\bar{\theta}] = 0.906(t)^{1/2}.10^9/\beta^2 \text{ ev. degrees.} \qquad 5.14$$

Other multiple scattering theories have been given by Goudsmit and Saunderson (1940), Moliere (1948), Snyder and Scott (1949), Nigan et al. (1959) and Nigam (1963). All these theories gave results within a few per cent of Williams's theory.

In Goudsmit and Saunderson's theory (1940) the distribution has been expressed as a series in Legendre polynomials.

In Moliere's (1948) and Snyder and Scott's (1949) theories an approximation of very small angle scattering, and hence, an expansion in Bassel functions have been used. For distribution of projected angles they use a Fourier integral.

A brief account of Moliere's theory has been given in Appendix (A). It shows that the scattering depends only upon a single parameter, describing the atomic screening. The scattering angle is obtained by making an exact quantum mechanical calculation of the cross-sections for single scattering.

/Nigam

Nigam et al (1959) (1963) has used the Dalitz (1951) relativistic expressions for single scattering cross-section derived in second Born approximation. It has been briefly described in Appendix (A). This theory could predict a small but finite difference in the multiple scattering of electrons and positrons, although the experimental value in a number of cases has been found to be greater than the theoretical.

In the case of heavy scatterer (high value of z) Modiere's theory gives better results, whereas Nigam's and Williams's theories give higher values. But in the case of light scatterer, Nigam's theory has been found more suitable.

Table 5.1 - List of earlier work on multiple scattering (m.s.) of cosmic ray muons.

Author	Energy Mev	Scatterer	Thickness	Technique	Whether agreement with theory	Degree of agreement Experimental Value / Theoretical value & remarks
Wilson (1940)	600	Pb Cu Au	1 cm 2 cm 2 cm	Cloud Chamber	Yes	
Code 1941	less than 2000	W	3.8 cm	Cloud Chamber	Yes	
Sinha 1945	93	pb	2cm	Cloud Chamber	No	47%
Crewe 1951	184	Pb	1 inch	Cloud Chamber	No	65%
Present work 1968	98	Pb	1 inch	Streamer Chamber	No	54%

Table 5.2 - List of earlier work on m.s. of electrons and positrons

Author	Energy Mev	Scatterer	Thickness	Technique	Whether agreement with theory	Degree of agreement Experimental Value / Theoretical value & remarks
Fowler 1938	5 to 10	Pb	0.015 cm 0.1695 gm/cm^2	Cloud Chamber	No	42%
Oleson et al 1939	5 to 8	C	0.75gm/cm^2	Cloud Chamber	No	58%
		Pb	0.072 gm/cm^2			
Sheppard and Fowler 1940	5 to 17	C	0.138 and 0.381 cm	Cloud Chamber	Yes	
		Pb	0.015 & 0.038 cm		No	60%
		Al	0.118 cm		No	85%
Kulchitsky & Latyshev 1942	2.25	Al	0.01 cm	Magn.lens and G.M. tubes.	No	94% (Moliere)
		Fe	0.002 cm		Yes (almost)	101.5%
		PB	0.0007 cm			
Groetzinger 1950	0.05 to 1.7	Ar		Cloud Chamber	Yes	
Gottstien et al. 1951	105 and 185	G_5	200 micron (cell length)	Nuclear emulsion	Yes	

Table 5.2 continued

Author	Energy Mev	Scatterer	Thickness	Technique	Whether agreement with theory	Degree of agreement Experimental value / Theoretical value
Hanson 1951	15.6	Be	0.257 gm/cm^2	Magnetic lens & ionisation chamber	Yes	Nigan(μ=1.12)
			0.49 gm/cm^2			Nigan(μ=1.8)
		Au	0.0187 and 0.0373 gm/cm^2			Moliere / Moliere
Hisdal 1952	0.59	G_5	17:6 micron (cell length)	Nuclear emulsion	No	60%
Voyvodic 1952	16.7	G_5	45 micron	Nuclear emulsion	Yes	
Bosley & Muirhead 1952	18	$\underline{G}_5$		Nuclear emulsion	Yes (almost)	Exptl.value slightly higher than theoretical
Hussain 1955	6.6 & 11.5	G_5	38,76 & 114 micron	Nuclear emulsion	Yes	
Bosley & Hughes 1955	10	G_5		Nuclear emulsion	Yes	for positrons
					No	for electrons exptl.value 10% higher than theory.

Table 5.2 continued

Author	Energy Mev	Scatterer	Thickness	Technique	Whether agreement with theory	Degree of agreement Experimental value / Theoretical value
Heymann & Williams 1956	1 1.5 2.5	G_5		Nuclear emulsion		85% 80% 95%
Henderson 1957	0.4	G_5	25 micron	Nuclear emulsion	Yes	
Strong & Roy 1963	0.3 to 1.8	N_2		Cloud chamber	Yes	Agreement with Williams's theory. Moliere's theory underestimates the results above 0.6 Mev

M.s of heavy ions (O^{16} and Ar^{40}) involving large values of Born parameter

$\Upsilon = -Zz/137\beta$

Simon 1964	(O^{16}) 164	Al	1.74 mg/cm^2	Nuclear emulsion	Yes	Agreement with Moliere's theory. Nigam's theory gives higher value.
		Ni	1.83 Mg/cm^2			
		Au	3.12 Mg/cm^2			
	(Ar^{40}) 400	Al	0.32 mg/cm^2			

Table 5.3.

List of works on multiple scattering difference between e^- and e^+

	Author	energy Mev	Scatterer	Technique	Whether agree-ment	K_-/K_+
1.	Groetzinger et al. 1952	3.55 (e^-) and 2.66 (e^+)	Ar	Cloud Chamber	No	1.1
2.	Cwsak and Scott (1955)	0.4	N_2	Cloud Chamber	No	0.08
			A	"	No	0.92
3.	Bosley and Hughes (1955)	10	G5	Nuclear emulsion	No	1.1
4.	Heymann and Willams (1966)	1	G5	Nuclear emulsion	No	1.08
		1.5			marginal	1.05
		2.5			No	1.17
5.	Strong and Roy (1963)	0.3 to 1.8	N_2	Cloud Chamber	Yes	1

K is called the scattering constant and is given by the relation

$$K = \theta \frac{pv}{z}\left(\frac{100}{t}\right)^{1/2} \qquad 5.15$$

Where θ is the mean angle of scattering, p,v and z are the momentum velocity and charge of the particle and t is the cell size in micron.

5.2. Survey of earlier work

The results of previous work have been condensed into Tables 5.1, 5.2 and 5.3. It may be seen that the observed amount of multiple scattering in most of the experiments does not agree with the theoretical values. The disagreement is generally in the case of lower energy particles scattered in thick specimens of heavy materials.

In all the experiments, agreement was found with the theory to the extent that the distribution in the product $(E\,\theta)$ of scattering angle (θ) and energy (E) of the scattered particle when plotted against θ was approximately Gaussian in form, and the product $(E\theta)$ was constant over a range of energies, and independent of the sign of charge of the scattered particles.

In the case of electrons scattered through heavy material agreement was obtained only when the energy was more than 15 Mev, and thickness of the foil very small, for example Hanson (1951). At the lower energies agreement was better in the case of aluminium and carbon laminae.

For muons scattered through thick ($\sim$1 cm) lead the agreement was obtained when the energy was more than 500 Mev. At lower energies, the experimental value was smaller than theoretical one, as has been found by Sinha (1945) and Crewe (1951).

When the multiple scattering was studied in photographic

/emulsion

emulsion plates, agreement with theory was found for energy about 10 Mev. But the experimental value at 1 to 2 Mev was only about 80% of the theoretical.

The multiple scattering has also been studied in gases. In nitrogen there is almost complete agreement with theory, but in Argon the experimental value is again less than theoretical.

All the work with emulsions and foils has been compared with Moliere's theory which gives a slightly lower (few per cent.) value than Williams's theory, in case of heavy scatterers.

Nigan's theory predicts about 1% difference in the multiple scattering of electrons and positrons, but larger differences, even more than 10% have been observed. Here, also the agreement is better when the energy is high and scattering angle small.

The multiple scattering of heavy ions (O^{16} and A^{40}) through very very thin metal foils (less than 2 mg/cm^2) has been found to be in agreement with Moliere's theory. The energies of the oxygen and argon ions were 164 and 400 Mev respectively.

5.3. Experiment

In the present experiment the scattering of cosmic ray muons in a one inch thickness of lead has been studied.

/The

The double gap chamber in the continuous streamer mode was used but with a lead scatterer (9 x 9 x 1 inch^3) placed between the gaps. The lead actually was sandwiched between two 1/16 inch (24inches square) aluminium plate electrodes. The experimental arrangement has been shown in figures 5.1. A scintillation counter was placed just above a 2 inches thick (8 inches square) lead absorber and an anticoincidence counter just below. The two earth electrodes were aluminium plates described earlier. Another scintillation counter was placed above the chamber on the joists used for clamping. The one inch lead scaterer along with the two thin aluminium plates served as the high voltage electrode. Above the top scintillator, there was placed 10 cm of lead to absorb the soft components of the cosmic ray particles.

The first and second scintillation counters were in coincidence; the third and the coincidence output were in anti-coincidence. Thus only the hard components of the cosmic ray particles which were able to pass through one inch of lead but stopped by the lower 2 inches of lead could give an anti-coincidence output which triggered the Marx-generator. The anti-coincidence system is described in Chapter VI. It was found to work quite satisfactorily. The spurious anti-coincidence output was almost negligible. The rate of genuine anti-coincidence output was about 5% of the coincidence output without any lead absorber.

/The

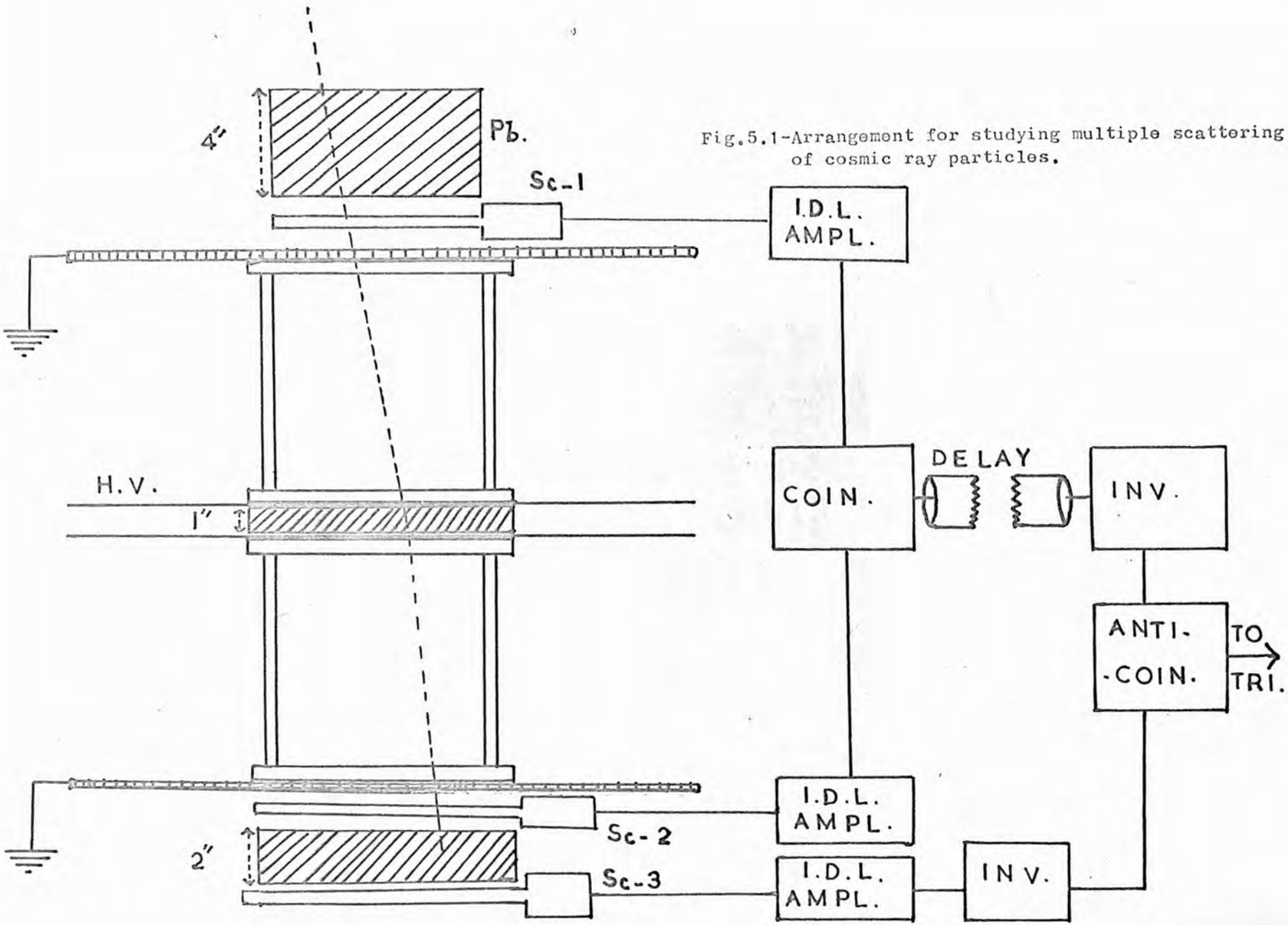

Fig.5.1-Arrangement for studying multiple scattering of cosmic ray particles.

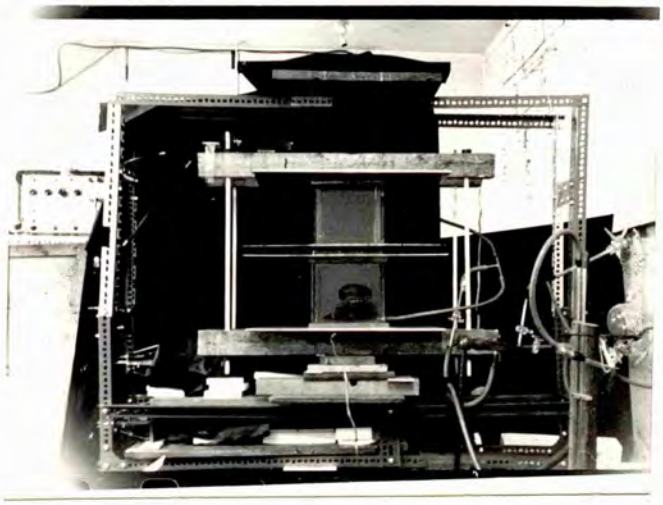

Fig.5.2-Photograph of the double gap chamber used for multiple scattering experiment.

The scattering in the thin aluminium high voltage electrodes and perspex plates was ignored in comparison with the scattering in lead, because previous observations had shown it to be negligible.

5.4. Results of present experiment

The tracks were scanned by the digitised microscope. Straight lines were constructed by the least squares method for the tracks above and below the scatterer, and the scattering angle was obtained from the difference of the slopes. In all 227 tracks were considered and they are displayed in Figure 5.4. The majority lie in the range 0° to 17°, although a few cases of larger angles were observed. Figure 5.3. shows some typical examples of the scatterings photographed. The accuracy with which the slopes can be determined is 0.09 degree and hence the probable error in the scattering angle is 0.11 degree.

The particles were grouped in the angular range 0°-1°, 1°- 2°, 2°- 3°,.....16°- 17° and so on, and their numbers were displayed in the form of a histogram (Fig. 5.4). It may be seen that there is some deviation from a Gaussian. The mean of all the small angle scattering is 4.45° and the root mean square value is 5.6°. A Gaussian of the mean value 4.45° can be seen in the Figure 5.4. In addition a Gaussian derived from the theory has been plotted and normalised to the experimental Gaussian. The discrepancies are obvious.

/From

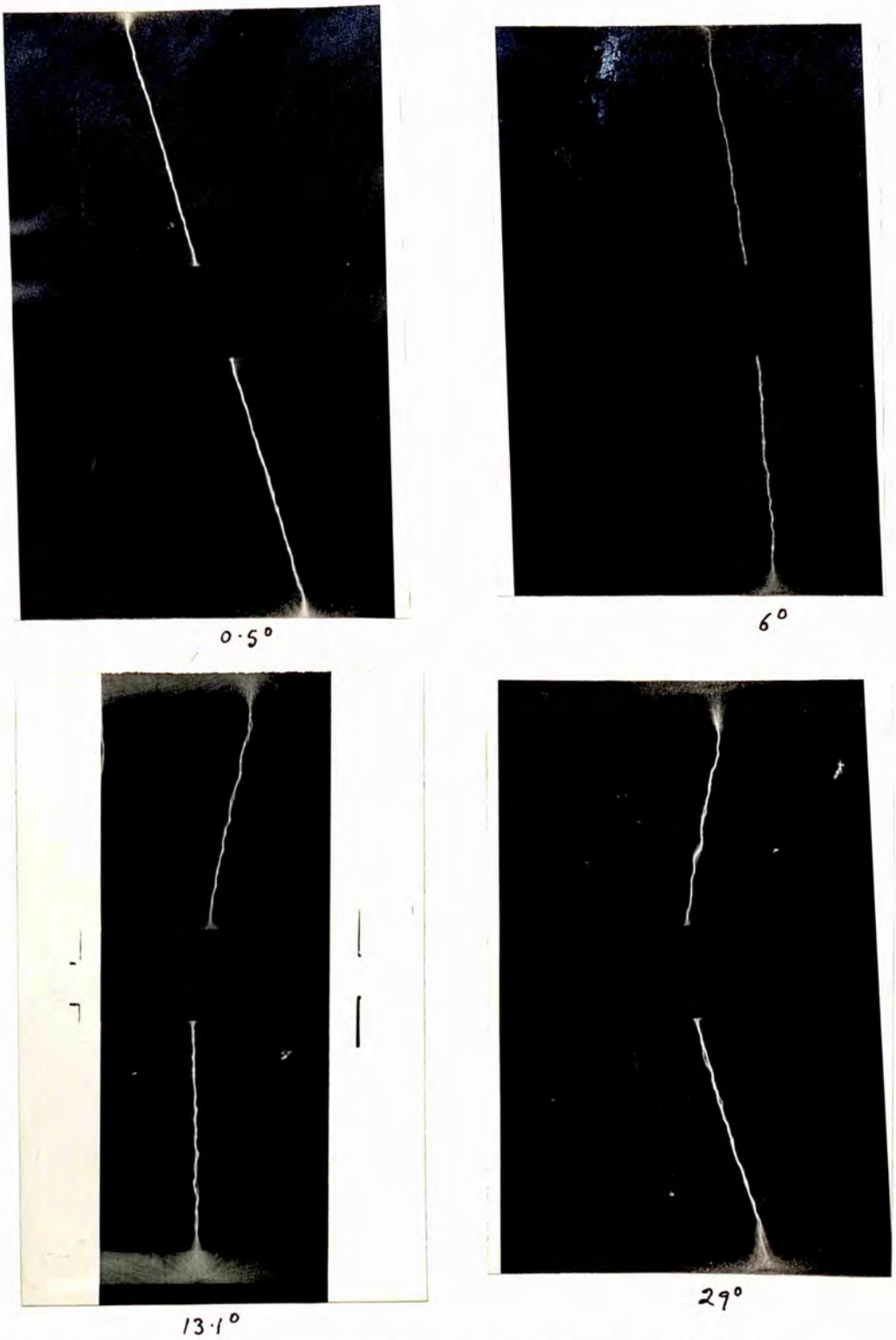

Fig.5.3-Cosmic ray muons scattered through one inch lead.

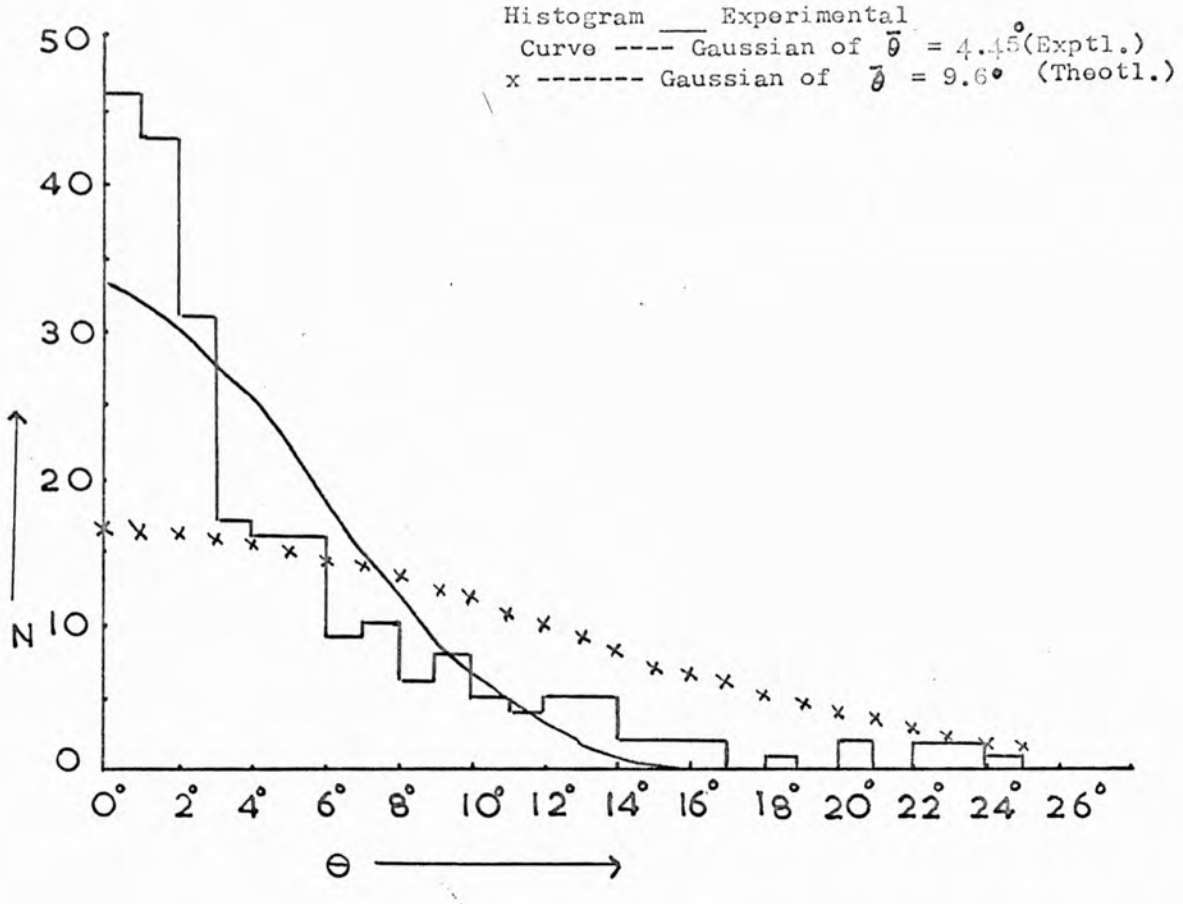

Fig.5.4-Distribution of cosmic ray particles scattered through one inch of lead, plotted against θ, the projected angle of scattering.

From the range-energy relation graph by Wick (1943) the kinetic energy of cosmic ray particles having a range of one inch in lead has been found to be 64 Mev, which was the lower limit of the energy range of particles selected by the anti-coincidence technique. The upper limit was fixed by the three inch range in lead which corresponds to 133 Mev. The mean kinetic energy is therefore 98 Mev over the small range of zenithal angle used in this experiment ($\pm$ 15°), the distribution of cosmic rays has been taken to be uniform (Rice-Evans and Mishra 1967).

The theoretical value of the product ($E\theta$) can be obtained from equation (5·14).

The total mean energy of the particles was about 200 Mev. Thus according to the equation

$$E = m_0c^2/(1-\beta^2)^{1/2}$$

$$2\cdot10^8 = 10^8/(1-\beta^2)^{1/2}$$

and $\beta^2 = 3/4$

thus ($E\theta$) = 1.90×10^9 ev degrees.

The experimental mean angle of scattering

$\bar{\theta} = 4\cdot45^\circ \pm 0\cdot25^\circ$ and $\theta_{r.m.s.} = 5\cdot7^\circ \pm 0\cdot2$

This value has been corrected with a geometrical factor to account for the small variation in the recording efficiency for the different angles. The correction has been found by a graphical method. In a scaled diagram of the whole

/arrangement

of the apparatus (counters, chambers, scatterer and extra lead absorber) as shown in figure (5.5), five equally spaced points were taken both on the upper counter and on the scatterer. The lines joining these points gave 25 typical trajectories of particles incident at different angles as allowed by the geometry. The sizes of the two counters and the scatterer are almost the same. The trajectories in the second gap representing the direction of the scattered particles were drawn taking the limiting cases which could be recorded by the instrument. The chance of a scatter through a certain angle was determined for each trajectory and the results combined to give an overall efficiency. Thus a correction factor was obtained for each angular group. Figure (5.6) shows the efficiency of different angles. It can be seen that there is a maximum decrease in efficiency of only 8% for angles greater than 15°. Application of these corrections increases the mean projected angle of scattering by only 4.7%, making it 4.66°. Then the r.m.s. value of the angle becomes 5.97°. This is the value that is used in the comparison with the different theoretical values.

The experimental situation in the present work differs slightly from the situation contemplated in Williams's theory. The projected distribution in a plane parallel to the front surface of the chamber has been measured in the present work, whereas Williams considered the plane containing the initial

/direction.

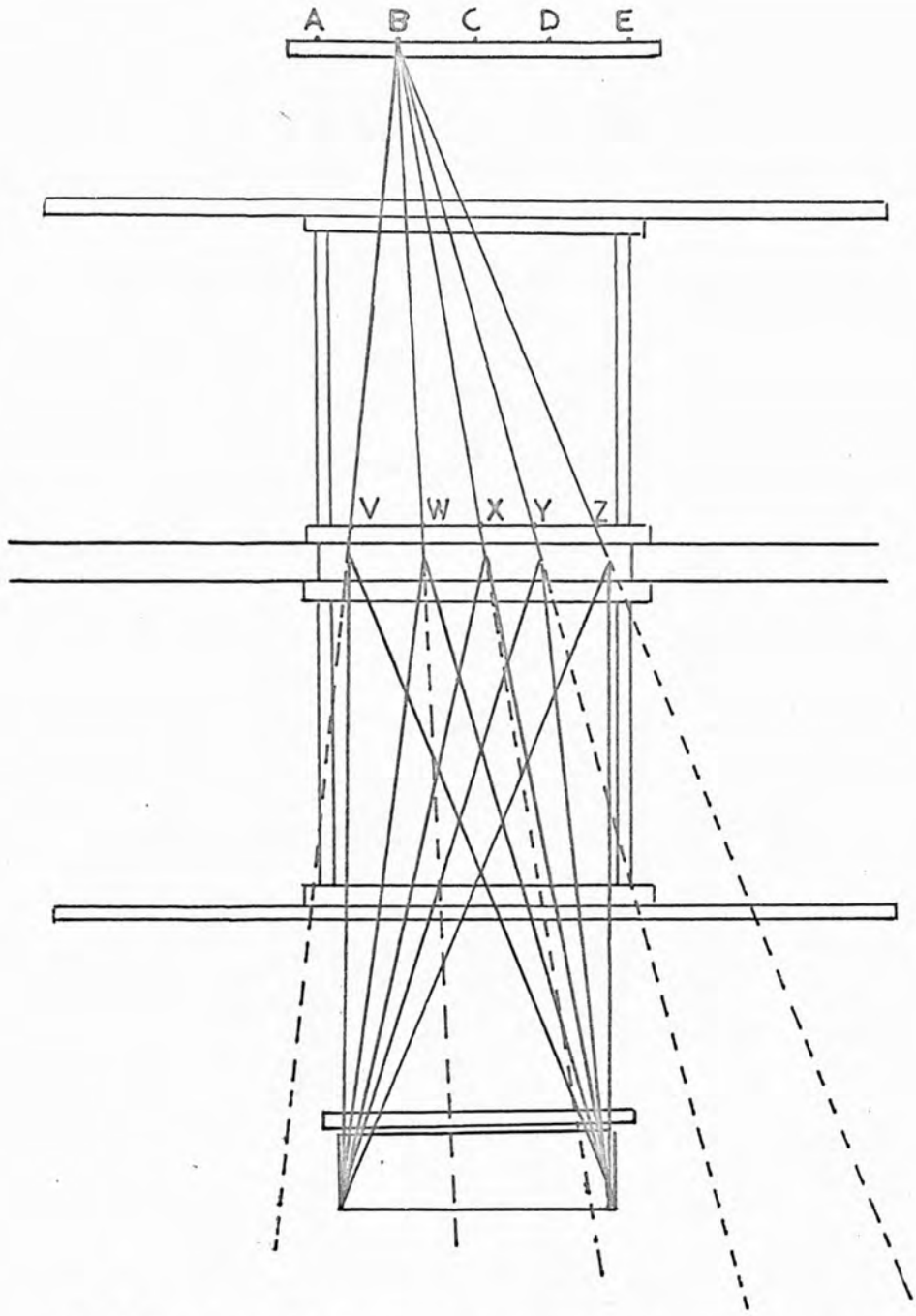

Fig.5.5-A typical diagramatic representation of the geometric limitations of the chamber for recording scattering.

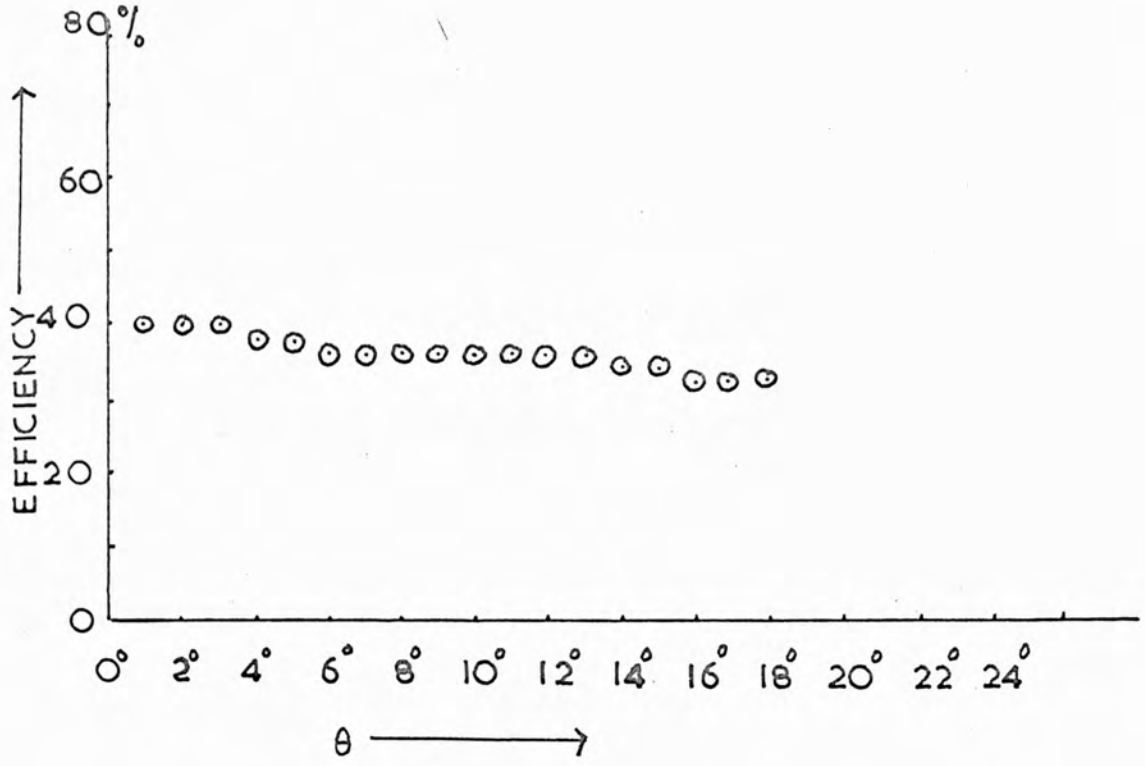

Fig. 5.6- Recording efficiency for different scattering angles.

direction. A graphical assessment has shown that the difference between the results in these two situations is only 3% for a particle incident at an angle of 20° and scattered through 10°. As the maximum angle of incidence in this work was only 15°, the actual correction would be much smaller.

A true spatial angle of scattering of 10° results in a mean projected angle (in a plane containing the initial direction) of 6.25°. In the case of incident particles not necessarily being in the plane of projection, Fig. 5.8 shows the modification that leads to an equivalent mean projected angle of 6.46°. Crewe and Latherland (1951) have given a mathematical treatment for such a case but it has not been employed because it is complex and the correction is small. Other authors seem to have ignored it altogether.

The results are shown in the table below.

	Value of θ r.m.s.	Agreement. θ exptl/θ theotl
Experimental	5.97°	
Williams	11.5	52%
Moliere	11.25	54%
Nigam (μ = 1.12)	12.7	47%
Nigam (μ = 1.8)	12.4	48%

It is seen that the disagreement between the experimental value of the mean scattering angle and the theoretical value is very large. This confirms what other physicists have found (see Fig.5.7c). The best agreement is with Moliere whose theory

/has

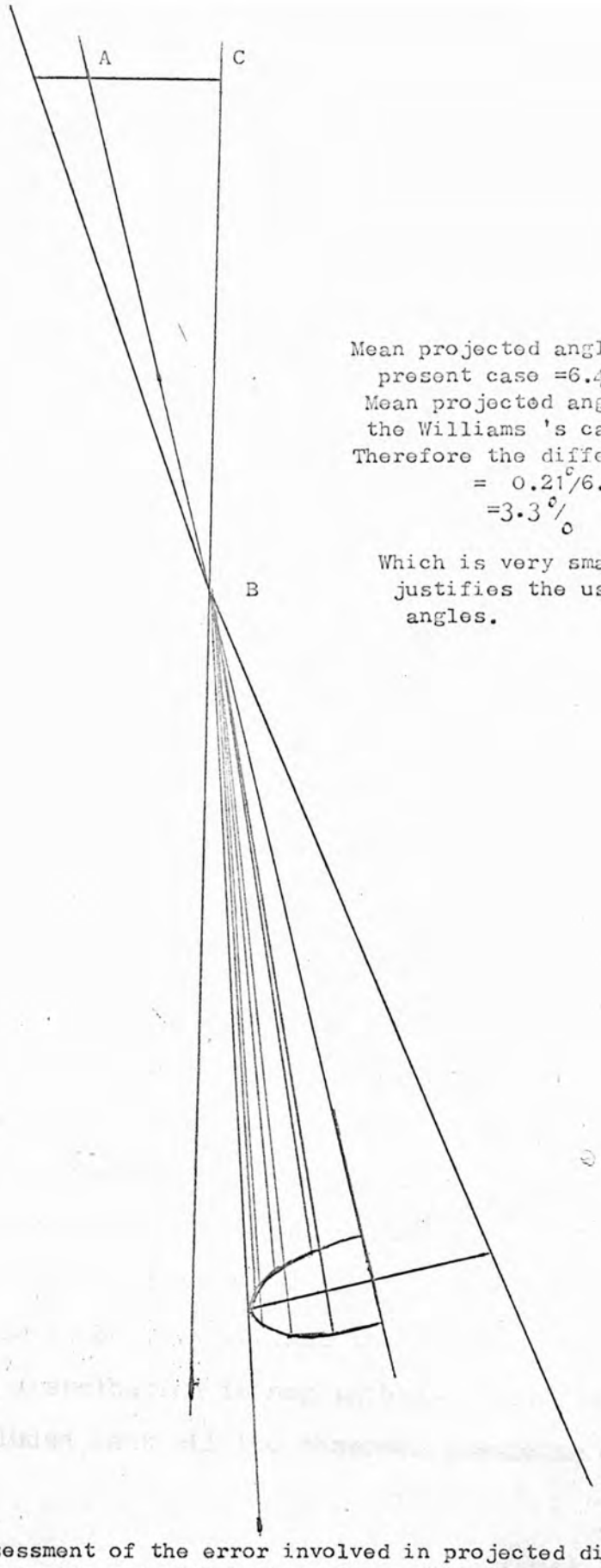

Mean projected angle in the present case $=6.46^{\circ}$

Mean projected angle in the Williams 's case $=6.25^{\circ}$

Therefore the difference

$= 0.21^{\circ}/6.25^{\circ}$

$=3.3\%$

Which is very small and justifies the use of projected angles.

Fig.5.8-Assessment of the error involved in projected distribution when compared with Williams's condition.

has a higher correction factor (than Nigam) attached to the critical screening angle where there is deviation from the first Born approximation in the case of scatterers of high atomic number. The justification for the smaller correction given by Nigam is that the deviation from the first Born approximation is very small at small angles which go into the definition of the screening angle. This shows that these theories might be fully applicable only in the case of very small angle scattering and hence for very high energy particles scattered through thin foils.

For these measurements in the present experiment electrons and protons have been excluded. Electrons would have to pass through at least five inches of lead without producing any shower. This is most unlikely. The protons cannot be excluded. But they have been estimated to be less than 5%. The mean kinetic energy of protons having range between one inch and three inches of lead is about 100 Mev. Thus the total energy would be of the order of 10^9ev. The velocity of these protons would therefore be smaller than for muons and would thus be scattered through larger angles. From equation (5.14) of Williams's treatment the mean angle of scattering comes to be 14.4°. Thus the contribution of protons to the distribution is negligibly small. It was therefore concluded that all the observed particles were muons.

/5.5.

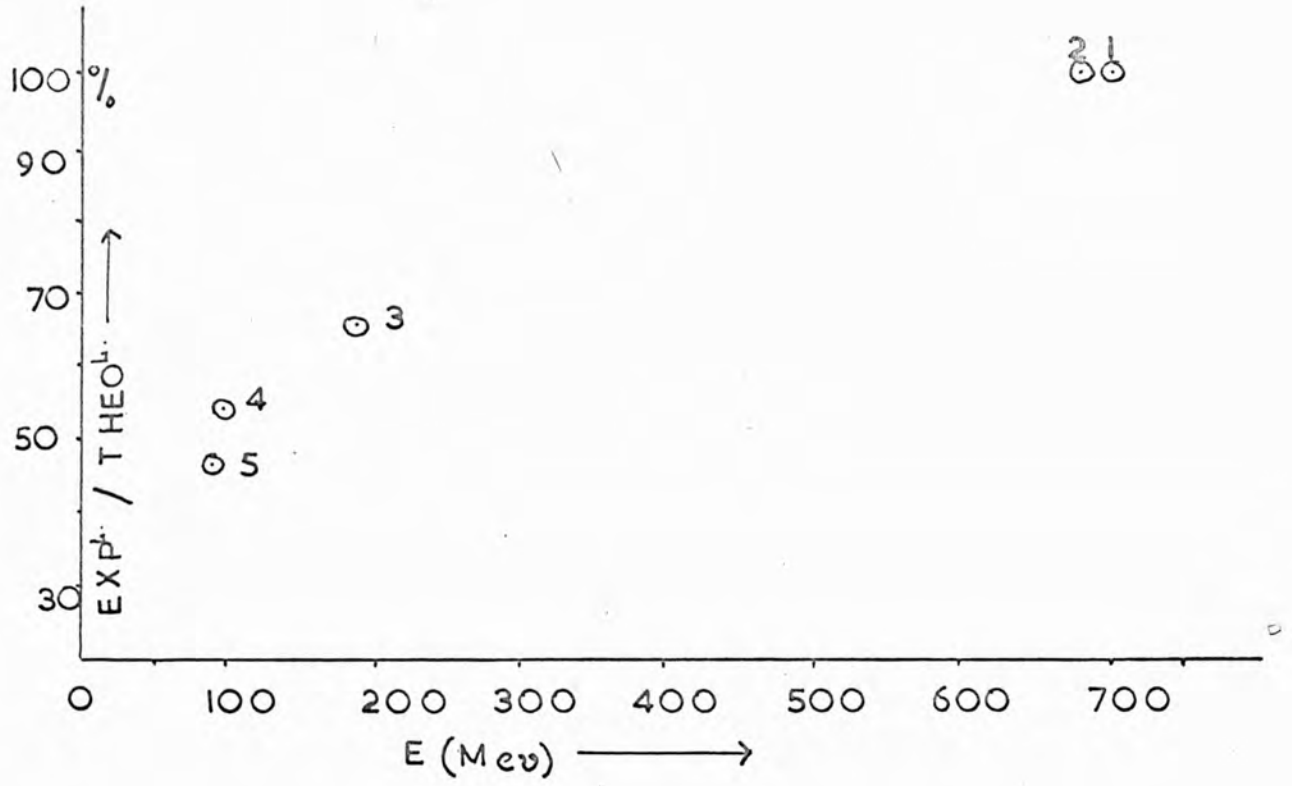

(1) Wilson (1940) (Pb.-1CM and Au. -2CM)
(2) Code (1941) (W--3.8 CM).
(3) Crewe (1951) (Pb. 1 inch)
(4) Present work (1968) (Pb.--1inch)
(5) Sinha (1945) (Pb. - 2CM)

Fig.5.7c-Dependence of ratio of experimental and theoretical values of mean scattering angle for muons in heavy and thick elements (lead and gold) .

5.5. Comparison with other results on muons.

In Figure 5.7a the amount of agreement of the present and other experiments with theory is plotted against energy. It appears that there is agreement at higher energies but the disagreement increases as the energy decreases. In each experiment a heavy scatterer was used (1 to 4 cm). From the combined results so far it is not possible to say at what energy the discrepancy begins, but 500 Mev would be a guess. The present value agrees well with the trend. For the theories to agree completely with the experimental value the critical screening angle $\bar{\Phi}$ min (or χ_α) should be about 100 times larger or alternatively $\bar{\Phi}$ max (χ_c) 10^{-2} times smaller than the estimated values. Such modified values would not appear to have any theoretical justification. It might be pointed out here, however, that the theorists have disagreed amongst themselves about the validity of their calculations (e.g. Nigam and Mathur (1961) doubt Moliere's treatment at high Z).

Williams's theory suggests that for muons of energy 100 Mev, one should expect the average number of collisions in one inch of lead to be $1.3\ 10^5$. But to account for the present results, a number of only 20 has to be substituted in the expression (5.7). This completely contradicts the sense of the theory.

/It

It is difficult to explain the discrepancies between the results and the theoretical statements - for low energy particles in heavy scatterers - with modifications for the form of the potentials, because the Fermi-Thomas and exponentially screened potentials used in the theories are well established.

5.6. Validity of Born approximation.

It has been pointed out by Parzen (1950) that the Williams's theory is based on the Born approximation which is not valid for heavy elements. It is a general property of Dirac's equation that if the potential is sufficiently strong, then no matter how high the energy of the scattering particle, the Born approximation will not be valid. This is in contrast with the Schrödinger equation, where Born approximation is always valid if the energy of the particle is large enough. The Born approximation gives good results when the potential is weak, that is, when the wave function is that of a free particle. In the Schrödinger theory as the particle energy increases the potential becomes effectively weaker, since the particle spends less time near scatterer. Thus even for strong potentials one can always find energies large enough for the potential to be considered weak. But

/in

in the relativistic Dirac's equation this is not the case. For if the particle is already travelling with almost the velocity of light, an increase in the energy will not decrease the time spent by the particle near the scatterer. If this is true, it is strange that Wilson's results for 600 Mev particles in 1 cm of lead and 2 cm of gold were in satisfactory agreement with theory. Code's result in 3.8 cm of tungsten agreed with Wilson's and thus the two results show that the Born approximation in lead might be valid for energies of the order of 10 times the rest energy of muons. But on the other hand Sheppard and Fowler (1940) found a large discrepancy for 5 to 17 Mev electrons in 0.015 cm and 0.038 cm of lead, and thus some doubt still remains on the validity of the approximation.

An attempt to modify the theory to account for this departure from the Born approximation has been made by Moliere (1948) and Nigam et al (1959) but their calculations produce only a small change and cannot explain the large discrepancies.

5.7. Comparison with the results on electrons:

Discrepancies similar to those observed with muons can be seen in the results on electrons (Fig.5.7 a and b). Although there are not many data on the scattering of electrons through metal foils the trend with energy is clear. It also

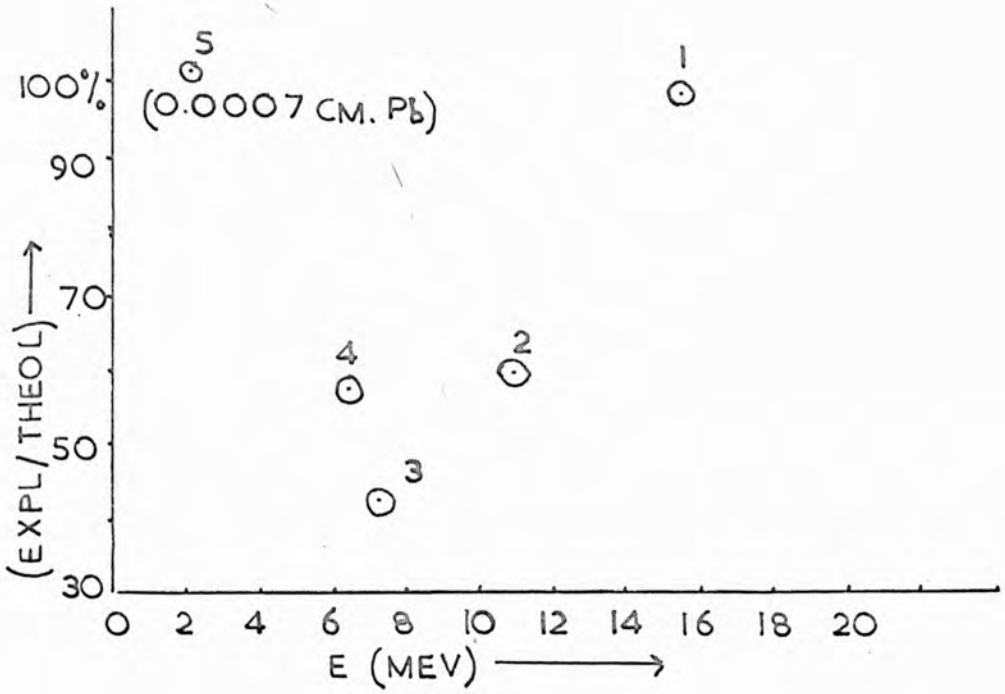

(1) Hanson (1951) (Au. -0.0187 and 0.0373 gm/ cm^2).
(2) Sheppard (1940) (Pb.-0.015and 0.038 CM.)
(3) Fowler (1938) (Pb.-0.015 cm.)
(4) Oleson (1939) (Pb.-0.072 GM/CM^2)
(5) Kulchitsky (1942) (Pb.- 0.0007 gm/cm^2)

Fig.5.7 a-Dependence of ratio of experimental and theoretical values of mean scattering angle for e^- & e^+ in heavy elements (lead and gold).

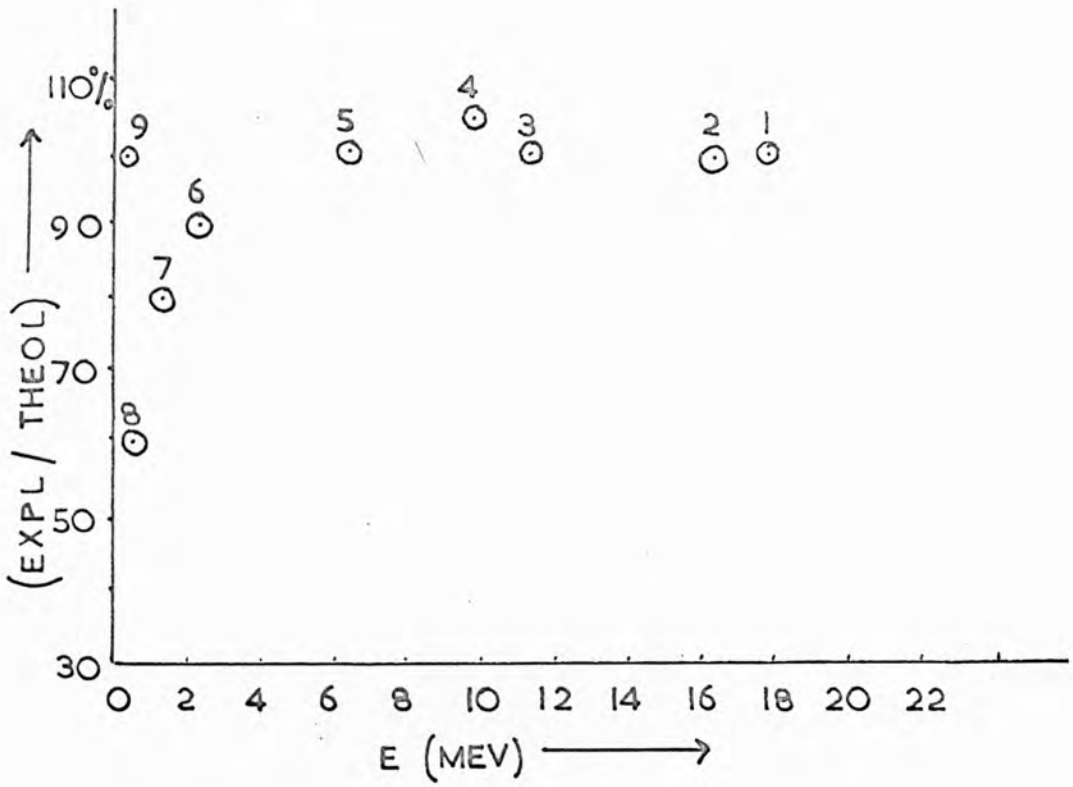

(1) Bosley and Muirhead (1952)
(2) Voyvodic (1952)
(3) Hussain (1955)
(4) Bosley and Hughes (1955)
(5) Hussain (1955)
(6) and (7) Heymann and Williams (1956)
(8) Hisdal (1952)
(9) Henderson (1957)

Fig.5.7b--Dependence of ratio of experimental and theoretical values of mean scattering angle for e^- & e^+ in G 5 (Ilford) emulsion.

appears that if the scatterer is made thinner, agreement with theory improves, e.g. (Fowler (1938) and Oleson et al. (1939), in which agreement goes up from 42% to 58%, When the thickness is reduced from 0.17 to 0.07 gm/cm^2. In the case of a very thin scatterer (e.g. 8 mgm/cm^2), Kulchitsky and Latishev, 1942) reasonable agreement was obtained even with electrons of energies as low as 2.25 Mev.

In the case of scattering in gases e.g. nitrogen in cloud chambers, there is a reasonable agreement between theory and experiment, but the experimental value has a tendency to be higher than the theoretical as the energy increases above 0.6 Mev (Strong and Roy 1963).

The study of the multiple scattering of electrons in emulsion plates also shows that there is considerable disagreement between theory and experiment, particularly at low energy as has been shown by Hisdal and in a number of other earlier experiments (table 5.2). The experiments of Bosley and Muirhead (1952) show agreement with theory but as the proportion of silver halide is decreased the experimental value exceeds the theoretical.

5.8. Discussion of the relevance of the different theories.

The above discussions clearly show the limited applicability of the theories. Williams's theory is suitable

for very high energy particles and lighter scatterers, Moliere's theory gives better results in the case of heavy scatterers and Nigam's theory explains the experimental values reasonably well in the case of thin, light scatterers, and predicts a difference between the multiple scattering of electrons and positrons (i.e. the particles of opposite charge). The latter theories modify the critical screening angle proposed by Williams. Moliere includes a correction factor which increases this angle with Z of the scatterer. In Nigam's theory a smaller correction has been used, with two impirically chosen multiplying factors, $\mu = 1.12$ and $\mu = 1.8$. In the experiment where the value 1.12 gives good results, 1.8 reduces the theoretical value to too low a value (Henderson and Scott, 1957). Also, Hanson's results (Table 5.2) show that when the scatterer thickness increases, $\mu = 1.8$ gives better results, whereas in gold Moliere's theory gives good results. In the case of Be (0.257 gm/cm^2) and Au(0.0187 gm/cm^2), $\mu = 1.8$ (Nigam) gives results 7% and 10% (respectively) smaller than theoretical.

5.9. Analysis of the present distribution of angles.

A close examination of the histogram (Fig.5.4) shows that it can be split up into two separate Gaussian distributions (Fig.5.9 a,b). The broader part if extrapolated to cover the range of 0° to 8°, with a nearly flat top, gives a mean angle

/of

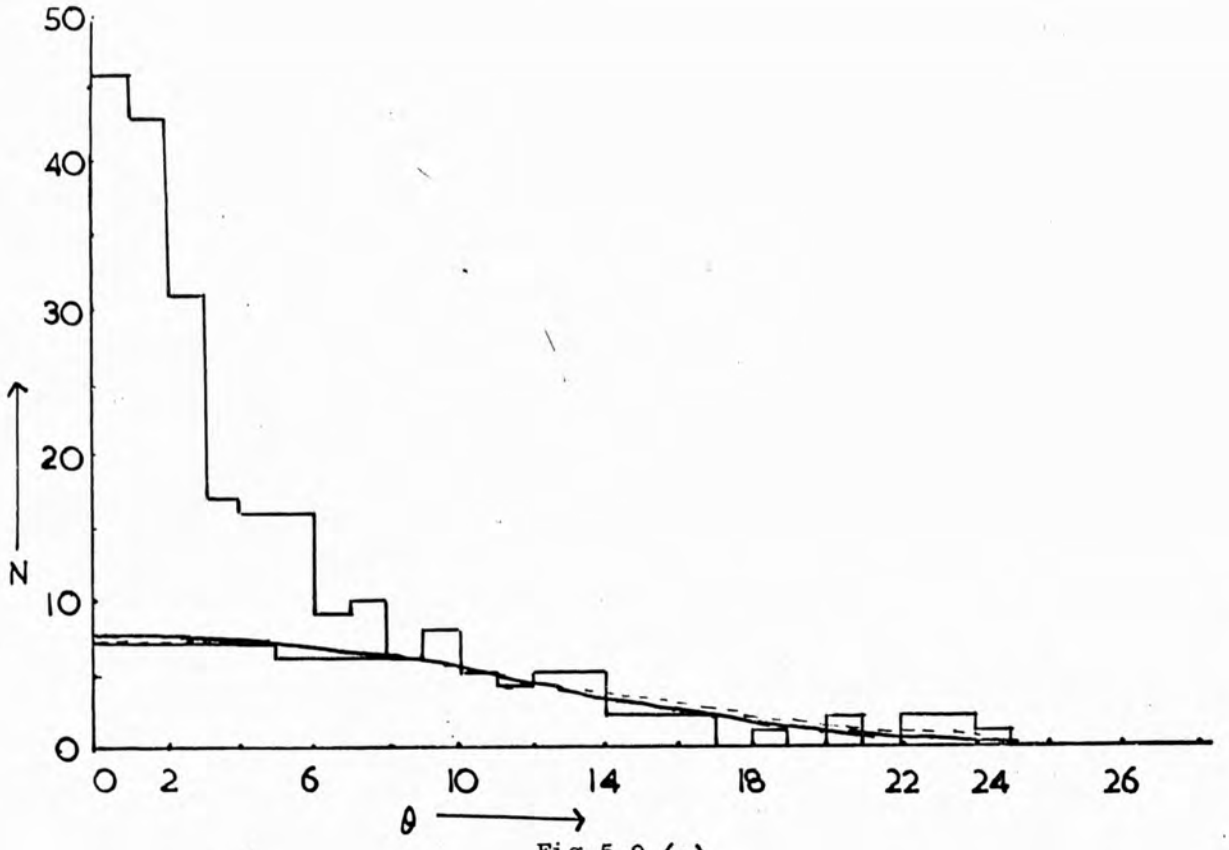

Fig.5.9 (a)

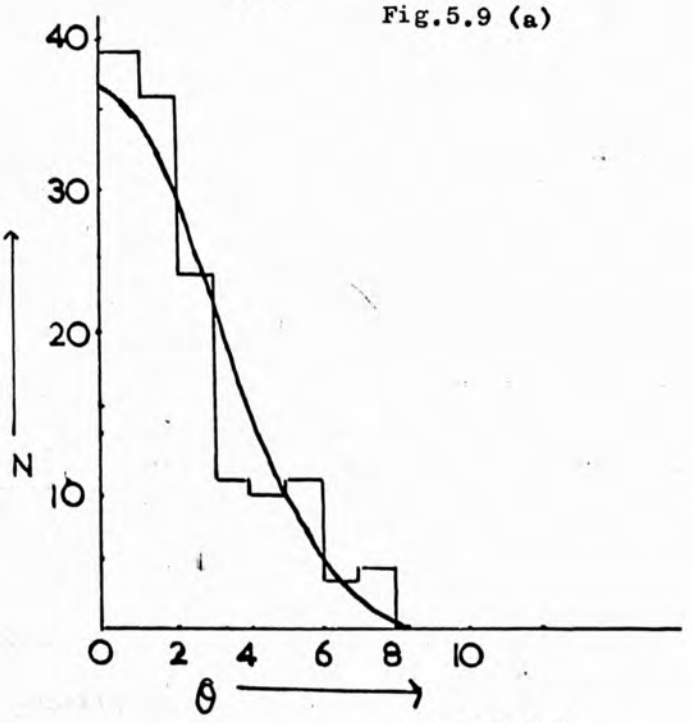

Fig.5.9 (b)

Fig.5.9 (a)-Histogram of total distribution of muons.The curve indicates an attempt to separate the distribution into two parts.The curve is a Gaussian of mean angle 8.1 °.
(b) -Histogram of subtracted component.The curve represents a Gaussian of mean angle 2.32 °.

of 8.1°, and this when corrected for geometrical factor, becomes 8.4°. The histogram compares reasonably well with the theoretical Gaussian corresponding to a mean angle of 9.4°. The value of 8.4° is 90% of the theoretical value.

The narrow component is contained in an angular range of 0° to 8°, and appears to be Gaussian in form with a mean angle of 2.32°. This second component cannot be explained by any of the theories on multiple scattering. It is interesting to note, however, that this distribution looks similar to the distribution of the charged particles emerging from a single crystal. In this case, the narrow component is considered to be due to "channelling" of particles in the inter atomic planes of the crystal (Dearnaley 1968). So far the experiments on channelling have been restricted to particles with low energies (of the order of a few Mev) traversing through very thin crystals (e.g. 20 microns), and the theories imply that this phenomenon will only be observed for low energies.

The lead plate used in the experiment was made by pouring into a one inch deep mould. The nature of the lead was investigated by polishing and etching an area. The etched surface was viewed with a microscope (x 7.5) and the crystalline structure was easily visible. Measurements indicated the average size of crystal to be about 0.2 mm, ranging up to a maximum of 0.5 mm.

Although "channelling" may explain some of the early discrepancies at the low energies, it does not appear that it can

/account

account for the narrow component of the histogram in the present experiment. It may be that a new effect is involved at these relatively high energies.

5.10. Conclusion on multiple scattering

The present work on the multiple scattering of 100 Mev muons in one inch of lead shows a large deviation from the theoretical predictions. It does not appear possible to modify the existing theories to account for the discrepancies. It may be that the explanation lies in the structure of the scattering material.

C H A P T E R V I

A SELF TRIGGERED STREAMER CHAMBER FOR LOW ENERGY PARTICLES

6.1. Low energy application

Practically all streamer chambers that have been used so far have been designed for the study of high energy particles. Such systems are normally triggered externally. In such cases the particles must pass through the scintillators and the metallic electrodes which is not feasible in the study of low energy particles. If alpha and beta particles from a radioactive source have to be studied, ideally the source would be kept inside the sensitive volume of the chamber, and so should the triggering device. In the case of intense beams random triggering might be used, but this suffers from the disadvantage that often long delays would occur, resulting in the diffusion of the primary electrons, so that the streamer would not represent the track faithfully.

In some applications neutral particles and electromagnetic radiation have to be studied by means of low energy charged particles produced in interactions. For such cases a streamer chamber with internal triggering could be very useful. An example might be the study of polarisation of fast neutrons by recording the recoil alpha tracks, if the chamber contains helium.

/In

In this chapter the design and operation of such a chamber is described. It has been found to work well with a weak thorium source.

6.2. Early work

C. Cavalleri et al. (1963) have reported a chamber, which they call a "light" or "gas amplified scintillation" chamber. The primary scintillation of the gas is picked up by a photomultiplier and used to trigger a pulse generator. A damped radiofrequency electric field from the pulse generator is applied to the chamber. The electron multiplication is caused by this field. The quality of the tracks obtained was not good. The authors said that the light output obtained restricted the method to the observation of particles of high ionisation density.

The next self-triggered spark chamber was reported by S. Yasumi, et al.(1964). This was actually a discharge chamber with a transparent H.V. electrode enclosed in a metal casing having a large glass window on the top for photography and a small quartz window on the side, through which a photomultiplier always looks inside the sensitive volume of the chamber. The Cerenkov light or the gas scintillation produced by the passage of the charged particles is picked up by the photomultiplier giving rise to a pulse which drives the high voltage circuit. They have used a photomultiplier protecting

/circuit

circuit, run by the same signal which triggers the high voltage circuit. The P.M. protecting circuit produces appropriate pulses of amplitude enough to make the voltage of the first and second dynode of P.M. equal to or less than that of the cathode during the breakdown of the chamber, and thus can protect the P.M. against a tremendous number of photons emitted at the time of sparking of the chamber.

The third self-triggered chamber was reported by Giacomich and Logonegro (1965). This was also a discharge chamber of sensitive volume 10 x 10 x 1 cm^3. On the bottom of the chamber a thin lining of ZnS(Ag) scintillator was placed and this was coupled to a photomultiplier tube. The ZnS coating was kept covered by a thin aluminium sheet of thickness equivalent to 100 Kev for 5 Mev alpha particles, to prevent the discharge light reaching the photomultiplier.

Ullman et al.(1968) have reported a double gap chamber of 4 cm gap spacing on each side and 53 cm diameter. The transparent electrodes were mylar covered wire planes, and the triggering was achieved with plastic scintillators placed outside the electrodes. The chamber was partially successful and has been used in the search for double beta decay.

6.3. Apparatus

An attempt was first made to convert the 20 cm double

/gap

gap chamber into a self-trigger device by introducing two wire grid counters in the gaps and connecting them in coincidence. First of all the detectors were tried as spark counters, but they were not successful. Next the proportional mode of operation was tried, but the signals were drowned by the pickup of the television signal on the large 60 x 60 cm^2) grids, which was as much as 10 mv. Finally, a plastic scintillator was introduced into a single 20 cm gap operated in streamer projection mode, and was found to work satisfactorily.

6.3.1. - Grid spark-counter (design and operation)

In the early attempt the double gap chamber was modified to include two wire grids within the sensitive volume as shown in Figure (6.1a). The winding of the 60 x 60 cm^2 grids has already been described, and the vacuum sealing was achieved with perspex cement and O' rings. Another such system was included in the second gap.- 1600 volts was placed between the outer plate and the first grid. When a particle passed, a localised spark occurred and the signal was taken out to trigger the Marx generator. The second grid was earthed and was included to allow the large chamber current to bypass the spark counter and its electronics. The spark pulse was sharply differentiated, giving very fast rising pulse with an

/amplitude

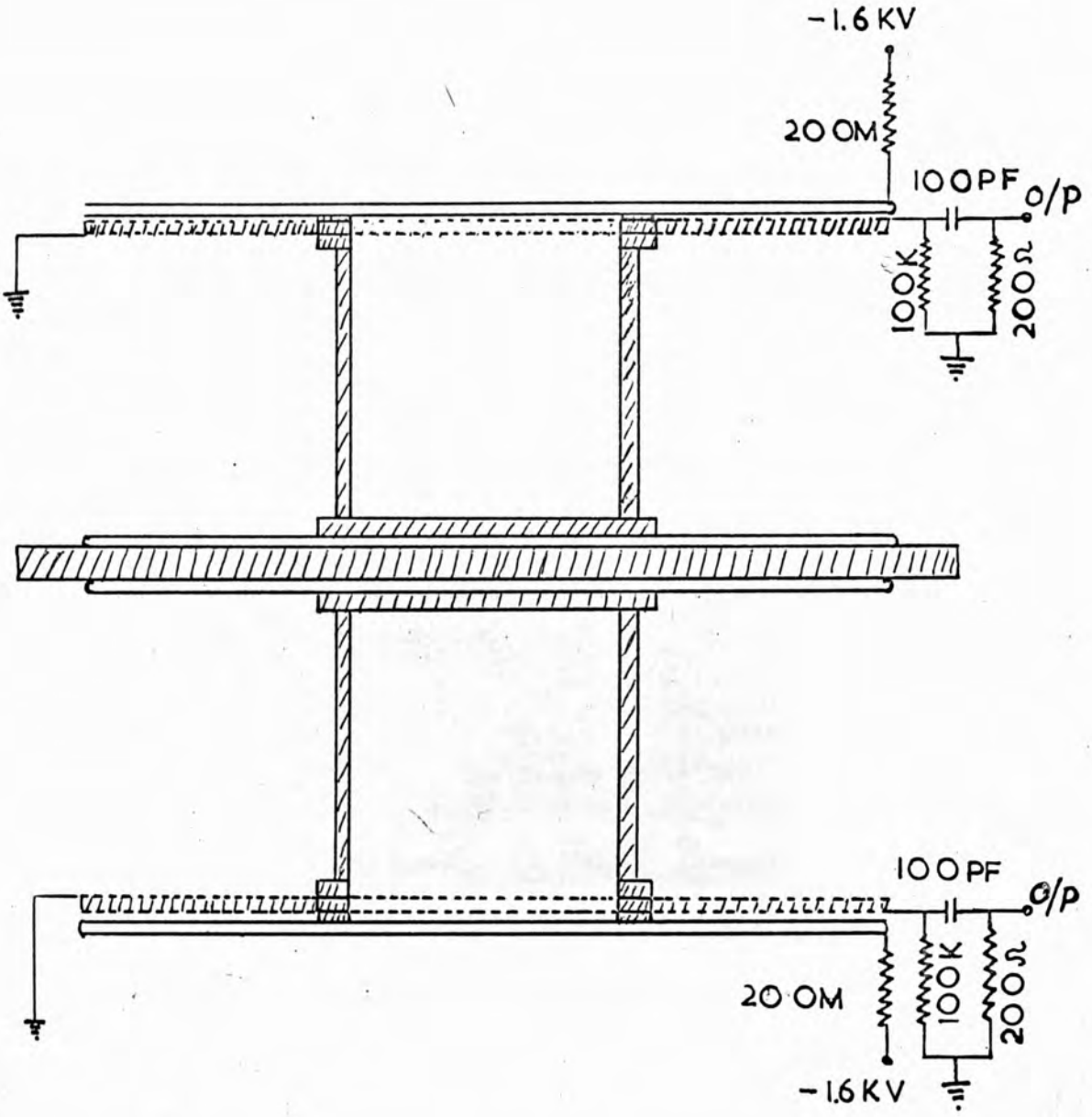

Fig.6.1a -Grid counters inside the sensitive volume of the chamber.

Fig.6.1b- Photograph of the chamber and some electronics.

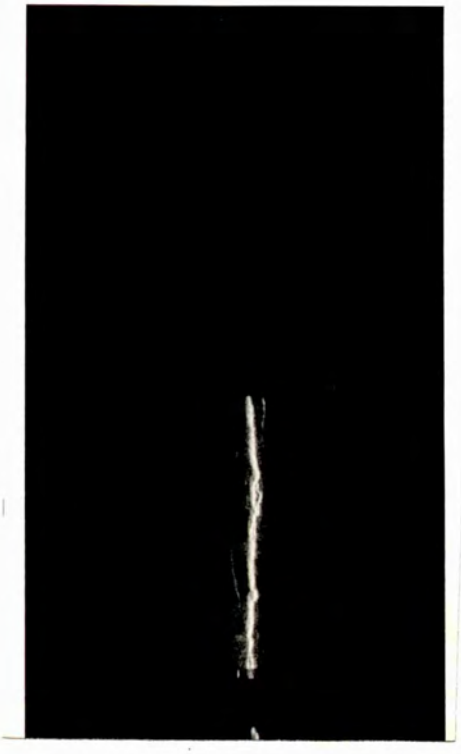

Fig.6.2-Discharge obtained on triggering by spark counter.

amplitude of about one volt. Fig. 6.1b shows a photograph of the chamber.

A quenching circuit similar to that described in section 6.4 was used. This was triggered by the counter pulse, and delivered a 250 volts 600 microseconds positive pulse to the aluminium electrode.

6.3.2. Performance

It was found that, it was difficult to operate two open spark counters in coincidence, because there was a mutual inducing of pulses between the two counters. Good electrical shielding was necessary. Another trouble was the emission of a large number of photons from the sparks in the counter. These gave rise to a large number of randomly placed ions in the sensitive volume of the chamber. These caused spurious discharges each time the chamber was triggered (see Figure 6.2). They also distorted the tracks. The tracks that were obtained were zig zag and diffused and often there was a sheet discharge along the sides of the chamber. This approach to triggering was thus abandoned.

6.3.3. Scintillator inside the sensitive volume

The Fig. (6.3) shows a nine inches square $\frac{1}{2}$ inch thick plastic NE 102A scintillator which was made to form the bottom of the chamber, the sealing being achieved with O'rings. The ceiling of the chamber was a 9 x 9 x $\frac{1}{2}$ inch^3 perspex plate with a central hole through which a source could be introduced.

/The

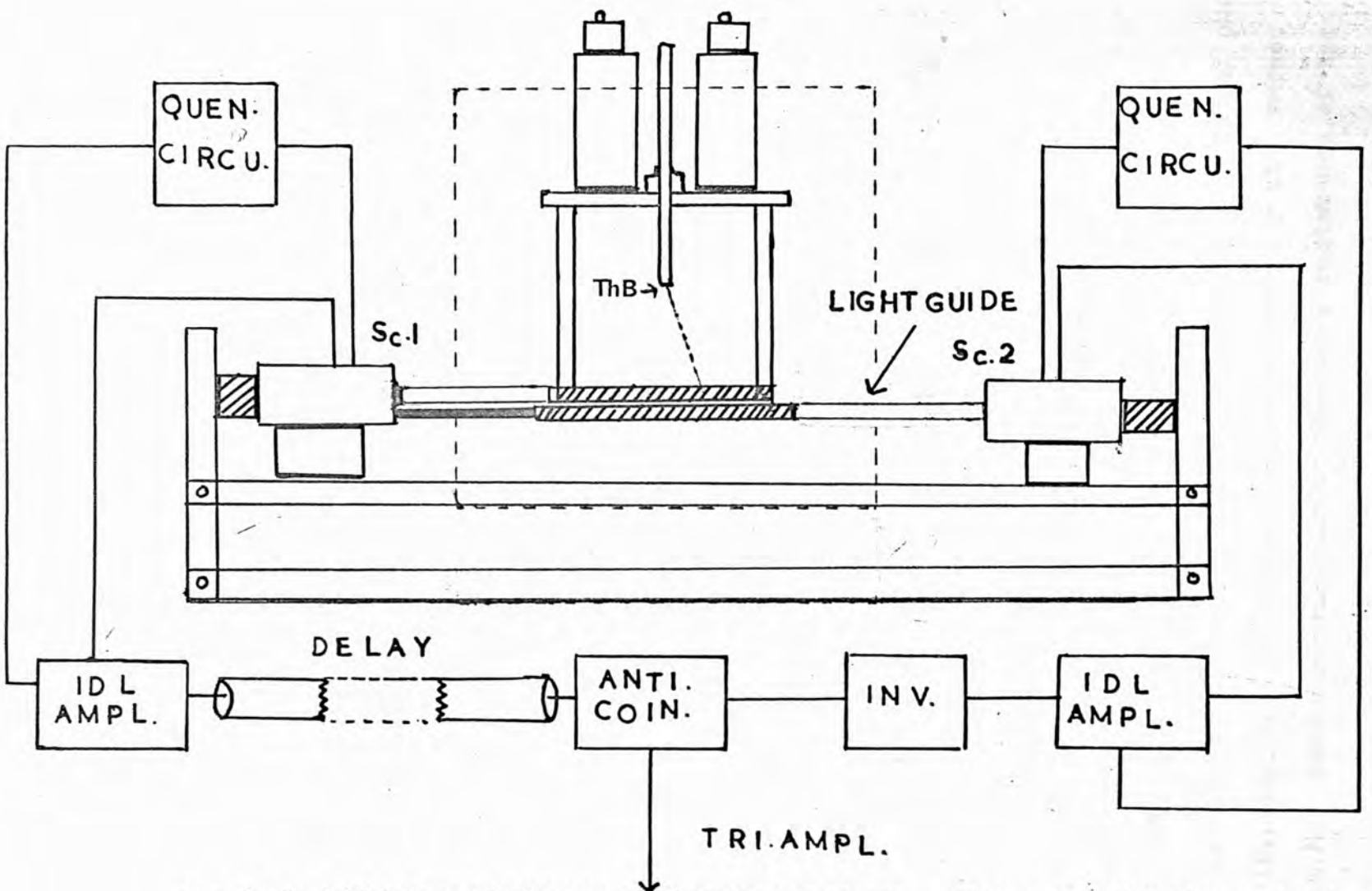

Fig,.6 .3- Self-triggered streamer chamber for low energy particles--Scintillation couter-Sc.2 in anticoincidence with ,Sc.1.The upper surface of Sc.1 is bare and the P.M. is protected by a -200V pulse of 8msec length,applied on first dynode within about 200 nsec of each event.

The light guide was a half an inch thick perspex plate. The length of the edge in contact with crystal was nine inches and that in contact with cathode of the photomultiplier was inch and a half. The light guide and the outside surfaces of the crystal was covered with thin sheets of white polystyrene foam and P.V.C. black tape to make it light.tight.

Particular care was taken to make the whole chamber light tight. The electrodes were clamped and the remaining two vertical surfaces were covered with sheets of polystyrene foam and black tape. The front surface of the chamber through which tracks were seen and photographed was surrounded by black cloth and the camera was placed inside (see Figure 6.4).

Arrangements were made to protect the photomultiplier from the photons of the discharge. An anticoincidence scintillation counter was placed just below the first counter to cutt off the cosmic ray background, as may be seen in Fig. 6.3.

6.4. Protection of the Photomultiplier

6.4.1 - High resistance potentiometer

The protection was ensured in two ways. First the potentiometer supplying voltages to different dynodes of photomultiplier, was a chain of resistances of very high value, 1.6 M each (see Fig. 6.5). The total resistance of the

/chain

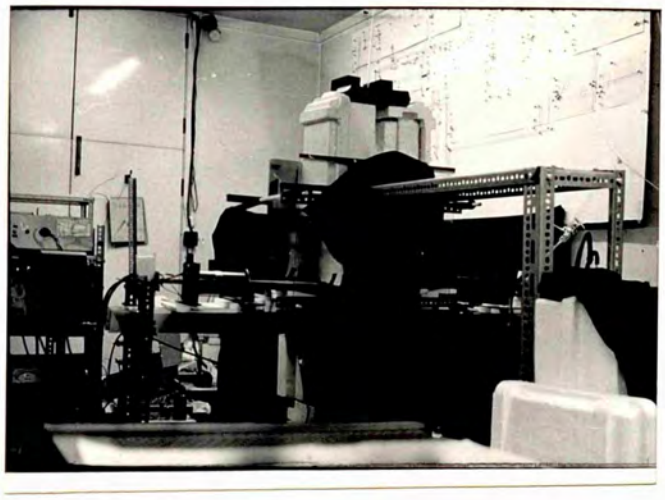

Fig.6.4- Self-triggered chamber.

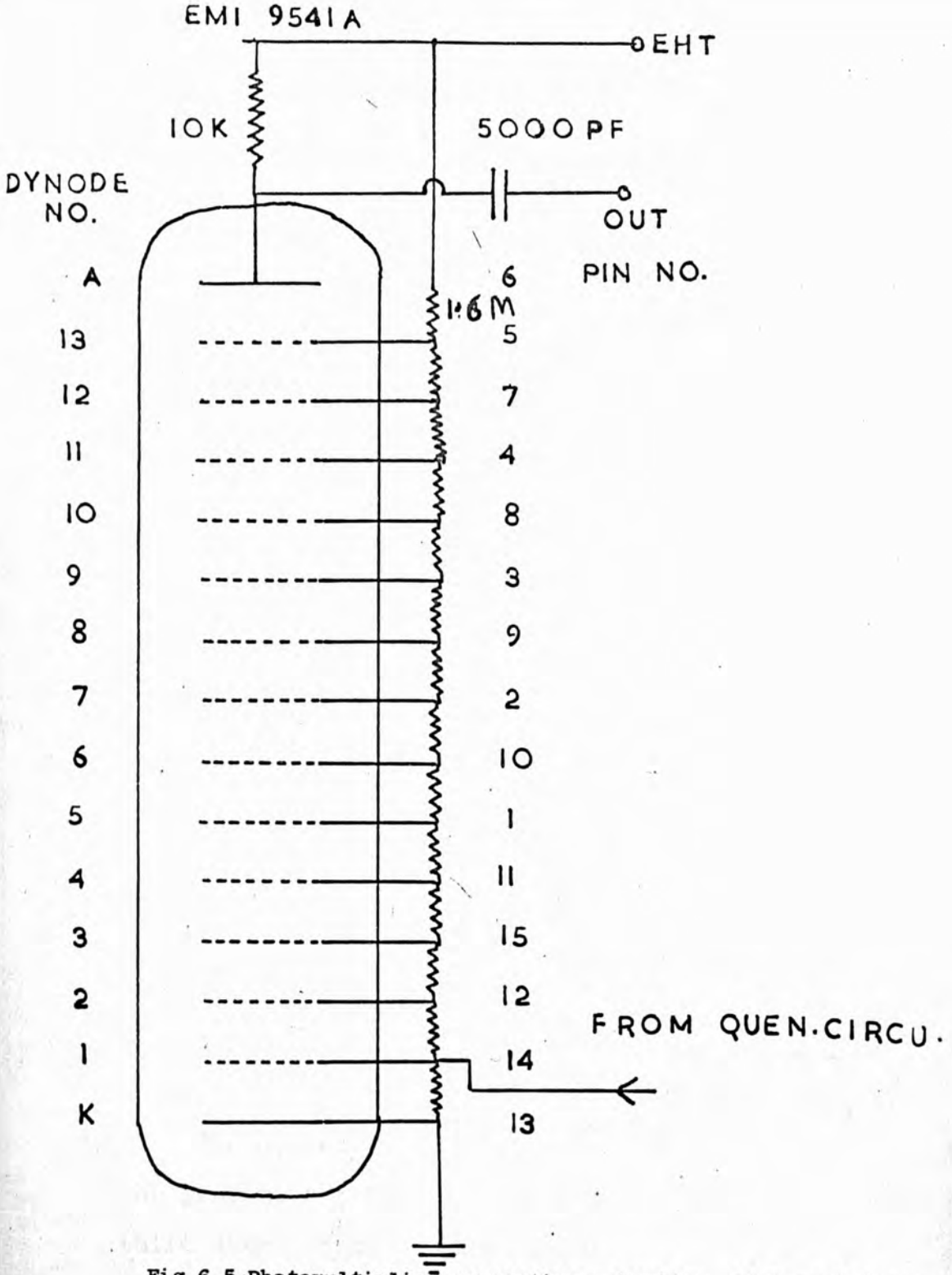

Fig.6.5-Photomultiplier connections showing high resistence potentiometer, with no bypass condensers, for protecting P.M..

chain in the 13 sstage tube was 14 x 1.6 = 22.4 M . The reason for protecting a photomultiplier is to protect the anode which may burn when a large current flows through it. The dynodes may not be affected. When there is a discharge in the chamber, a huge current flows through the chain and reduces the voltage very much and hence decreases the anode current.

6.4.2 -

Quenching Circuit - The second method which was thought to be more reliable was a quenching circuit, which gives a negative pulse of amplitude 200V and length about 8 m sec, rising in about 150 n sec.

The quenching circuit actually consisted of three stages (Figure 6.6). The first stage was a multivibrator. The valve was a double triode ECC 91. It was initiated by a 15 volts positive pulse from the amplifier/discriminator.

The second stage consists of a valve EL 360 used as an amplifier. Normally this valve remained cut off. A 40 volts positive output from the multivibrator turned it on almost completely, giving out the required quenching pulse.

The quenching pulse was applied to the first dynode of the photomultiplier through a cathode follower which was the third stage of the quenching circuit.

The 150 n sec rise time of the quenching pulse ensured

/its

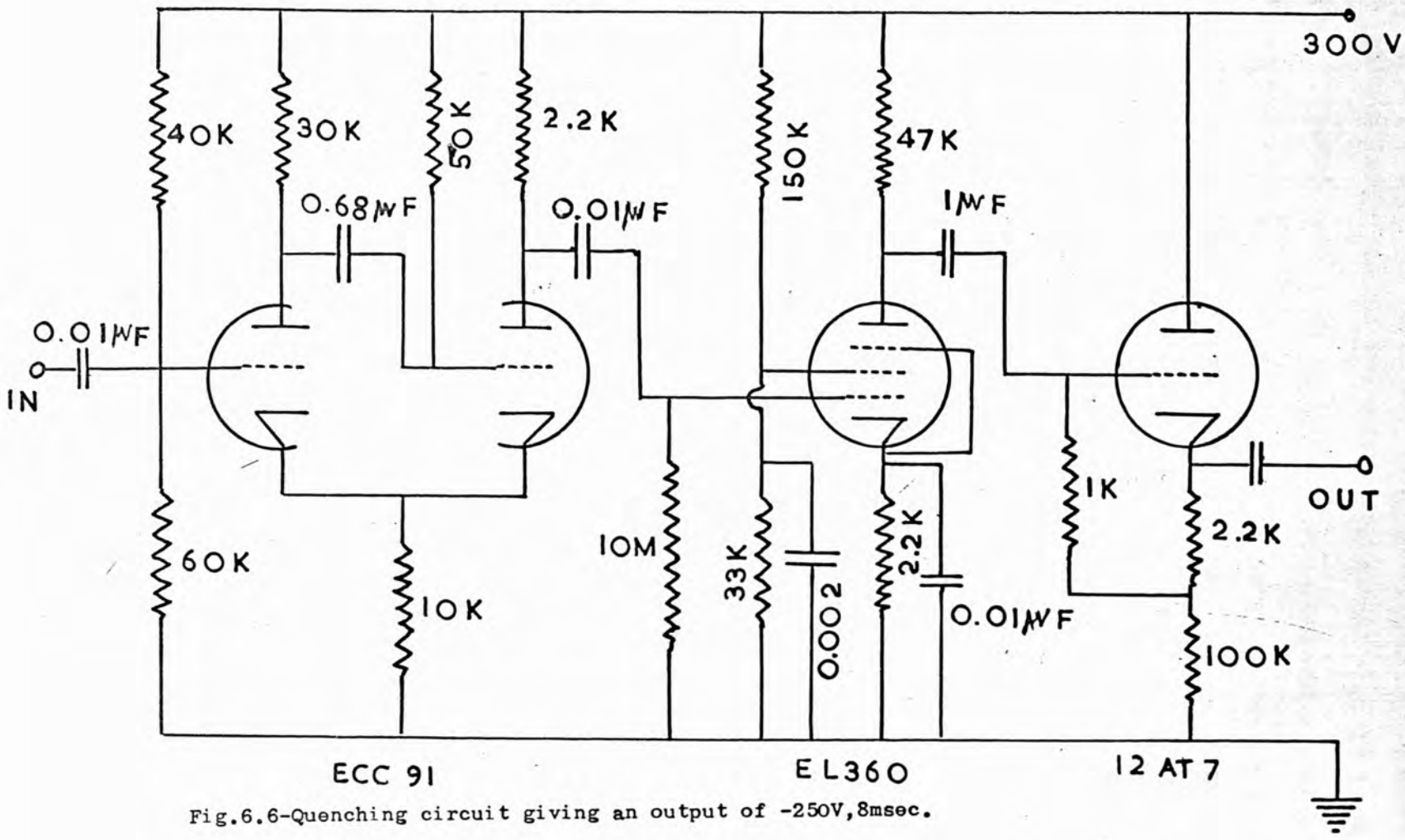

Fig.6.6-Quenching circuit giving an output of -250V,8msec.

its application to the first dynode before the chamber discharged. During this pulse the first dynode remained negative with respect to the cathode, preventing the electrons reaching it. The quenching pulse was long enough dynode to keep the first/negative until the discharge in the chamber ended completely.

With this circuit included in the system, an oscilloscope showed clearly that no pulses were obtained from the scintillator for the duration of the quenching pulse.

6.5. Anticoincidence

An anticoincidence arrangement was necessary to cut off the cosmic ray background. For this purpose, a 10 x 9 X ½ inches^3 plastic NE102A scintillator, with a similar light guide and photomultiplier was used in anticoincidence with the first scintillator.

The anticoincidence stage was a 6 BN6 valve. A bias of -3v was applied to the first grid and +0.8 volt to the third (Figure 6.6). Normally the valve remained cut off. It was switched on only when a positive pulse arrived at the first grid from the upper scintillator. If a simultaneous negative pulse arrives from the lower scintillator, the valve remains cut off. Thus the 6 BN6 only gives an output when the particle is stopped in the upper crystal. Because, most of the cosmic ray particles passed through both scintillators they produced no anticoincidence output. It

It was ensured that the negative pulses were lengthened and always arrived before the positive pulses.

On testing with no source present the system was found to trigger once or twice a minute. But when a radioactive source was introduced into the chamber, the system appeared to work well. The inverter and anticoincidence circuits are shown in Figure 6.7.

6.6. Results and discussion.

With a weak Thorium B source inserted the chamber was triggered at random, and as expected the tracks were broad and diffused. They have been shown in Figure 6.8. The photography was done in the projection mode from a distance of about 4 ft. with a stop 2.8.

In the self-triggered mode the source was placed at different distances (e.g. 18, 10 and 5 cm) above the bare upper crystal. With the anticoincidence system triggering the chamber, good tracks were obtained.

Thorium B emits two alpha particles with energies of 6.1 and 8.6 Mev in its decay to stable lead. The ranges in the neon-helium mixture were estimated to be 12 cm and 17 cm respectively. In addition the source emits beta particles with a variety of energies up to 2.25 Mev, and these of course have much larger ranges.

A selection of tracks with the source in the middle of the chamber is shown in Figure 6.9.

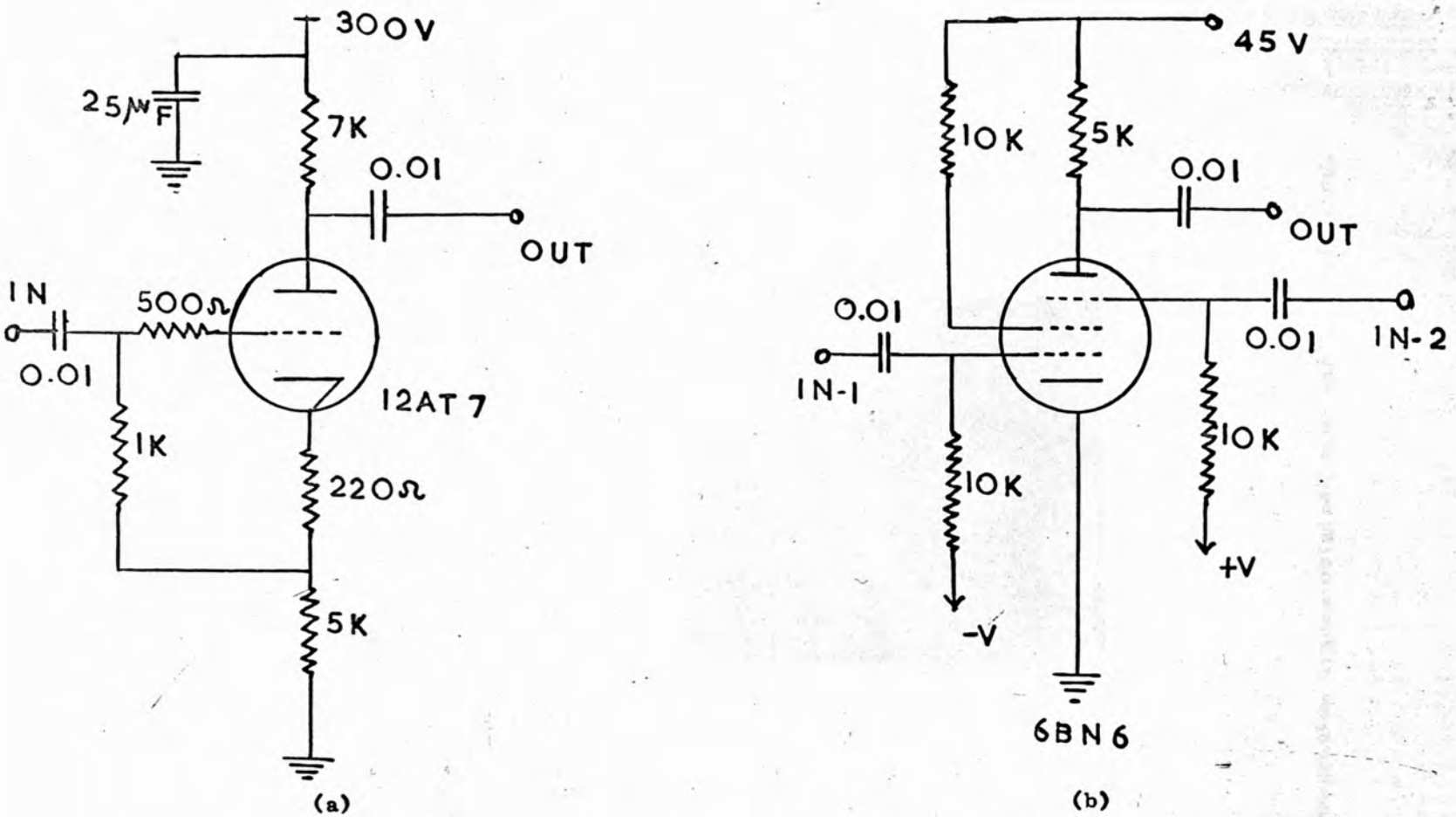

Fig.6.7 (a)- Inverter, (b) - Anticoincidence stage.

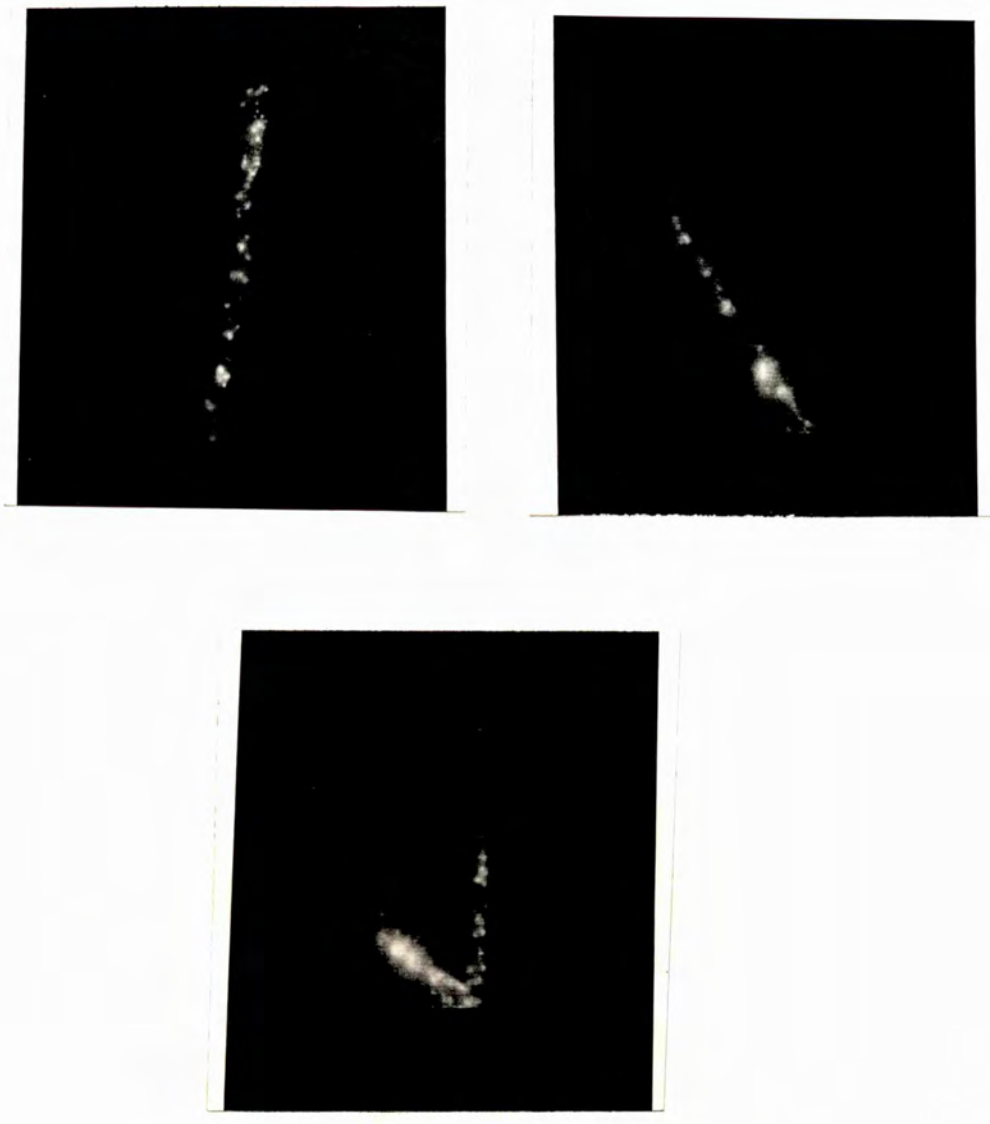

Fig.6.8- Projection tracks obtained with random triggering.

6.9 (a) Shows a typical alpha track.

6.9 (b) Shows an alpha that triggered the chamber together with a randomly coincident alpha moving horizontally.

6.9 (c) The decay of Th C is such that a beta particle is often emitted immediately after the alpha ($\sim$ 300 n sec) and the figure shows both the particles. The alpha track is characterised by a much brighter track.

6.9 (d) Shows a similar case to (c) but the triggering has been done by the beta only, and the alpha appears to have stopped in the gas. The brighter end of the track corresponds to the greater ionisation just before stopping.

6.9 (e) This shows a beta track. Because the β tracks in the negative are much fainter than the alpha, a high contrast print is required and consequently the exposure time has to be adjusted carefully.

In the projection mode the alpha tracks are quite different from those of cosmic rays. The light emission appears to be very high and this corresponds to a high primary ion density, which is of the order of thousand/cm. The avalanches probably coalesce before they grow to full size, when inhibition takes place. The small side tracks in Figure 4.10 have a similar look. The high primary ion density is also the reason for the tracks being a bit thicker than the cosmic ray tracks.

/The

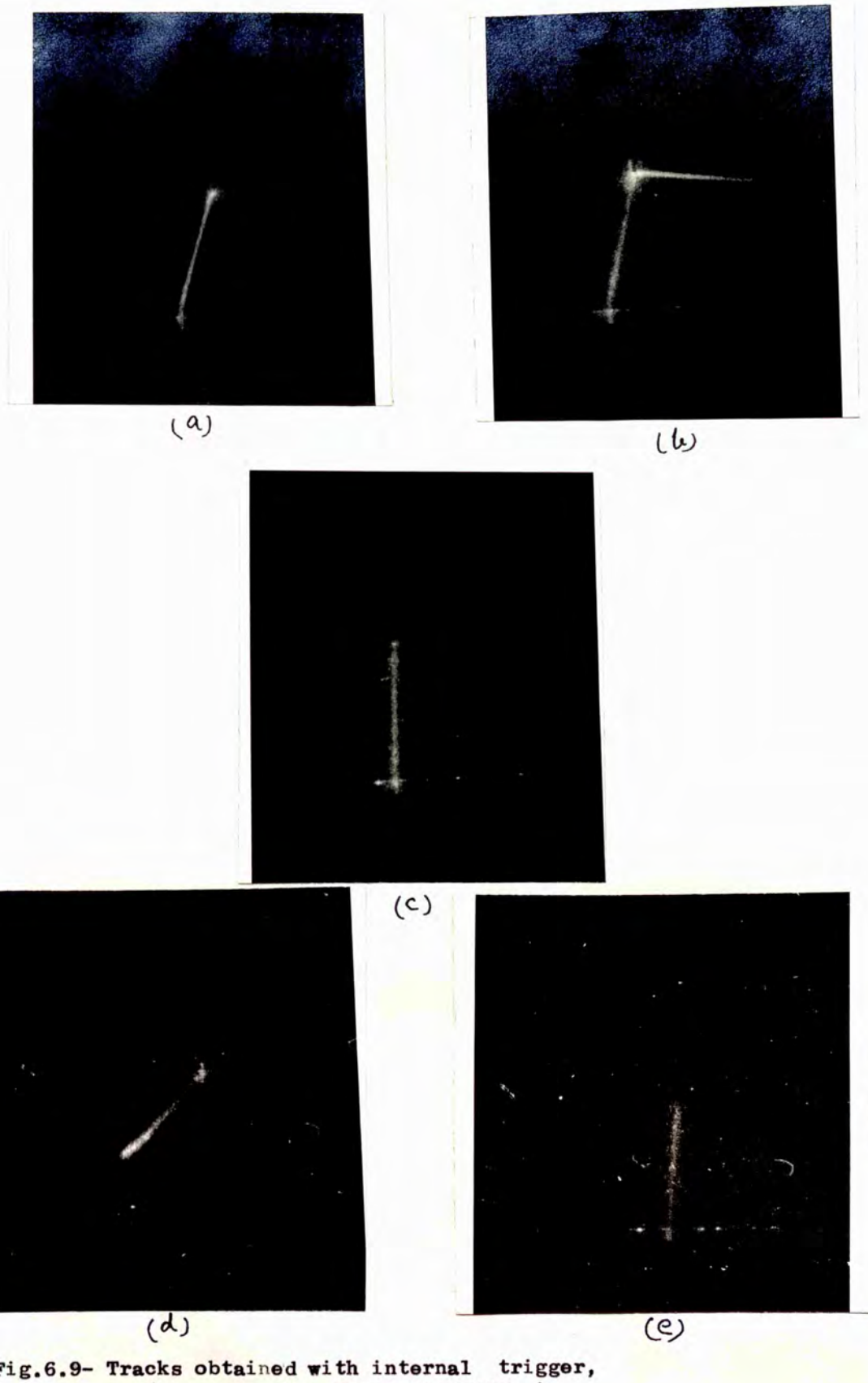

Fig.6.9- Tracks obtained with internal trigger,
(see page 113 for explanation).

The quality of the tracks in this self triggered chamber is better than those previously reported. The chambers by Cavalleri et al. (1963) and Giacomich and Lagonegro (1965) were not so successful because the light emission was very small.

A streamer chamber which has just been reported by Ullman et al (1968) for use in low energy application, is not strictly internally triggered because the scintillators were outside the wire electrodes, which was the cause of a lot of spurious discharges.

One advantage of the present device is that the source can be kept anywhere in the chamber. This would enable one to put a target right inside the sensitive volume and one could observe the products of reactions.

This chamber can also be operated in the continuous streamer mode (Chapters II and IV), by changing the configuration of the electrodes and scintillator. In that case, if a lead HV electrode is used, the precise determination of the direction of gamma rays can be made by studying the pair production.

This method of self-triggering might thus be applied to a variety of problems in which the directions of low energy particles must be recorded.

A P P E N D I X A

Moliere's theory of multiple scattering

Moliere adopts a method originally invented by Wenzel (1922) which consists of first determining separately, contributions to the scattering distribution due to the particles scattered once, twice ..... n times in a layer of matter, then summing these contributions to obtain the total angular scattering distribution. The improvement due to Moliere is the evaluation of these angular distributions on the basis of quantum mechanical solution of single scattering problem. He uses approximation of small angle scattering and therefore an expansion in Bessel function. Fourier integral has been used for the distribution of projected angles.

In this theory it has been shown that the scattering depends only upon a single parameter, describing the atomic screening, the critical screening Φ min, which can be calculated for the Fermi-Thomas distribution of electrons in atom, or for any more accurate electron distribution.

The Fermi-Thomas electronic screening field

$$V(r) = -\frac{zZe^2}{r}\,\omega(r\lambda_0) \qquad \text{A.1}$$

$\omega(r\lambda_0)$ is Fermi-Thomas function represented by a sum of three exponentials. Using this potential and first Born

/approximation,

approximation, he obtains an expression for the critical screening angle which is valid at both limits $\gamma << 1$ and $\gamma >> 1$ and also holds good with sufficient approximation in the intermediate cases.

$$\Phi_{min} = \Phi_0 (1.13 + 3.76\gamma^2)^{1/2} \qquad A.2$$

$(1.13 + 3.76\gamma^2)^{\frac{1}{2}}$ represents Moliere's correction factor

$$\Phi_0 = (\hbar/p)(z^{1/3}/0.885 a_0) = (\hbar/p)\lambda_0 \qquad A.3$$

a_0 = Bohr radius = 0.529×10^{-8} cm

$$\Phi'^2_{min} = 1.167 \Phi^2_{min} \qquad A.4$$

Wenzel's method of calculation leads to the definition of the parameter B which is given by the expression

$$B - \log B = b \qquad A.5$$

$$b = \log(\pi\delta^2/\Phi'^2_{min}) = \log(\Omega_4) \qquad A.6$$

where Ω_4 is a measure of the average number of collisions.

For approximation to be valid $1/B^n$ must be negligible for $n > 2$. This would be the case for $B \geq 4.5$, a condition satisfied by all materials for $t \geq 10^{-3}$ cm.

The root mean square value of the projected angle of scattering is given by

$$\langle\theta\rangle = \delta B^{1/2}[1 + 0.982/B - 0.117/B^2] \qquad A.7$$

Nigam's theory of multiple scattering

Nigam (1963) derived expression for the mean projected angle of multiple scattering, using the distribution function for multiple scattering derived by Nigam et al. (1959). He says that although Moliere's theory has been widely applied in interpretation of experimental results, Nigam et al. have pointed out that the formula given by Moliere for the scattering cross section of a charged particle by an atom in his theory of multiple scattering is inconsistent. The reason is that the Moliere's calculation of the scattering amplitude includes an inconsistent expansion of the phase-shift in powers of $\gamma = Z/137.\beta$

Dalitz's relativistic expression for the single scattering cross section derived in the second Born approximation for the scattering of spin half charged particle by exponentially screened coulomb field has been used and the distribution function for multiple scattering has been calculated in powers of γ in a consistent manner by Nigam et al.(1959)

The exponentially screened coulomb potential is

$$V(r) = (zZe^2/r)\exp(-\lambda r) \qquad \text{A.8}$$

Where the screening parameter $\lambda = \mu\lambda_0 \cdot \mu$ is an adjustable parameter of the order of unit, which compensates for the use of a single exponential as the screening factor of the coulomb field of an atom instead of a sum of three exponentials as done by Moliere.

/The

The expression for the screening angle has been derived from the distribution function

$$\chi_\alpha = \chi_0\left\{1 + 2\alpha\chi_0\left[\frac{1-\beta^2}{\beta}\log\chi_0 + \frac{0.231}{\beta} + 1.448\beta\right]\right\}$$

where $\chi_0 = \mu(\hbar/p)(z^{1/3}/0.885a_0)$, $\alpha = -zZ/137$ A.9

The Moliere's correction term $3.76\gamma^2$ is large for high Z. Thus, the effect of the deviation from the first Born approximation on the screening angle, as estimated by Nigam et al. is much smaller than as given by Moliere. This is as it should be since the deviation from the first Born approximation is very small at small angles which go into the definition of screening angle.

The equation (A 9) shows that there are different screening angle and hence different multiple scattering for negatively charged particles (z = -1) and positive charged particles (Z = +1). In Moliere's theory α appears in even power, giving the same value for the particles of both the charges.

The parameters in terms of which multiple scattering is described are χ'_α, ξ, b and B defined by the following expressions

$$\left.\begin{aligned} \log(2/\chi_\alpha) &= \log(2/\chi'_\alpha) - \tfrac{1}{2} + C - (2\alpha\chi_0/\beta)(1-\beta^2)(1-C) \\ \xi &= 1 + (2\alpha\chi_0/\beta)(1-\beta^2) \\ b &= \xi\log(\chi_c^2/4) - \log(\chi'^2_\alpha/4) \\ b &= B - \xi\log B \end{aligned}\right\} \text{A.10}$$

where c = 0.577215 is the Eauler's constant. ξ is very close to unity and its value may be of any importance only when comparing the multiple scattering of particles of equal mass and energy but of opposite charges.

/The

The root mean square projected angle of scattering

$$\theta = \varphi \chi_c \sqrt{B} \qquad \text{A.11}$$

where

$$\varphi = k\left\{\bar{\varphi}_0 + \frac{1}{B}(\bar{\varphi}_1' + \bar{\varphi}_1) + \frac{1}{2!B^2}(\bar{\varphi}_2' + \bar{\varphi}_2) + \ldots\right.$$

$$\left.\begin{aligned}
&\bar{\varphi}_0 = \frac{1}{\sqrt{\pi}}(1 - e^{-\delta^2}) \quad , \quad \delta = \pi / \chi_c \sqrt{B} \qquad \text{A.12}\\
&\bar{\varphi}_1 \simeq 0.5538\,\delta - \delta^{-1} - \delta^{-2}\\
&\bar{\varphi}_2 \simeq -0.1320 - \tfrac{1}{3}\delta^{-3}\left(\log(2\gamma\delta) + \tfrac{1}{3}\right) \qquad \text{A.13}\\
&\bar{\varphi}_1' \simeq (-2\alpha\beta\chi_c\sqrt{B})\left[0.01804 - \log\delta + 0.75\,\delta^{-2}\right]\\
&\bar{\varphi}_2' \simeq (-4\alpha\beta\chi_c\sqrt{B})\left[0.2886 + \delta^{-2}(1.5\log\delta - 0.0945)\right]\\
&k = \mathrm{Exp}\left\{\frac{\chi_c^2 B}{16}\left[1 + \frac{\delta\pi\alpha\beta}{B} + \frac{2\xi\log\xi}{B} + \right.\right.\\
&\qquad \left.\left.\frac{8(\beta^2 + \pi\alpha\beta)}{B}\left(c - \log(\chi_c\sqrt{B})\right)\right]\right\}
\end{aligned}\right\}$$

and

$$\chi_c^2 = 4\pi N t e^4 z^2 Z(Z+1)/(p\alpha\beta)^2 \qquad \text{A.14}$$

When

$$\chi_c\sqrt{B} \longrightarrow 0$$

$$\theta = (1/\sqrt{\pi})\left[1 + 0.982/B - (0.117/B^2) + \cdots\right] \qquad \text{A.15}$$

which is the same as that obtained by Moliere's theory.

A P P E N D I X B

ON FLUCTUATING DELAY IN SPARK COUNTER

It was reported by Singh and Saha (1961) that a multiwire spark counter can give very fast rising pulses which can be used in fast coincidence work. But Marinescu et al. (1967) measured the fluctuating delay between the passage of the charged particle and the appearance of the pulse. The experiment was done in air and they found a standard fluctuation of about 150 n sec. which shows that spark counters cannot be used for fast coincidence work.

In the present work an attempt was made to measure this time fluctuation in the neon-helium spark counter described in Section 6.3. Because it was difficult to use two open spark counters in coincidence due to their mutual inducing of pulses it was decided to use a scintillation counter and a spark counter in coincidence.

A time to pulse height converter shown in Figure B.1 consisting of a 6 BN 6 valve and E 180 F limiters was built. The output was amplified and fed into a multichannel analyser. Figure B.2 shows shift produced by a delay of 55 n sec, when the spark pulses were split up into two before being sent to limiters.

To obtain satisfactory measurements a fast discriminator would be required in the scintillation counter arm. At this stage, however, it was decided to give priority to the steamer chamber development and this line was abandoned.

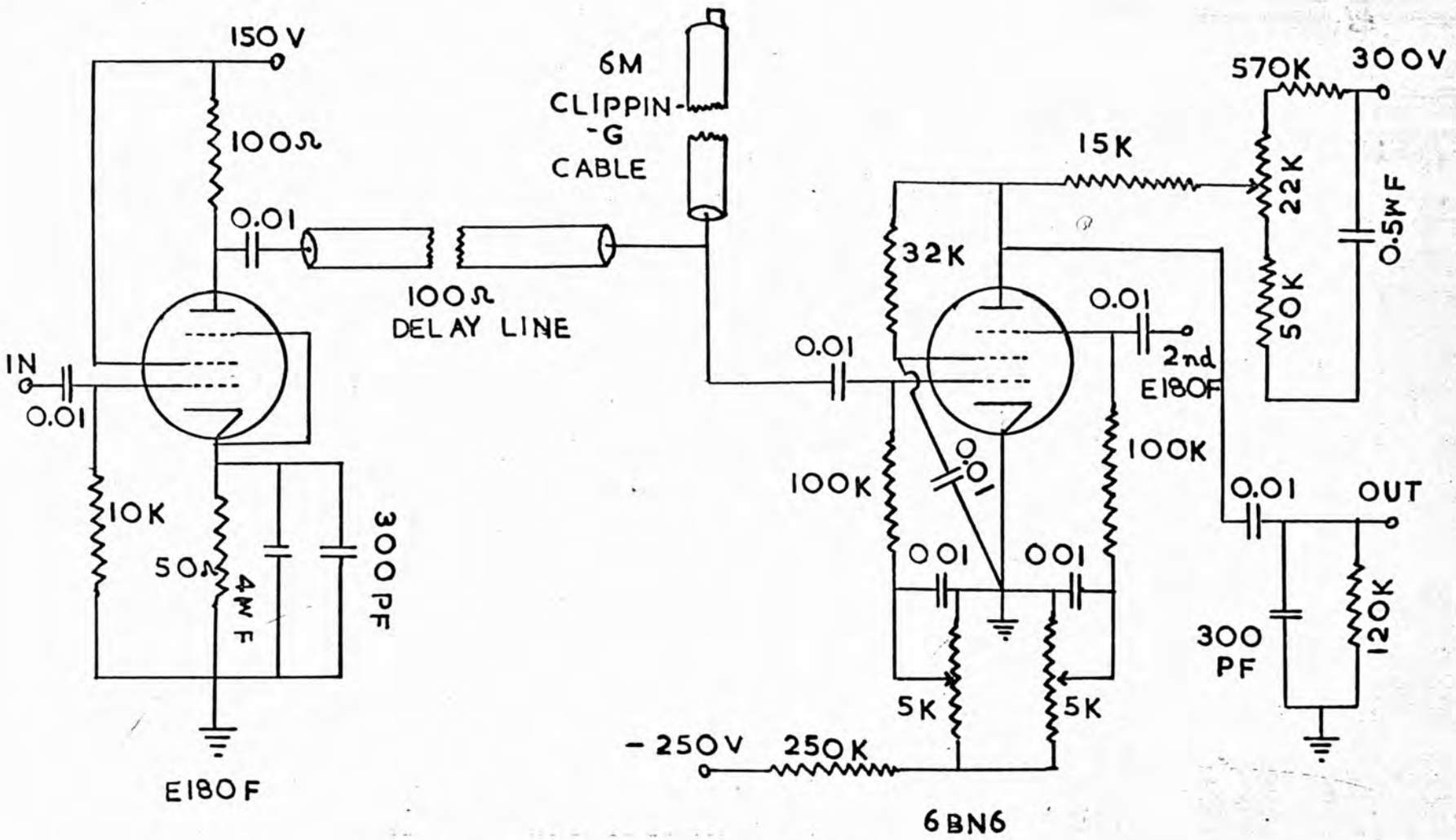

Fig. B.1- Time to pulse height coverter.

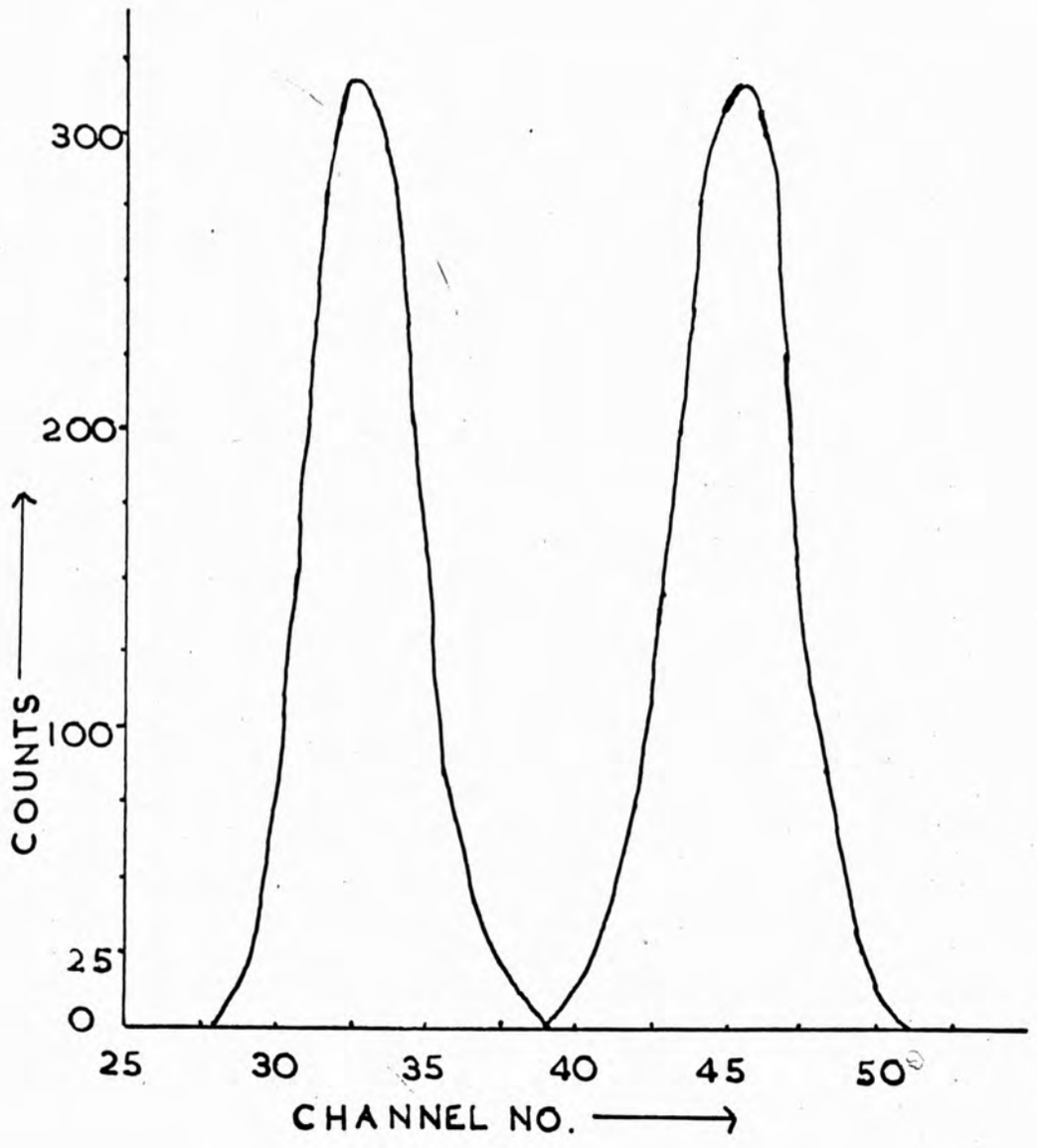

Fig. B.2-Promt curve obtained when the spark pulses were split up into two before being sent to limiters.The shift has been produced by 55 nsec delay.

A C K N O W L E D G E M E N T

I am extremely grateful to Dr. P. Rice-Evans for his excellent supervision throughout the work, and to Professor H. O. W. Richardson and Mr. R. N. Thomas for their interest. I thank Professor F. F. Heymann of University College (London) who allowed me to use the digitised microscope and Mr. Cecil Kaplinsky for his help in computation.

I would like to thank the Central Research Fund and the Science Research Council for their help to purchase some of the equipment. I am grateful to Bedford College and University of Bihar (Muzaffarpur) for support.

I would also like to thank Mr. W. A. Baldock, Mr. A. K. Betts, Mr. F. A. Grimes and Mr. J. Kavanagh for their technical assistance, and Miss J. Franklin for typing.

My warm thanks go to my wife for her encouragement and sacrifice.

REFERENCES

Alikhanian, A.I., Asatiani, T.L., Matervosian, A.M. and Sarkhatunian, R.O., Physics Letter, 4,295, 1963.

Alikhanian, A.I.
Prog. in Nucl.Tech. and Inst., North Holland Publication 1965.

Atikhanian, A.I., Asatiani, T.L., Materovosyan, E.M., Nazaryan, A.A., Sharkhatunyan, R.O., Jr.Expt. and Theo.Phys.(U.S.S.R.), 45, 1684, 1963. J E T P (U.S.A.), 18, 1154, 1964.

Bolotov, V.N., Devishev, M.I. and Klimanova, L.F. Nucl.Inst. and Meth. 44,77,1966.

Bolotov, V.N., P.T.E. No.2 50-57 March 1964

Borizov, A.A., Dologoshein, B.A. and Luchkov, B.I., P.T.E., No.2, 170, March, 1962.

Bose, D.M. and Choudhary , B. Nature, 147, 240, 1941.

Bosley, W. and Hughes, L.S. Phil. Mag. 46, 1281, 1955.

Bosley, W. and Muirhead, H. Phil. Mag.43. 62, 1952.

Brookes, G.R., and Garvey, J. Nucl. Inst. and Meth. 33,335,1965.

Bulos, F., Odian, A., Villa, F. and Yount, D. SLAC Report No.74 Sept. 1967.

Bunaciu, T., and Kullander, S. Nucl.Inst. and Meth. 58, 173, 1967.

Cavalleri, C., Gatti, E., and Redaelli. Nucl.Inst. and Meth. 20,238,1963.

Charpak, G. and Massonet, L.Rev. Sc. Inst. 34, 664, 1963.

Chikovani, G.E., Roinishvili, V.N., and Mikhalov, V.A. Nucl.Inst. and Meth. 29, 261, 1964.

Chikovani, G.E., Roinishvite, V.N., Mikhalov, V.A. and Javrishvili, A.K., Nucl.Inst. and Meth. 35, 197, 1965.

Code, F.L. Phys.Rev. 59, 229, 1941.

Conversi, M. and Gozzini, A.. Nuov.Cimen.2, 189, 1955.

Cork, B. . Rev. Sc. Inst. 32, 486, 1961.

Cranshaw, T.E. and de Beer, J.F., Nuo.Cime. 5,1107, 1957.

Crewe, A.V. Proc. Phys. Soc. (London) A64, 660, 1951.

Crewe, A.V. and Lutherland, A.E., Jr. Sc. Inst. 28, 182, 1951.

Cusak, N. and Scott, P. Phil.Mag. 46, 632, 1955.

Dalitz, R.H. Proc. Roy. Soc. A206, 509, 1951.

Dearnaley, G., Mitchell, I.V., Nelsoh, R. ., Farmery, B.W., Thompson, M.W., Phil. Mag. 18, 985, 1968.

Di Munari, G.M., and Mambriani, G. Phys.Rev. 153,388,1967.

Dickey, F.R. Jr. Appl. Phys. 23, 1336, 1952.

Dolgoshien, B.A., Rodionov, B.U. and Luchkov, B.I. Nucl. Inst. and Meth. 29, 270, 1964.

Druyvesteyn, M.J. and Penning, F.M. Rev. Mod. Phys. 12, 87, 1940.

Eschstruth, P.T., Franklin, A.D., Hughes, E.B., Gilles B. W., Murphy, F.V., Reading, D.H., and Wright, K.E. Nucl. Inst. and Meth. 63, 96, 1968.

Fowler, W.H. Phys. Rev. 54, 773, 1938.

Fukui, S. and Miyamoto, S. Nuo, Cime, 11, 113, 1959.

Fukui, S. and Miyamoto, S. Jr. Phys. Soc., Japan, 16, 2574, 1961.

Garçon, J.P., Grossman, D. and Strauch, K. Rev. Sc. Inst. 36, 264, 1964.

Giacomich, R. and Lagonegro, M., Nucl.Inst. and Meth.34, 347, 1965.

Gottstein, K., Menon, M.G.K., Mulvey, J.H., Ceallagh, G.O. and Rochat, O. Phil. Mag. 42, 708, 1951.

Goudsmit, S.A., and Sanderson, J.L. Phys. Rev. 57, 24, 1940.

Goudsmit, S.A. and Clement. Nuo. Cene. 7, 331, 1950.

Groetzinger, G., Berger, M.J. and Ribe, F.L.
Phys. Rev. 77, 584, 1950.

Gygi, E. and Schneider, ., CERN report 66 - 14, 1966.

Henderson, C. and Scott, A. Pro. Phys. Soc. A70, 188, 1957.

Hanson, A.O., Lanzl, L.H., Lyman, E.M. and Scott, M.B.
Phys. Rev. 84, 634, 1951.

Heymann, F.F. and Williams, W.F. Phil. Mag. 1, 212, 1956.

Hisdal, E. Phil. Mag. 43, 790, 1952.

Hussain, A. Proc. Phys. Soc. (London) A68, 45, 1955.

Kaye, G.W.C. and Laby, T.H., Physical and Chemical constants,
1966.

Keller, L.P. and Walschon, E.G., Rev. Sc. Inst. 37, 1258, 1966.

Keuffel, J.W., Rev. Sc. Inst. 20, 202, 1949.

Kulchetsky, L.A., and Latyshev, D.G. Phys. Rev. 61, 254,
1942.

Lavoie, L., Parker, S., Rey, C. and Schwartz, D.M.
Rev. Sc. Inst. 35, 1567, 1964.

Lawrence, A.S.C., "The Scientific Photographer"
Cambridge, 1941.

Lynhimov, V.A., and Pavlovsky, F.A.
Nucl. Inst. and Meth. 27, 346, 1964.

Marinescu, L., Petrascu, M. and Vorculescu, G.
Nucl. Inst. and Meth. 54, 327, 1967.

Meek, J.M. Phys. Rev. 57, 722, 1940.

Meek, J.M. and Craggs, J.D. "Electrical Breakdown in gases"
Oxford 1953.

Menon, M.G.K., and Rochat, O. Phil. Mag. 42, 1232, 1951.

Mishra, S.R. M.Sc. project report, 1966.

Mohr, C.B.O. Proc. Phys. Soc. (London) A70, 730, 1954.

Moliere, G. Zeits f. Naturforsch. 3a, 781, 1948.

Neilson, G.C. and James, D.B. Rev. Sc. Inst. 26, 1018, 1955.

Nigam, B.P., Sundaram, M.K., and Wu, T.Y.
Phys. Rev. 115, 491, 1959

Nigam, B.P. and Mathur, V.S. Phys. Rev. 121, 1577, 1961
Nigam, B.P. Phys. Rev. 131, 238, 1963.

Oleson, N.L., Chao, K.T., Halpern, J. and Crane, H.R.
Phys. Rev. 56, 482, 1939.

Parzen, G. Phys. Rev. 80, 261, 1950.

Raether, H., Arch. Eleck. 34, 49, 1940.

Reed, R.D. Phys. Rev. 138 A1000 1965.

Rice-Evans, P. and Mishra, S.R. Amer. Jr. of Phys. 35, 357, 1967.

Ruthergten, J.G., and Patterson, J.M.
Rev. Sc. Inst. 32, 522, 1961.

Scott, W.T. Rev. Mod. Phys. 35, 231, 1963.

Sharpe, J., E.M.I. Electronics Technology, June & July 1961.

Sheppard, C.W. and Fowler, W.A., Phys. Rev. 57, 273, 1940 and
56, 849, 1939.

Simon, W.G. Phys. Rev. 136, B410, 1964.

Sing, G. and Saha, N.K. Nuc. Inst. & Meth. 13, 322, 1961.

Sinha, M.S. Phys. Rev. 68, 153, 1945.
Snyder, H.S. and Scott, W.T. Phys. Rev. 76, 220, 1949
Strong, I.B. and Roy, R.R., Phys. Rev. 131, 198, 1963.

Ullman, J.D., Bardin, R.K., Gollon, P.J., and Wu, C.S.
Nucl. Inst. & Methods. 66, 1, 1968.

Voyvodic, L., and Pickup, E. Phys. Rev. 85, 91, 1952.

Wentzel, Ann. der Physik, 69, 335, 1922.

Wick, G.C. Nuo.Cime, 1, 302, 1943.

Williams, E.J. Phys. Rev. 58, 292, 1940

Williams, E.J. Proc. Roy. Soc. A169, 531, 1939.

Wilson, J.G. Proc. Roy. Soc. A174, 73, 1940.

Wilson, J.G. Nature, 158, 414, 1946.

Yasuni, Z.S. Itoh, H. Masaike, A. and Miyake, K.
Nucl. Inst. and Methods. 31, 343. 1964.

NUCLEAR INSTRUMENTS AND METHODS 67 (1969) 337-340; © NORTH-HOLLAND PUBLISHING CO.

A WIDE-GAP STREAMER CHAMBER

P. RICE-EVANS and S. R. MISHRA

Department of Physics, Bedford College, Regent's Park, London, N.W.1, U.K.

Received 15 July 1968

A 20-cm gap streamer chamber is described together with details of the high voltage circuitry. An analysis of measurements on the tracks in the various modes of operation shows that an angular resolution of 1.5 mrad is attainable.

1. Introduction

The multigap spark chamber has become a powerful instrument in particle physics. Systems for recording the data have been developed to such a degree that they now offer automatic determination of spark addresses and on-line computer analysis of the results. Simultaneously, development has occurred both of the wide-gap spark and streamer chambers. Although they exhibit many advantages, few experiments have yet been reported in which they were employed. In the case of the most promising, the streamer chamber with its potential for isotropic response, the major difficulty lies in the limited light output from the streamers.

In the latter case, it has been found possible to photograph the tracks with fast film; but, of course, this is not ideal because of the delays involved in development. On the other hand, the detection of tracks by sonic or magnetostrictive techniques would seem inappropriate. However, it may safely be predicted that it is only a matter of time before a method similar to vidicon-scanning will be possible, either directly or with an image intensifier. Indeed the new English Electric "image isocon" may well prove to be sensitive enough for direct viewing.

It is important that knowledge of the capabilities of these chambers should not wait on the development of techniques for automatic recording. Accordingly, in this paper, the design of an isotropic streamer chamber with its associated high voltage pulse electronics is described; photographs of particle trajectories with the chamber operating in a variety of modes are presented; and quantitative estimates of the spatial resolution attainable under the different modes are given.

2. Apparatus

The streamer chamber shown in fig. 1 has a sensitive volume with dimensions: $20 \times 20 \times 20$ (cm). The 12 mm walls of the perspex box had "O" ring grooves milled in them to allow both a flexible arrangement of electrodes and evacuation prior to filling with gas. In accord with the findings of Garron et al.[1]), to ensure reasonable uniformity of electric field, large electrodes were constructed with dimensions: 61×61 (cm). Both 6.4 mm aluminium plate and also wire-grid (2 mm spacing, 0.1 mm dia. stainless steel wire) electrodes were made. The latter were wound under tension on a $61 \times 61 \times 0.64$ (cm) perspex former with a 20×20(cm)

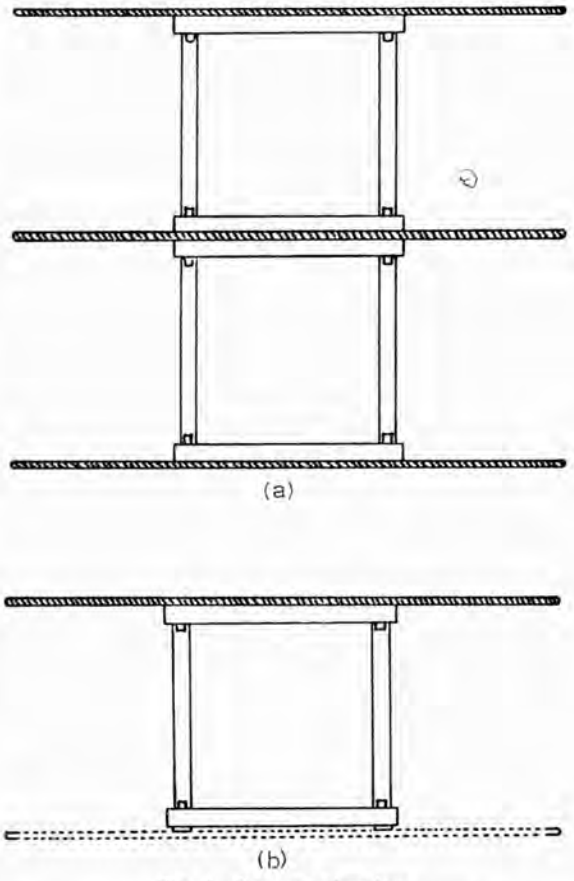

Fig. 1. Streamer chamber.

a. For continous streamer mode of operation, with aluminium plate electrodes;
b. For projection mode, photography through transparent wire-grid electrode.

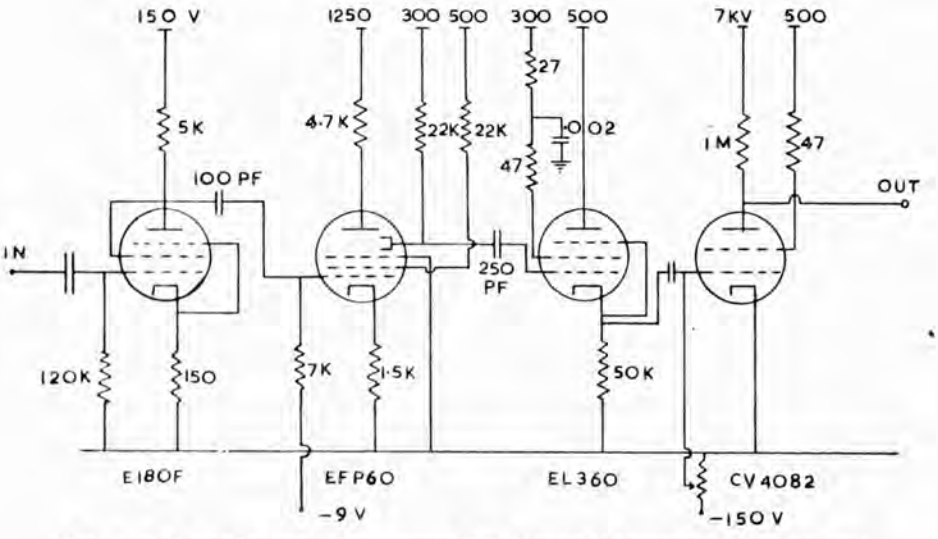

Fig. 2. a. Amplifier providing negative 6000 V pulse to trigger the first spark gap;

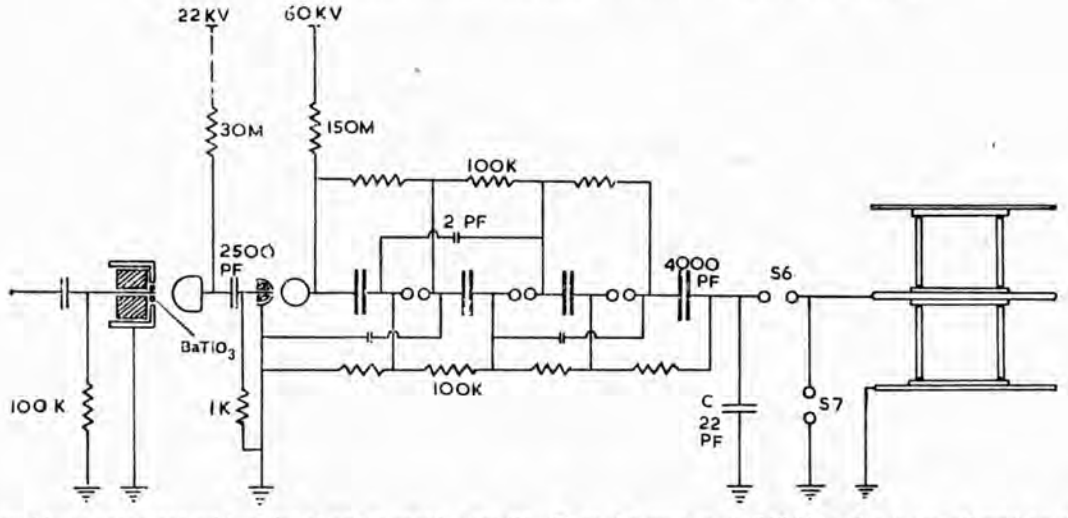

b. Four stage Marx generator with pulse shaping spark gaps S6, S7 at the output. A 240 kV pulse is transferred to the chamber electrode.

hole in the centre to correspond to the sensitive region, and thus constituted a double-plane grid. To allow "O" ring sealing, perspex spacers were cemented (I.C.I. "tensol", no. 7) so that the wires were sandwiched in the cement. The sensitive gas was a mixture of 70% neon and 30% helium. In some configurations the rear interior wall of the box was painted matt black to preclude reflections.

The high voltage electronics is shown in fig. 2. Two volt coincidence pulses from the particle counters are amplified in the valve circuit in which the CV4082 produces a sharp 6 kV output pulse. This pulse triggers the first spark gap, in which barium titanate has been used successfully to facilitate the sparking[2]). Breakdown of the 22 kV at this gap transfers the charge from capacitance 2500 pF to the first gap of the Marx generator[3]).

This generator consists of four cylindrical rapid-discharge capacitances mounted coaxially with the stainless steel spark electrodes. Each capacitance charges up to 60 kV. When triggered, the spark gaps break down as they are over-voltaged; and the final output pulse – being the series sum of the voltages – has a magnitude of 240 kV. To facilitate rapid breakdown, small (2 pF) polystyrene dielectric by-pass condensers are connected as shown[4]); and the components and walls of the generator are painted white to reflect the uv light from one gap to the next.

The rather large inductance of the Marx generator (0.8 μH) increases the rise time of the output pulse.

However, this handicap may be overcome with the use of the series-shunt spark gap method of pulse shaping[5,3]) The Marx output pulse charges up the enhanced stray capacitance C(22 pF constructed from aluminium foil and blocks of polystyrene foam). Suddenly, the series gap breaks down and the charge is rapidly transferred to the chamber electrode. The requirement of a rapid rise in voltage is important as it reduces the ion drift within the chamber. The shunt gap is adjusted to allow a pulse of suitable duration, typically 50 ns, to arrest the chamber discharge appropriately. The overall delay between the passage of the particle and the application of the high voltage is 420 ns.

3. Qualitative performance

The initial experiments have been performed with cosmic rays, the triggering being achieved with plastic scintillation counters mounted above and below the chamber. The flexible design allows the performance in the various modes to be studied.

The spark mode, with the bare electrodes exposed to the sensitive gas, was not very successful. Straight sparks were obtained but because of the large effective capacitance of the Marx generator they were very thick. We found it difficult significantly to reduce the current in the spark by using low value shunt resistors across the chamber, whilst simultaneously maintaining the high efficiency of the instrument.

When 12 mm thicknesses of perspex are interposed between the electrodes and the gas, streamer action results, that is, the only ions present in the visible track are due to multiplication in the gas and are not supplied by the electrodes. In an applied field of 12 kV/cm, for tracks lying near the direction of the

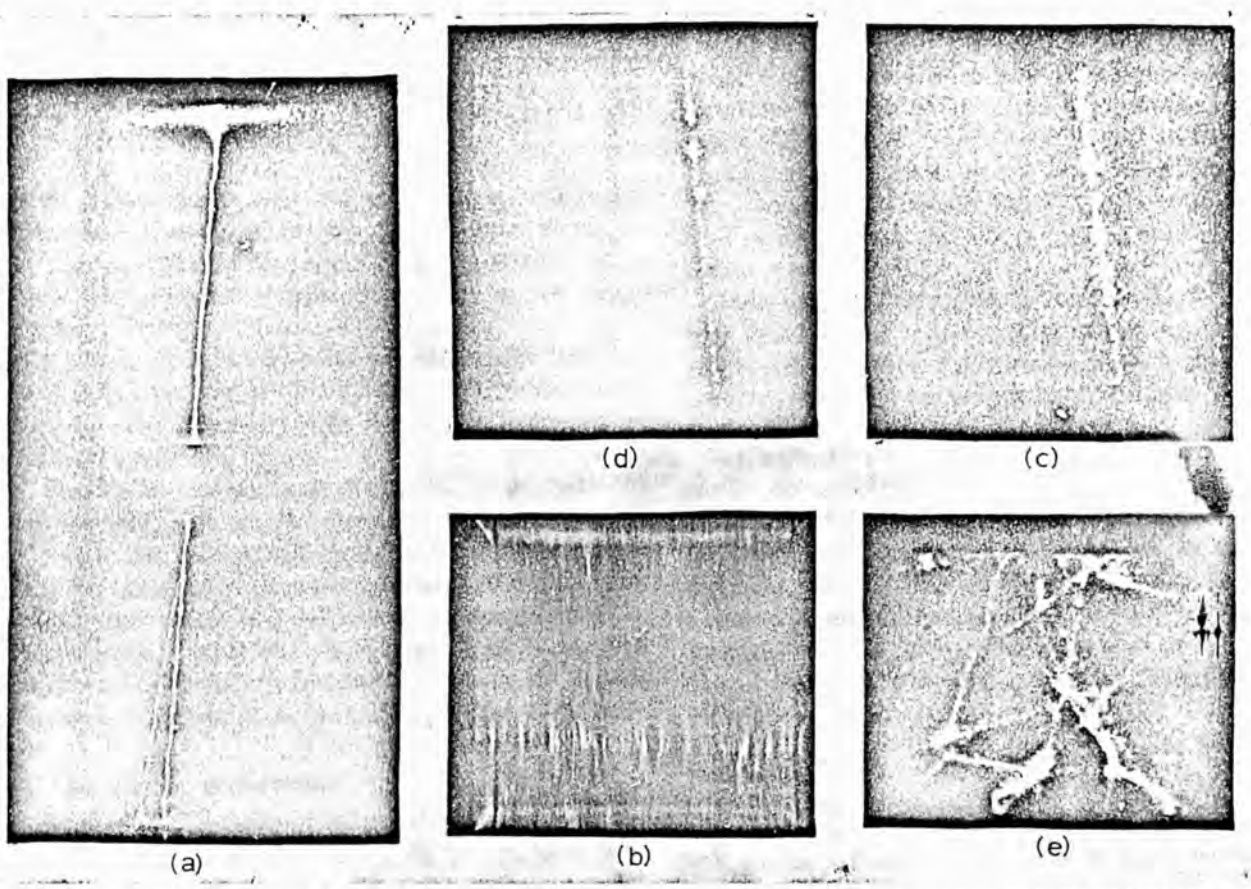

Fig. 3. Photographs of streamers taken with a 35 mm camera, at a distance of about 1 m, with aperture *f*/1.9. Ilford HP4 film used, which when developed with microphen at 20°C for 16 min has a speed of 1200 ASA.

a. Double gap continuous streamers. Photo shows knock-on particle from central electrode;
b. Streamers, viewed from side;
c. Streamer projection mode, photographed through wire-grid electrode (12 kV/cm);
d. Streamer projection mode (24 kV/cm);
e. Curious, instantaneous results from a shower seen in the projection mode.

TABLE 1

Analysis of measurements on cosmic ray tracks. The values are averages as explained in the text. The angular uncertainty is the standard deviation,

$$\{\sum_i (m_i - m)^2/(n-1)\}^{\frac{1}{2}} \text{ with } n = 10,$$

of the orientation of the track. The last column refers to the degree to which the selected measuring points lie off the computed line.

The field strengths are nominal, not measured values.

Mode	Field strength (kV/cm)	Angular uncertainty (mrad)	Standard deviation (mm)
Continuous streamer (fig. 3a)	12	1.5 ± 0.1	0.34 ± 0.02
Streamer projection (fig. 3c)	12	2.2 ± 0.24	0.41 ± 0.03
Streamer projection (fig. 3d)	24	1.5 ± 0.08	0.44 ± 0.02
Disconnected streamer (fig. 3b)	12	4.2 ± 0.6	0.90 ± 0.07

field, the primary ions are accelerated, avalanches grow and coalesce to form a fine streamer as shown in fig. 3a. This coalescing holds for angles up to about 35°, but the efficiency declines at the larger angles.

For directions nearly perpendicular to the field, the avalanches proceed in the direction of the field. Tracks therefore are indicated by the centres of a large number of short streamers, fig. 3b.

Finally, in the streamer projection mode, with the photography along the direction of the field and through the transparent grid electrode, fine tracks, [illegible] obtained with pulses of about 50 ns duration. Along the tracks the individual streamers may be distinguished as bright spots, fig. 3c, d. Very high multitrack efficiency is obtained in this mode; in one instance thirty simultaneous trajectories were recorded.

4. Quantitative performance

Numerical estimates of the spatial resolution of the chamber operating in a variety of modes have been obtained with the use of a digitising microscope that records film coordinates to an accuracy of 2 μm.

In our analysis, each cosmic ray track has been measured ten times. Each measurement consisted of selecting ten (twenty in the projection mode) arbitrary coordinate points along the track. The best straight line was then computed on the London Ferranti Atlas with a least-squares fit. Ten independent values of the track direction were thus obtained from which the probable angular uncertainty was calculated. The average standard deviations of the ten points off the computed line have also been determined, to give an indication of the trajectory straightness to be expected in a typical measurement of ten arbitrary points.

The results of the analysis on 50 tracks in the various modes are given in table 1, in the form of averages. The measurements on the mode depicted in fig. 3 are included in spite of their lower resolution, as this mode assumes considerable significance if three-dimensional determinations are contemplated.

5. Conclusion

The results of the analysis, for example, the 1.5 mrad uncertainty in track orientation, demonstrate the sensitivity of the streamer chamber. In the design of experiments, if the particle trajectories be mainly in the forward direction then the continuous streamer mode might prove best in view of the good resolution – viewed from all sides – coupled with the brighter trace. Furthermore, the uniform intensity of the trace might make it easier to detect with a scanning device. The streamer projection mode operated at a high field would be most suitable in cases when an isotropic response is required.

Although the quantitative results have been obtained with the aid of the human eye, we do not expect that an automatic recording device need show a diminished sensitivity. Indeed, the reverse might be true.

It is a pleasure to thank Professor H. O. W. Richardson for his advice; Mr. Cecil Kaplinsky for considerable help with the programming; and Professor F. F. Heymann for generously allowing us to use his digitising microscope at the University College, London. The work has been supported by the Science Research Council. One of the authors (S.R.M.) would like to thank the University of Bihar (Muzzaffarpur) for support.

References

1) J. P. Garron, D. Grossman and K. Strauch, Rev. Sci. Instr. **36** (1965) 264.
2) L. Lavoie, S. Parker, C. Rey and D. M. Schwartz, Rev. Sci. Instr. **35** (1964) 1567.
3) A. I. Alikhanian, T. L. Asatiani, A. M. Matevosian and R. O. Sharkhatunian, Phys. Letters **4** (1963) 295.
4) E. Gygi and F. Schneider, CERN 64-46.
5) G. E. Chikovani, V. N. Ruinishvili, V. A. Mikhailov and A. K. Javrishivili, Nucl. Instr. and Meth. **35** (1965) 197.
6) F. Bulos, A. Odian, F. Villa and D. Yount, SLAC no. 74 (1967).